November 2016

Biopolymer Electrospun Nanofiber Mats to Inactivate and Remove Bacteria

Katrina Ann Rieger
University of Massachusetts Amherst

Biopolymer Electrospun Nanofiber Mats to Inactivate and Remove Bacteria

A Dissertation Presented

by

KATRINA A. RIEGER

Submitted to the Graduate School of the
University of Massachusetts Amherst in partial fulfillment
of the requirements for the degree of

DOCTOR OF PHILOSOPHY

September 2016

Chemical Engineering

Biopolymer Electrospun Nanofiber Mats to Inactivate and Remove Bacteria

A Dissertation Presented

by

KATRINA A. RIEGER

Approved as to style and content by:

_____
Jessica D. Schiffman, Chair

_____
David M. Ford, Member

_____
Susan B. Leschine, Member

_____
Susan C. Roberts, Member

_____
John Klier, Department Head
Chemical Engineering

ACKNOWLEDGEMENTS

This work was partially funded by an NSF-BRIGE grant (EEC-1342343), the James M. Douglas Career Development Faculty Award, the NSF-sponsored ICE IGERT program (DGE-0654128), the UMass Center for Hierarchical Manufacturing (CHM), NSF Nanoscale Science and Engineering Center (CMMI-1025020) and Fulbright. I want to thank my advisor, Dr. Jessica Schiffman, who gave me her time, patience, and enthusiasm. I can't imagine a better advisor to help me grow as a person and a researcher. I also want to thank my committee, Dr. David Ford, Dr. Sue Leschine and Dr. Sue Roberts, for their insightful comments guiding my research. I am grateful to Shana Passonno and Dr. Mike Knolder, who provided mentorship and Lauren Barney, for her friendship. I want to thank the Schiffman Lab, Nate Birch, Kris Kolewe, and Kerianne Dobosz, and the undergrads, Emma Klinkhamer, Maureen Hoen, Hiu Yueng, Nat Eagan, and Michael Porter, who worked with me. I want to thank, Dr. David Ford, Raghuram Thyagarajan, Dr. Wei Fan, Dr. Paul Dornath and Hong-Je Cho, for our fruitful collaborations. I am thankful to Dr. Christos Dimitrakopoulos, Dr. Klaus Muellen, Dr. Mischa Bonn and Dr. Sapun Parekh, to helping me study at Max Planck in Mainz, Germany on Fulbright. Thanks to Lou Raboin, Dr. Shelly Peyton, Lauren Barney, Dr. Julie Goddard, Luis Gutierrez, Dr. David A. Reckhow, Dr. Weiguo Hu, Sekar Thirunavukkarasu, Dr. Sue Leschine, Jesus Alvelo and Jack Hirsch for access to and help in research equipment. Last but not least, I want to thank my parents, Linda and Jim, and my siblings, Andrew and Claire, for their support and encouragement. I want to express my boundless appreciation for husband, Cole, who through the ups and downs over these years has been my most enthusiastic cheerleader and my best friend so it only seems right that I dedicate this dissertation to him.

ABSTRACT

BIOPOLYMER ELECTROSPUN NANOFIBER MATS TO INACTIVATE AND REMOVE BACTERIA

SEPTEMBER 2016

KATRINA A. RIEGER

B.S., OREGON STATE UNIVERSITY

M.S., UNIVERSITY OF MASSACHUESETTS-AMHERST

Ph.D., UNIVERSITY OF MASSACHUSETTS - AMHERST

Directed by: Professor Jessica D. Schiffman

The persistence of antibiotic resistance in bacterial pathogens remains a primary concern for immunocompromised and critically-ill hospital patients. Hospital associated infections can be deadly and reduce the successes of medical advancements, such as, cancer therapies and medical implants. Thus, it is imperative to develop materials that can (i) deliver new antibiotics with accuracy, as well as (ii) uptake pathogenic microbes. In this work, we will demonstrate that electrospun nanofiber mats offer a promising platform for both of these objectives because of their high surface-to-volume ratio, interconnected high porosity, gas permeability, and ability to contour to virtually any surface. To provide biodegradability, biocompatibility, and little or no antibacterial resistance, biopolymers and plant essential oils will be used. The first system explores the engineered incorporation, characterization, delivery, and antibacterial activity of two structurally different essential oils from chitosan-poly(ethylene oxide) nanofiber mats and chitosan thin films. The incorporation of both chitosan and the essential oil, cinnamaldehyde, produced a wider range of antibacterial efficacy against *Escherichia coli* and *Pseudomonas aeruginosa* than when chitosan or cinnamaldehdye were used alone. The second system features cellulose fibers to fundamentally study the use of nanofibers for the collection of bacteria. Nanofiber mats outperformed the two commercial fibrous materials, by collecting high quantities of three medically relevant bacteria strains. Additionally, polyelectrolyte-functionalized cellulose nanofiber mats demonstrated the ability to tune both the collection and inactivation of bacteria for specific applications. Overall, biopolymer nanofiber mats electrospun in this work demonstrate the successful collection and inactivation of medically relevant bacteria, and thus, are an ideal platform for biomedical applications.

TABLE OF CONTENTS

LIST OF TABLES

Table **Page**

LIST OF FIGURES

Figure **Page**

LIST OF ABBREVIATIONS

AA: acetic acid

AA-d_4: deuterium acetic acid

AgNP: silver nanoparticles

B. anthracis: *Bacillus anthracis*

BET: Brunauer–Emmett–Teller

CDC: Center for Disease Control and Prevention

Ce: chain of entanglement

CFU: colony forming unit

CIN: cinnamaldehyde

DA: degree of acetylation

DAPI: 4′,6-diamidino-2-phenylindole

D_2O: deuterium oxide

DS: degree of substitution

E. coli K12: *Escherichia coli* K12

FTIR: Fourier transform infrared spectroscopy

GA: glutaraldehyde

HAIs: hospital-acquired infections

H-CIN: hydrocinnamic alcohol

HFIP: 1,1,1,3,3,3-hexafluoro-2-propanol

H_2SO_4: sulfuric acid

KCl: potassium chloride

LB: Difco Luria-Bertani broth

LTA: Linde Type A

MIC: minimum inhibitory concentration

MMP: matrix-metalloproteinase

NaCl: sodium chloride

Na_2HPO_4: sodium phosphate dibasic anhydrous

$Na_2H_2PO_4$: sodium phosphate monobasic anhydrous

NaOH: sodium hydroxide

$NaNO_3$: sodium nitrate

NH_4OH: ammonium hydroxide

PAA: poly(acrylic acid)

P. aeruginosa: Pseudomonas aeruginosa

PBS: phosphate buffered saline

PCL: poly(caprolactone)

pDADMAC: polydiallyldimethylammonium chloride

PEI: polyethyleneimine

PEO: poly(ethylene oxide)

PI: Propidium iodide

PLA: poly(lactic acid)

PLCL: poly(L-lactide-*co*-ε-caprolactone)

PLGA: poly(lactide-*co*-glycolide)

PMMA: poly(methyl methacrylate)

p:o: total polymer:oil mass ratio

PVA: poly(vinyl alcohol)

PVAc: poly(vinyl acetate)

PSf: polysulfone

PU: polyurethane

S. aureus: Staphylococcus aureus

SEM: Scanning electron microscopy

Span®80: sorbitan monooleate

SWNTs: single-walled carbon nanotubes

TGA: Thermogravimetric analysis

TMAOH: tetramethylammonium hydroxide

Wt %: Weight percent

XPS: X-ray photoelectron spectroscopy

XRD: X-ray diffraction

CHAPTER 1
INTRODUCTION

1.1 Motivation

1.1.1 Biofilms Produce Difficult to Treat Infections

Ubiquitously, planktonic bacteria attach to surfaces and develop into communities of microorganisms called biofilms[1]. The stages of biofilm development include the (i) initial reversible attachment, (ii) irreversible attachment, (iii) early maturation, (iv) maturation, and (v) dispersion of the bacteria (Figure 1). When free-floating, the microorganisms attach to virtually any surface and start to form a 3-dimensional structure known as a biofilm. The close proximity of cells within this structure facilitates a cell-to-cell communication mechanism known as quorum sensing (QS), which coordinates the growth and maturation of most biofilms[2,3]. Although antibacterial agents damage the outer layer of a biofilm, the community can develop resistance in the protected inner layers. Thus, bacteria becomes 1000 times more resistant to antibiotics in a biofilm than when the bacteria were in the planktonic state.[2,4]

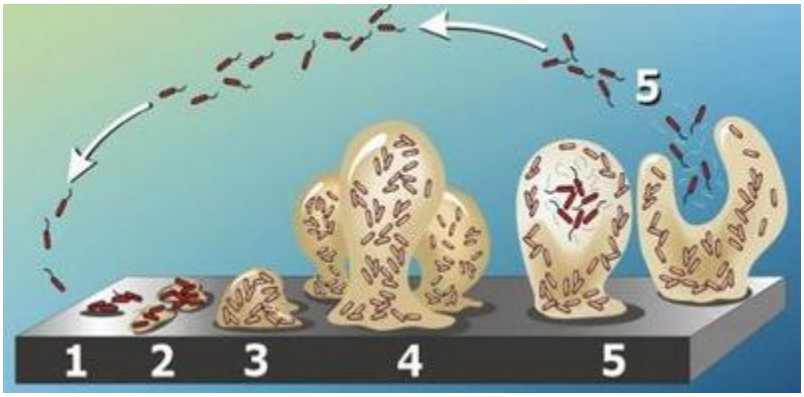

Figure 1**:** Biofilm formation starts when (1) planktonic bacteria cells (2) attach to a surface and start to (3) proliferate (4) maturing into a biofilm to (5) become a source of dispersion. Image acquired from Center for Biofilm Engineering at MSU-Bozeman (2003) by Paul Stoodley and Peg Dirckx.

In the medical field, antibiotic resistance plays a critical role in hospital associated infection (HAIs). Each year two million patients are diagnosed with HAIs, with approximately 23,000 resulting in death[5]. However, these statistics do not include those who have a preexisting condition and acquire an infection. In addition to the challenge of treating patients who acquire such an infection, there is also a reduction in the success of medical advancements (cancer therapy, organ transplants and chronic disease such as diabetes) that rely on antibiotics to treat infections[5]. Furthermore, hospitals face a financial burden of $20 billion in excess cost and society faces a loss of $35 billion in productivity[5].

Hospitalized patients who are critically ill, have a 40-60% likelihood of dying from an infection caused by the leading Gram-negative opportunistic human pathogen, *Pseudomonas aeruginosa* (*P. aeruginosa*)[6,7]. In U.S. hospitals alone, 51,000 cases are diagnosed each year with 6,700 cases resulting in bacterial resistance and 440 resulting in death[5]. The severity of nosocomial pseudomonas infections is augmented by the increasing tolerance of this microorganism to nearly all current antipseudomonal drugs, such as piperacillin, ceftazidime, imipenem, and ciprofloxacin[8,9]. With 8% of all infections occurring being a resistance strain of *P. aeruginosa*, this bacteria has recently been labeled as a serious threat by the Center for Disease Control and Prevention (CDC).

P. aeruginosa has an intrinsic resistance to antibiotics due to the low permeability of its outer membrane. Additionally *P. aeruginosa* relies on QS to control population density and bacterial virulence. During an infection, *P. aeruginosa* can utilize QS to coordinate the expression of a tissue-damaging factor[10]. A multi-layered hierarchical interconnected QS system (Figure 2) can be activated within *P. aeruginosa* consisting of four QS signaling networks: LasR, RhIR, PqsR and IqsR[11]. The quorum sensing signals also known as auto-

inducers are small diffusible signal molecules that can move freely across the cell membrane. For *P. aeruginosa*, the QS signals include N-(3-oxododecanoyl)-homoserine lactone (OdDHL), N-butyrylhomoserine lactone (BHL), 2-heptyl-3-hydroxy-4-quinolone (Pseudomonas Quinolone Signal, PQS), and 2-(2-hydroxyphenyl)-thiazole-4-carbaldehyde.

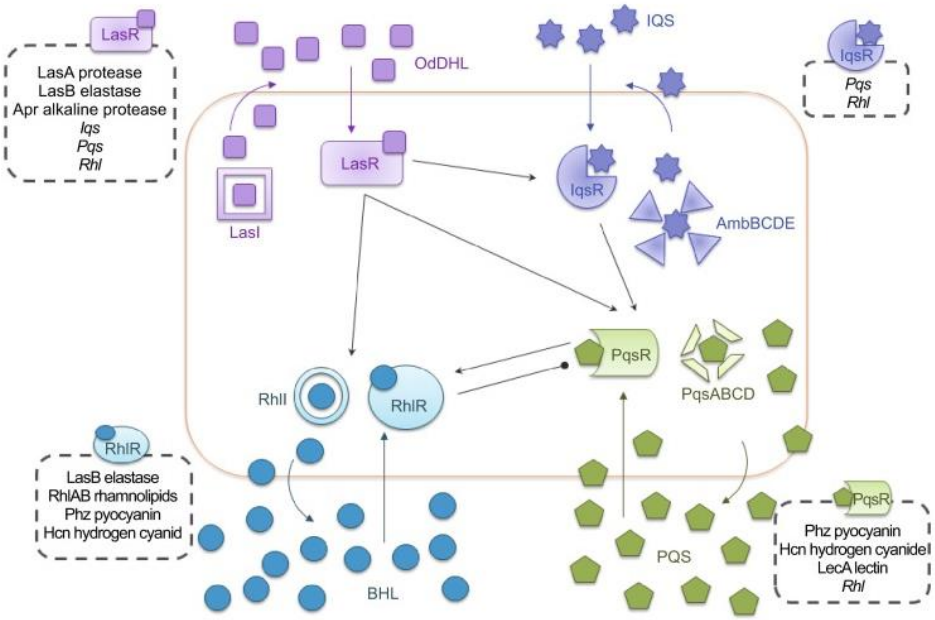

Figure 2: Schematic representing the QS 4 multi-layered hierarchal signaling networks, LasR, RhIR, PqsR and IqsR found in *P. aeruginosa*[11].

1.1.2 Need for Alternative Antibiotics

While antibiotic resistance is an innate process, it is accelerated through the application of incorrect or an insufficient quantity of antibiotics to the bacterial infection.[12] As demonstrated in Figure 3, the time lapse between the development of an antibiotic and the first observed resistance is decreasing. Furthermore, a steady decrease in the number of antibacterial new drug application approvals demonstrates a need to develop new antimicrobials to combat antibacterial resistance.[5] Notably, according to the 2013 CDC

report, 50% of antibiotics prescribed are either not needed or not optimally effective.[5] Widespread use of antibiotics is prevalent in medical, food, and agriculture industries, resulting in further increase in antibiotic resistance.

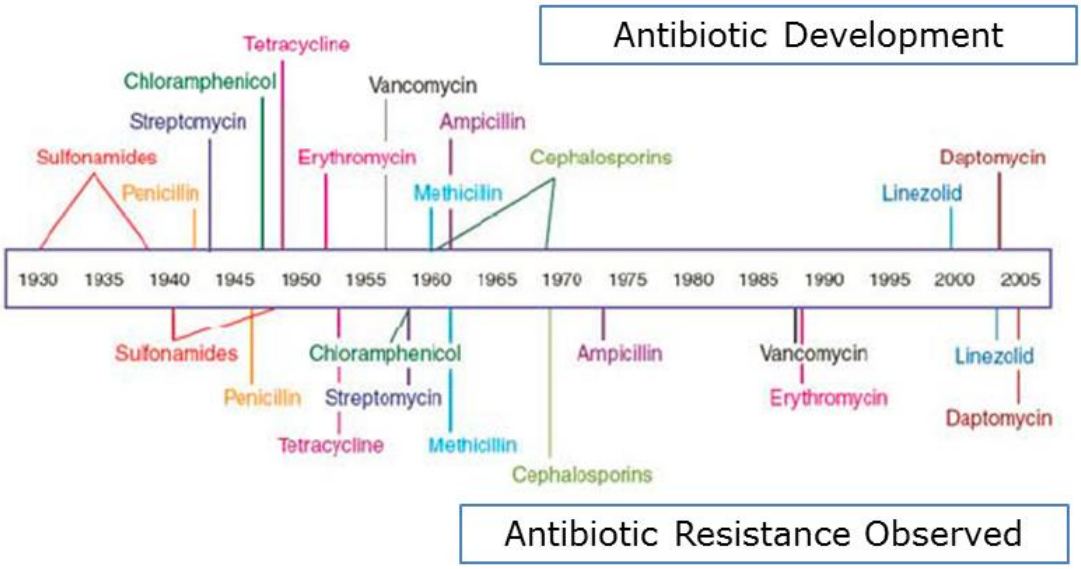

Figure 3: A timeline correlating the development of an antibiotic to initial observance of antibiotic resistance for various antibiotics. This demonstrates the increasing trend of antibiotic resistance[12]**.**

Antibiotics are a limited resource and therefore the CDC has proposed four core strategies to fight antibiotic resistance. These tactics include preventing the spread of resistance, tracking resistance in bacteria, improving use of antibiotics, and promoting development of new antibiotics and new diagnostic tests for resistance[5].

1.1.3 Essential Oils as a Potential Alternative

Essential oils are a natural resource that have been exploited for their intrinsic properties since the Middle Ages. These secondary metabolites of aromatic plants are known for their fragrance and can be extracted via distillation[13]. Composed of a variety of molecules including both aromatic and aliphatic, essential oils are plants' natural antibiotics exhibiting inactivation of bacteria, viruses, funguses, parasites and insects.[13]

There are approximately 300 different essential oils with each oil containing various concentrations of 20-60 components[13]. Nearly all 300 of them rely on one of three chemical structures – phenols, aldehydes and alcohols – to exhibit bioactivity, Figure 4 [13].

Unlike commercial antibiotics, essential oils nonspecifically attack a wide assortment of bacteria resulting in little to no bacterial resistance.[13] This is in part due to the structurally complex compounds found in essential oils. The antimicrobial mechanisms of many essential oils have been investigated and are the subject of numerous review articles.[14–16] The hydrophobicity of the small terpenoid and phenolic compounds found in essential oils is related to their complex antimicrobial mechanism — they can easily permeate the cell membrane leading to a depletion of the proton gradient and subsequent disruption of adenosine triphosphate (ATP) synthesis or cell lysis.[15] Since their exact antimicrobial mechanism is complex, the development of resistance by bacteria is hindered. Kavanaugh and Ribbeck have demonstrated that concentrations of essential oils (cassia, peru balsam, and red thyme) were as effective as similar concentrations of commercial antibiotics against both planktonic cells and biofilms of *P. aeruginosa* (PA01) and *P. putida* (KT2440).[17]

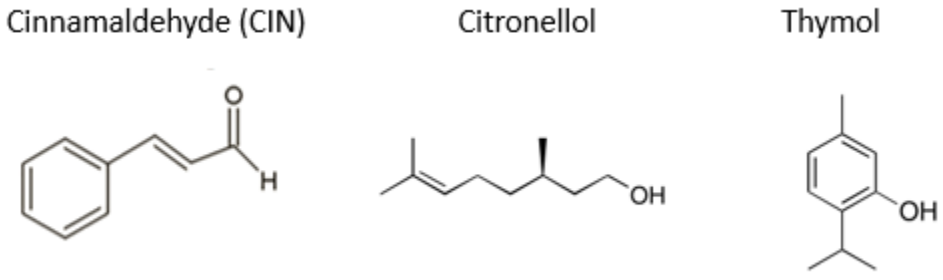

Figure 4: Three natural essential oils, cinnamaldehyde (CIN), citronellol and thymol, represent the three major chemical structures –aldehydes, alcohols, and phenols – used to exhibit bioactivity.

One well studied essential oil, which will be a focus of this work, is cinnamon oil, whose major component is cinnamaldehyde (CIN), **Error! Reference source not found.**. CIN decreases metabolic activity and the replication rate of *P. aeruginosa*[18]. In *P. aeruginosa*, exposure to CIN can inhibit the QS system. Specifically, CIN is structurally similar to the N-acyl homoserine lactones (AHLs) and can dock at the substrate binding sites of the LasI network interfering with the QS communication system[19].

1.2 Polymers

1.2.1 Biopolymers

Polymers, chains of covalently bonded monomeric units, can be classified as either natural or synthetic.[20] Natural polymers, known as biopolymers, are found in biological systems, display well defined specific structures with a polydispersity of one and are synthesized for a specific biological function such as storage or structure.[21] Biopolymers derived from renewable resources are becoming increasingly beneficial for limiting the dependence on synthetic materials produced from limited petroleum resources.[20] For instance, by using the waste products from fishing and farming industries, natural materials are readily available and also help to make other industries more eco-friendly.

Biopolymers of either plant or animal origin are being applied to many fields such as biomedicine, defense and agriculture as they pose many advantages over synthetic polymers because they also offer numerous intrinsic benefits (antimicrobial, hemostatic, etc). In addition to being economical, non-toxic and renewable, biopolymers are both intrinsically biodegradable/compatible and are easily chemically modified for increased functionality.

Unfortunately, there are numerous challenges that arise when working with natural polymers, since they suffer from batch-to-batch variability. The raw source may contain heavy metals and microbes thus challenging their product consistency.[22] In comparison to synthetic materials manufactured in a controlled environment, climate growth conditions, natural production rate tends to result in higher product variations.[21] Thus, further characterization and understanding of natural materials, specifically biopolymers, is needed in order to harness their functionalities for a variety of fields.

1.2.2 Polysaccharides

Polysaccharides are long chains of monosaccharide units linked together by glycosidic bonds. This important class of biological polymers is either linear or branched depending on whether its purpose is structure or storage, respectively. Starch and glycogen are both branched polysaccharides that primarily serve as storage whereas cellulose and chitin are examples of structure. The abundance and renewability of these polymers has led to their use in many industries.

Polysaccharides, such as chitosan[23–27], cellulose[28–31], and hyaluronic acid,[32,33] as well as proteins, collagen[34–36] and silk[37–40] are advantageous for biomedical applications because they display specific properties that promote wound healing.[41] For instance, chitosan exhibits both antibacterial and hemostatic activity. While certain polysaccharides are expensive such as proteins and hyaluronic acid, cellulose and chitosan are relativity cheap and very abundant in the form of raw biomass.[21] Therefore, the utilization and engineering of cellulose and chitin for a variety of new applications is highly appealing due to the lower production costs associated with the use of the raw biomass of these biopolymers and will be the focus of this work.[21]

As the most abundant polysaccharide on earth, cellulose is found as the structural material in plant cell walls, algae, and it is also produced by some bacteria species. It is a waste product of the agriculture industry. Composed of linear chains of D-glucose linked via β(1→4) with extensive hydrogen bonding, cellulose displays excellent thermal and mechanical properties, Figure 5.

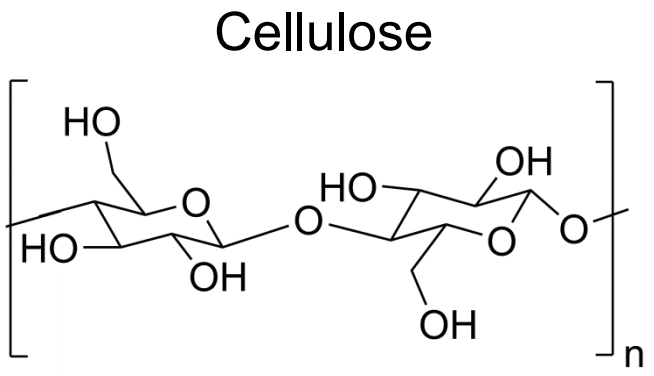

Figure 5: Cellulose, a polysaccharide composed of linear chains of D-glucose units linked via β(1→4) is the most abundant organic polymer on Earth as a structural material in plants and algae.

Chitin is the second most abundant biopolymer on earth (Figure 6) from which chitosan can be synthesized. Chitin is the main structural component in cell walls of fungi and in the shells of crustaceans. Thus, the seafood industry commonly disposes chitin — on the order of millions of tons per year. Composed of linear units of 2-acetylamino-2-deoxy-D-glucose joined by β(1→4) bonds, chitin can be deacetylated into a copolymer of 2-acetamido-2-deoxy-D-glucopyranose and 2-amino-2-deoxy-D-glucopyranose units linked together through β(1→4) bonds. This copolymer, chitosan contains free amino groups, which give it antibacterial and hemostatic activity[42,43].

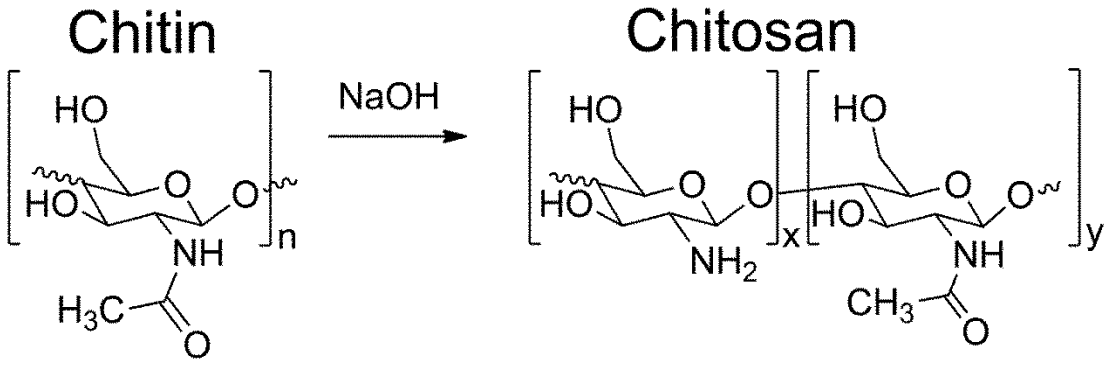

Figure 6: Chitin, the main structural component of crustaceans shells, is composed of 2-acetylamino-2-deoxy-D-glucose units joined by β(1→4) bonds. The deacetylation of chitin results in a copolymer of 2-acetamido-2-deoxy-D-glucopyranose and 2-amino-2-deoxy-D-glucopyranose units known as chitosan, which exhibits amine functionality based on its degree of deacetylation.

1.2.3 Synthetic Polymers

The appropriate polymer matrix, natural, synthetic, or a rational combination of polymers, should be selected to match the desired biomedical applications.[44] Synthetic polymers commonly used for biomedical applications include, poly(ethylene oxide) (PEO)[45–47], poly(lactic acid) (PLA)[48–52], poly(caprolactone) (PCL)[53], and poly(vinyl alcohol) (PVA).[54] While the majority of synthetic polymers are not biodegradable, these polymers are all biocompatible and have received regulatory clearance from the FDA for medical applications.

There are a few important items to note when choosing between natural and synthetic polymers. While synthetic polymers are not intrinsically biocompatible or biodegradable, they display other properties that are needed to develop a scaffold such as higher mechanical properties. Batch variation is minimal for synthetic polymers; in terms of processing, synthetic polymers are compatible with a wider range of solvents than biopolymers.[55] A blend of synthetic and natural polymers can be chosen to gain a wider range of properties, which can be tuned based on polymer type and blend ratio.[56]

1.3 Electrospinning

1.3.1 Process and History

The current electrospinning process originates from early understandings of electrodynamics. Starting as early as the 1500s, Gilbert demonstrated the change of droplets of water from spherical to conical shape due to the presence of charged amber.[57] The use of an electric field to excite a dielectric liquid was reported three hundred years later by Lamor.[58] Further development, specifically in apparatus design and spinning solutions was documented in patents published by Cooley, Morton, and Formhals in 1902[59,60] and 1934.[61–63] A variety of polymer solutions were placed in electric fields using systems that featured multiple spinnerets, a moving collection target, and a collector composed of parallel electrodes. Today, commercial and laboratory electrospinning set-ups resemble these initial systems. While there have been numerous significant lulls in electrospinning research over the past five hundred years, current interest in this inexpensive nano- and macro- fiber fabrication technique continues to be on the rise (Figure 7A).[64]

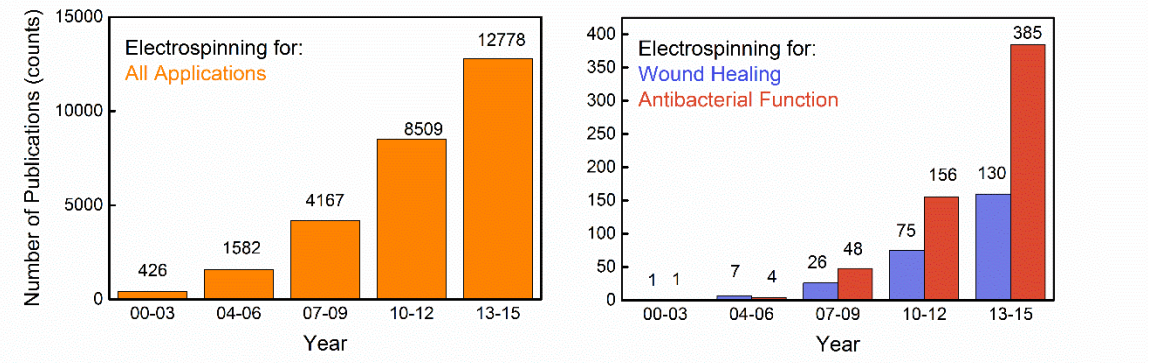

Figure 7: The number of publications on (A) electrospinning and (B) electrospinning for wound healing and antibacterial function exhibit an upward trend over the past dozen years. The SciFinder Scholar database was used to determine the total number of unique results from searching (A) “electrospinning” and (B) “electrospinning” plus “wound healing” or “antibacterial”. Data analysis was conducted on February 23, 2016.

Electrospinning, an inexpensive and scalable process, generates nonwoven fibers through the use of an electric field.[64–66] Conventionally, an electrospinning apparatus includes a high voltage power supply, a grounded collector, and a spinneret, Figure 8. The spinneret is connected to the grounded collector via electrodes to complete the circuit and produce an electric field. A precursor solution — typically a polymer, sol-gel, or melt —is loaded into the spinneret and advanced at a low feed rate using an advancement pump. The precursor solution will form a pendent drop held at the tip of the spinneret via surface tension. The pendent drop will pull into a conical shape known as a Taylor Cone due to repulsive electrical forces once the voltage is increased.[67,68] From the tip of the Taylor Cone, a liquid jet will emerge once the electrical forces overcome the surface tension forces. During travel, the liquid jet is pulled and whipped due to a bending instability allowing the solvent to evaporate before fibers are collected on the target. The liquid jet will reach the collector as smooth, cylindrical fibers in 18 nanoseconds.[69] Inconsistent fiber morphologies such as beading will result for polymer solutions of insufficient viscosities due to a Rayleigh instability experienced during travel from the spinneret to the collector.

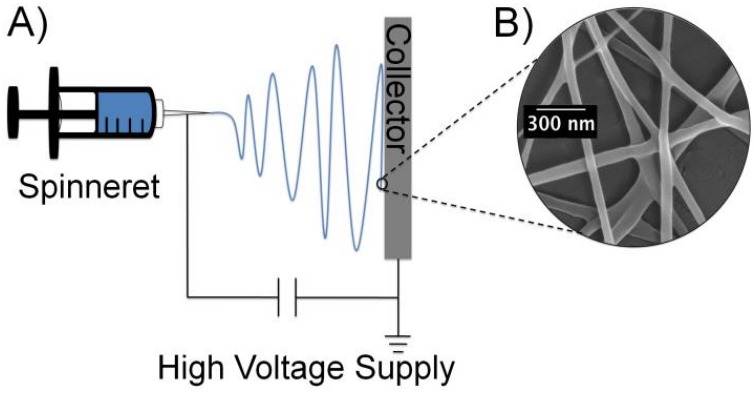

Figure 8 (A) The schematic displays an electrospinning apparatus, which is composed of a spinneret, a high voltage supply, and a collector. Typically, an advancement pump is used to regulate the flow rate of the polymeric solution. (B) The scanning electron micrograph displays the nanofiber morphology present in a typical electrospun non-woven mat, a 300 nm marker is displayed.

1.3.2 Processing Variables

Fabrication of fibers via electrospinning is dependent on the precursor solution, processing variables, and ambient conditions. The extent of chain entanglement (C_e) within a polymer solution is directly related to the ability to electrospin fibers. Only once the polymer concentration is above the critical concentration, can fiber spinning ensue.[26,70,71] Other properties of the precursor solution — conductivity, surface tension, viscosity, and polymer concentration — can be optimized by appropriate polymer and solvent selection. Different solvents and salts can be used to adjust the conductivity and surface tension of the system.

Controlling particular electrospinning apparatus parameters directly influences the resultant mean diameter and arrangement of the accumulated fibers. An increase in voltage or a decrease in feed rate will facilitate a reduction in fiber diameter.[72] The separation distance needs to be sufficient for solvent evaporation but close enough to enable the desired fibrous morphology.[73] Ambient parameters — temperature and humidity — should be controlled and monitored through the process since they affect fiber formation. For example, an increase in temperature will decrease the average fiber diameter, due to a decrease in solution viscosity. While an increase in humidity will increase the average fiber diameter due to polymer swelling.[74–76] Additionally, high humidity can result in insufficient solvent evaporation, leading to no fiber formation. Fiber alignment can be achieved through the manipulation of the electric field profile and appropriate collector selection.[66] Rotating drums,[35] parallel electrodes,[77] and an array of counter-electrodes[78] are example collectors, which have been implemented to generate a controlled arrangement of fibers.

1.3.3 Techniques to Manipulate Fiber Design

A number of apparatus designs either *in situ* (during the spinning) or post-electrospinning allow for the tailoring of fibers for a specific application. Active agents can be housed within or coated on the outside of fibers based on fiber modifications. Blend, core/shell and emulsion electrospinning (Figure 9) are techniques that place active ingredients within the fibers in situ, while post processing allows for the placement of active ingredients on the outer surface of the fibers.

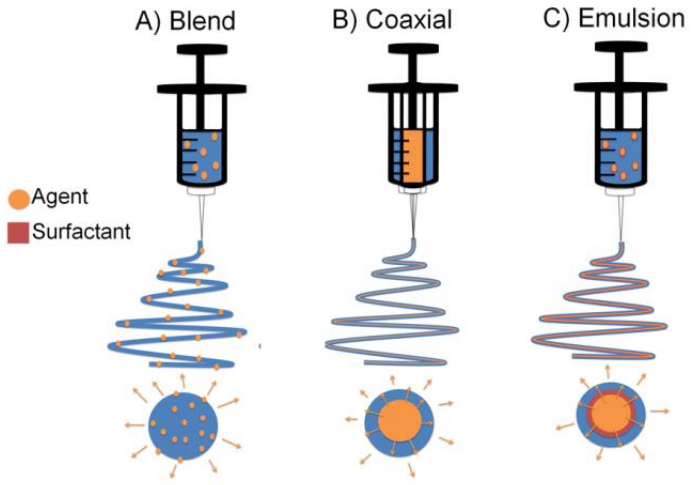

Figure 9**:** (Top) Schematic displaying a spinneret loaded with a bioactive agent for (A) blend, (B) coaxial, and (C) emulsion electrospinning. Coaxial electrospinning requires the use of a concentric spinneret configuration. (Middle) Blend electrospinning often yields fibers that contain the active agent dispersed throughout the fibers, whereas coaxial and emulsion electrospinning lend well to the synthesis of a core/shell morphology. (Bottom) Cross-sections of an individual fiber produced via the three methods displayed.

1.3.3.1 Blend Electrospinning

Blending[79], consists of suspending a drug,[80] an active agent,[81] or a precursor agent (e.g., silver ions[82]) that can be reduced to an active agent (e.g., silver nanoparticles) into the electrospinning solution, Figure 9A. The as-spun mats can contain the agent dispersed throughout or at the surface[83,84] of the fibers. This technique requires the traditional

electrospinning apparatus and can be used to incorporate a multitude of polymers and agents.[85]

Ojha et al.[84] demonstrated that polymer/agent blend fibers can accumulate the agent along the surface of the fibers, which occurs *in situ* as the solvent is being evaporated. As a result, these blended fibers exhibit a high initial release of drug known as a burst release.[86] Non-steroidal anti-inflammatory drugs (NSAIDs) are a group of agents where a burst release would be favorable. A PLGA electrospun mat containing ibuprofen was shown to reduce pain immediately and prevent the response of fibroblasts to major pro-inflammatory stimulators due to a burst release of medicine characteristic of polymer/agent blend fibers.[87]

A high initial release of an antibiotic is desirable at the site of a wound to eliminate bacteria, while a subsequent slow release of drug aids in preventing an infection. Jannesari et al.[54] electrospun composite PVA/poly(vinyl acetate) (PVAc) nanofiber mats containing ciprofloxacin HCl, whose initial burst release rate was doubled when the drug content was increased from 5 to 10 weight percent (wt%). By blending the hydrophobic polymer, PVAc, into the fibers, the hydrophilic model drug would be more likely to migrate to the surface of the fibers during solvent evaporation. Additionally, the PVAc mats were better engineered for wound healing because they demonstrated a slower sustained release rate and were more flexible.

Additionally, researchers have further tailored the functionality of fibers by loading solid agents into the polymer precursor solutions, including TiO_2/graphene for increased electrical performance,[88] quantum dots for fluorescent detection,[89] and single-walled carbon nanotubes for antibacterial activity.[79] In these cases, the solid agent was suspended

in a concentrated polymer solution, which provided the chain entanglement necessary to "carry" the solid agent along the electrospinning process.[90]

1.3.3.2 Coaxial Electrospinning

When a burst release is not desired or the bioactivity of the agent is sensitive to harsh solvents, encasing the agent in a polymeric shell is necessary. Coaxial electrospinning[91–95] produces core/shell fibers by using a "coaxial" or concentric needle arrangement, which features an inner and an outer channel to separate two or more solutions, Figure 9B. In the context of synthesizing mats containing biologics, an outer polymer shell can be used to encase the active agent. To do this, the active agent is fed through the inner channel. The outer shell provides a protective barrier from the electric field, as well as from harsh solvents, which might be needed to electrospin the polymer located in the outer channel of the syringe.[96] Additionally, non-spinnable material such as inorganic nanomaterials can be electrospun into the core of the fiber by placing a polymer in the outer channel to carry the non-viscous material through the process.[97]

While the addition of an inner channel increases the processing parameters that need to be optimized, this electrospinning technique is superior for obtaining controlled drug release via eliminating a burst release. Su et al.[98] compared the release rates of heparin encapsulated in the core of poly(L-lactide-*co*-ε-caprolactone) (PLCL) fibers and fibers composed of heparin blended with PLCL. The composite fibers showed a high initial release while heparin, once located in the core of the fiber, demonstrated a stable sustained release over two weeks. It was deduced that the release from the core/shell fibers was governed by a coupled diffusion/degradation mechanism.

1.3.3.3 Emulsion Electrospininng

Another route towards achieving a core/shell morphology is to employ an emulsion as the precursor solution,[99–103] Figure 9C. Here, a surfactant is used to separate the distinct phases. This type of electrospinning allows for the incorporation of protein, DNA, and peptides by preventing their exposure to harsh organic solvents.[103] A handful of reports used harsh organic solvents to emulsion electrospin specific polymers, by relying on a surfactant to carry the immiscible phase biological cargo ─ proteins,[102,104] DNA,[105] and water-soluble drugs[101,106] ─ and protect them against coalescence.[99,101,103,104,107–109]

Yang et al.[102] demonstrated the use of emulsion electrospinning as a carrier for therapeutic proteins via electrospinning an emulsion consisting of a water phase containing the model protein, bovine serum albumin, and an organic phase using the polymer, poly(DL-lactide). In addition to keeping the encapsulated protein bioactive, the initial burst could be reduced through lowering the volume ratio of aqueous to organic phase.

Water in oil (W/O) emulsions have been electrospun wherein the oily phase consists of a polymer dissolved in an organic solvent and the water phase contains the active agent. This system is ideal for the delivery of a hydrophilic drug because a hydrophobic shell is needed to protect the drug from dissolving instantaneously in the blood stream.[101] For example, by spinning from an emulsion pre-curser solution, TCH (a hydrophilic antibiotic) was successfully encapsulated within the core of poly(ethylene glycol) PEG-PLA nanofibers.[110] As characteristic of emulsion electrospinning, these fibers showed a stable release rate, elimination of an initial burst release, and protection of the active agent incorporated.

1.3.3.4 Post-processing of Electrospun Mats

The surface of an electrospun mat might lack the properties needed for a specific bio-application. As a result, as-spun fibers can be modified post-spinning via electrostatic

attachment,[111] dip-coating,[112,113] layer-by-layer assembly,[114] or by performing surface chemistry,[115–117] Figure 10.

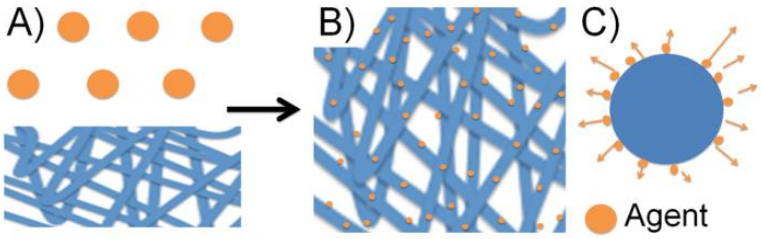

Figure 10: Post-production, (A) as-spun mats can be modified with functional agents (e.g., polymers, drugs, biomolecules) to (B) alter their surface chemistry and functionality. (C) A cross-section of an individual post-modified fiber mat displays that the new functional units are located on the surface of the fibers.

Coating consists of submerging a fabricated electrospun mat into a solution in order to transfer desirable properties to the mats. Chitosan has been used to coat PVA electrospun fibers by submerging the fibers in a 1.0 wt% chitosan solution for 1 hr at 30 °C.[112] In addition to using this facile process, another advantage of this coating is that chemically, chitosan more closely resembled glycosaminoglycans in the extracellular matrix than their control (chitosan-PVA blend fibers). In order to provide immediate hemostatic activity, Spasova et al.[113] also chose chitosan to coat their wound healing electrospun PLA and PLA/PEG mats.

Performing chemical modifications to functional groups located on the surface of the fibers can enable the attachment of bio-functional molecules or tune the degree of hydrophilicity of the mat. The addition of a bio-functional molecule can promote certain biological activities such as cell proliferation and migration.[116] This is specifically important in treating diabetic ulcers, where the natural wound healing process is compromised, thus leading to chronic wounds and in some cases amputation. EGF, the epidermal growth factor, was chemically immobilized to functional amine groups on the

surface of PCL and PCL-PEG block copolymer blended fibers to treat diabetic ulcers.[117] *In vivo* wound studies demonstrated an increase of keratinocyte-specific genes as a result of the EGF conjugated fibers. Thus, the incorporation of a growth factor facilitated gene expression, which in turn accelerated wound healing.

Through the attachment of biomolecules onto the surface of fibers, the mat can be functionalized to make use of the body's natural enzymes. A MMP-responsive release dressing was electrospun as a local gene delivery system to treat diabetic ulcers, which display high levels of MMPs.[115] Linear polyethyleneimine (PEI) was chemically attached through an MMP-cleavable peptide linkage to amine groups, which were already present on the surface of PCL-PEG nanofibers. The mat was further modified through the electrostatic attachment of negatively charged DNA to the positively charged PEI. The ability to release DNA in the presence of MMP makes this system ideal for local gene therapy of diabetic ulcers.

1.3.4 Polysaccharides Nanofibers

Most biopolymers have been electrospun for localized drug delivery or as wound healing dressings. Polysaccharides such as chitosan,[23–27,118,119] cellulose,[28–31,120,121] and hyaluronic acid,[32,33,122] as well as proteins, collagen,[34–36,123] gelatin,[55,124,125] silk,[37–40,126] alpha-elastin[127,128] and tropoelastin[127,129] have all been electrospun.[44] Electrospinning of polysaccharides presents a unique set of challenges, which usually include purification steps prior to electrospinning and limited solvent choices due to high crystallinity and poor mechanical properties. Additionally, standardization of the electrospinning parameters to polysaccharides is challenging because of high sample variation due to purity and origin of material.

One polysaccharide that is challenging to electropsin due to its high crystallinity is cellulose. Expensive solvents, manipulation of temperature, and microwave irradiation have all been employed to dissolve cellulose for electrospinning. Frey et al.[130] used ethylenediamine and potassium thiocyanate salts to successfully prepare cellulose nanofibers. However, the process was time intensive with multiple freeze-thaw cycles to completely dissolve the cellulose. The use of expensive room temperature ionic liquids capable of dissolving both polar and nonpolar compounds was utilized by Viswanathan et al.[131] Cellulose was dissolved in 1-butyl-3-methylimidazolium chloride with the help of microwave irradiation, electrospun at 100 °C and collected into an ethanol bath for solvent removal. Recently, the relationship between utilizing a co-solvent system to electrospin cellulose and the resultant fiber properties was performed to gain better understanding of electrospinning cellulose directly.[132] While a variety of solvents have been employed to spin cellulose, such as *N*-methylmorpholine-*N*-oxide, manipulation of processing temperature is still sometimes required and the overall process is challenging.[133]

These challenges associated with electrospinning cellulose have led to investigations into using cellulose derivatives as an alternative. Cellulose derivatives are produced via the hydroxyl group, which can be partially or fully reacted to give cellulose esters or cellulose ethers. One cellulose derivative, cellulose acetate, is fiber forming and can be electrospun in common solvents such as acetone or acetic acid.[134] Another advantage of electrospinning cellulose derivatives is the ability to regenerate the fiber mats into cellulose through the deacetylation of cellulose acetate using sodium hydroxide (NaOH), Figure 11. The degree of regeneration is based on the NaOH solvent solution. Alcoholic NaOH results in a complete regeneration of cellulose whereas aqueous NaOH

regenerated cellulose on the surface of the fibers but the core of the fibers remains cellulose acetate.[134] Additionally, cellulose nanofibers can be further processed into carbon nanofibers.[120] Overall cellulosic nanofibers produced from electrospinning have been explored for applications in the biomedical field,[121,135] food science[136] and filtration.[137]

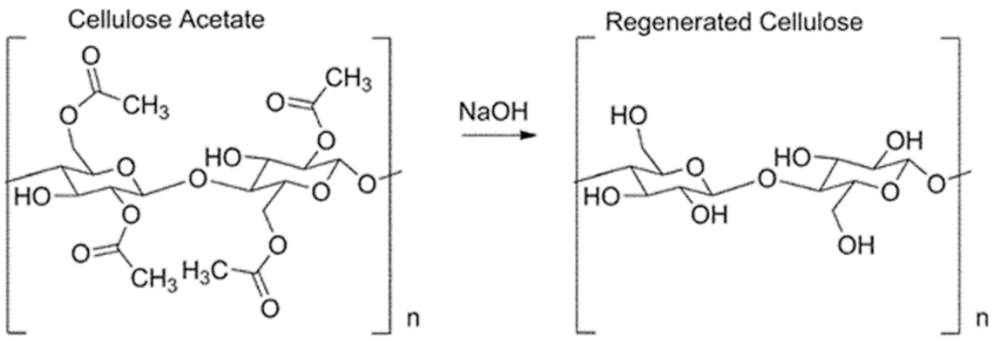

Figure 11: While cellulose is challenging to dissolve with common solvents, modifying the hydroxyl groups on cellulose yields cellulose acetate. Cellulose acetate is easily dissolved in aqueous acetic acid or acetone, can form fibers, and can be deacetylated to form regenerated cellulose. [134,138]

Chitin and chitosan have both been extensively used in the electrospinning field due to the antibacterial and hemostatic properties associated with chitosan. Pure chitosan solutions have been electrospun in solvents such as trifluoracetic acid[139] and fluoracetic acid and dichloromethane[140]. However, electrospinning of pure chitosan relies on harsh solvents and has proven challenging due to the viscosity scaling law associated with incorporating polyelectrolytes into solutions.[70] Thus, the majority of chitosan fibers fabricated via electrospinning are blended fibers containing a second polymer. When electrospun in conjunction with a synthetic polymer, the mechanical, degradation, and/or morphological features of the porous fiber mats can be fine-tuned. Synthetic polymers are compatible with a wider range of solvents, which can facilitate the spinning process.[55]

Additionally, minimal variations of synthetic polymers results in uniform behavior during electrospinning. Based on polymer ratio, overall polymer concentration and choice

of solvent, chitosan has been electrospun into defect free nanofibers with a variety of syntetic polymers including poly(lactide-co-glycolide) (PLGA),[141] PLA[48], and PEO[142]. It has also been paired with a second biopolymer including zein,[34] and collagen[143], creating nanofibers that have additional properties promoting wound healing. Another method to electrospin pure chitosan nanofibers is electrospin chitin.[144] Chitin dissolved in 1,1,1,3,3,3-hexafluoro-2-propanol (HFIP) can be electrospun and subsequently deacetylated into chitosan nanofibers through the use of NaOH.

1.3.5 Antibacterial Nanofibers

Prevention of an infection is essential to complete wound repair. The addition of antibacterial agents — inorganic, organic, or metallic — into electrospun mats has continually been an important research focus, Figure 7B, especially as antibiotic resistant bacteria strains increasingly emerge. Electrospun nanofiber mats specifically offer a promising solution specifically to the management of wounds where bacteria resistant infections occur by accelerating the healing process. Nanofibers generated using the electrospinning process exhibit high levels of porosity, gas permeation, and offer a high surface-to-volume ratio. These properties promote cell respiration, skin regeneration, moisture retention, removal of exudates, and hemostasis.[84] Thus, a wide range of biocidal nanofibers is imperative to effectively treat both the gram-positive and the gram-negative bacteria present during wound healing and for the prevention of hospital-acquired infections.

Metals have been incorporated into electrospun mats as antibacterial agents; the most common of these agents is silver.[27,82,83,111,145] Silver displays a wide spectrum of biocidal activity and a low bacterial resistance as compared to other antimicrobials agents.

Bacterial membranes uptake the free Ag^+ ions, which disrupts ATP production and DNA replication, generating reactive oxygen species (ROS) that directly damage cell membranes. In wound healing, silver decreases surface inflammation and promotes surface calcium, stimulating epithelialization. In order for silver to be incorporated, a reducing method must be utilized to prevent cytotoxicity to mammalian cells. This can be achieved by using an aqueous route instead of an organic agent.[145] Nyugen et al.[83] took advantage of the ability of PVA to be a reducing agent for silver nanoparticles/PVA blended fibers. Once electrospun, a heat treatment process was employed to draw silver nanoparticles to the surface of the fibers where they can be the most effective. The use of PVA as a reducing agent allowed for a faster, simpler and more economical process than conventional methods. Silver has additionally been reduced *in situ* while electrospinning a number of other polymer mats.[146,147] The bactericidal efficacy of silver nanoparticle (AgNP)-coated electrospun fiber mats has been demonstrated for the first time by Schiffman et al.[111] Here, polysulfone (PSf) fiber mats were electrospun and then surface-modified using an oxygen plasma treatment, which allowed for the facile irreversible deposition of cationically charged PEI-AgNPs via electrostatic interactions. Time-dependent bacterial cytotoxicity studies indicate that the optimized PSf–AgNP mats exhibit a high level of inactivation against both *E. coli*, and *B. anthracis* and *S. aureus*. Although silver, like many other metals, displays excellent antibacterial properties, it can also cause irritation and bind to DNA preventing replication, both of which can hinder the healing process.

Inorganic materials, specifically titania, have been incorporated within electrospun bandages. Pure and iron (Fe)-doped titania nanofibers, spun from ceramic-polymer precursor solutions, demonstrated photoactivated antimicrobial activity against *E. coli*

using multiphoton infrared spectroscopy for three seconds.[148] Titania also exhibited antibacterial efficiency against *P. aeruginosa* and *S. aureus* when loaded into polyurethane (PU) electrospun fibers.[149] Testing performed in solution on titania mats doped with 0.4 and 1.6 μg/mL of zinc (Zn)[150] demonstrated an inhibition of *E. coli* and *S. aureus* growth, respectively.

Carbon-based nanomaterials are cytotoxic to bacteria.[151–153] Of this class of materials, single-walled carbon nanotubes (SWNTs) exhibit the highest toxicity and they can kill microbes on contact.[154,155] For the first time, Schiffman et al.[79] has demonstrated that even at a low weight percent loading of incorporated SWNTs, their antibacterial activity is retained. Four different weight percents of well-characterized, small diameter (0.8 nm) SWNTs were incorporated into electrospun polysulfone (PSf) mats. Electrospun PSf-SWNT mats were observed to be flexible and composed of continuous, cylindrical, and randomly oriented fibers. Loss of bacteria (*E. coli*) viability was observed to directly correlate to increased SWNT incorporation within the mat, ranging from 18 % for 0.1 wt% SWNTs to 76 % for 1.0 wt% SWNTs. Time-dependent bacterial cytotoxicity studies indicated that the antimicrobial action of the PSf-SWNT mats occurs after a short contact time of 15 minutes or less.

Alternatively, researchers have been inspired by nature for antibacterial agents. Plant-based antimicrobials, shikonin and alkannin, loaded into polymeric fibers demonstrated biocidal activity against both *S. aureus* and *E. coli*. The fiber mats additionally provided aid in both the inflammation and proliferative phases of wound healing.[156,157] Fusidic acid, a protein synthesis inhibitor derived from fungus, was blended into PLGA fibers to prevent the growth of bacteria.[50] The drug release from these fibers

was dependent on the severity of the wound. Both lightly and heavily infected wounds were treated via bioburden-triggered drug release of fusidic acid from PLGA mats. Lysostaphin, a cell lytic enzyme with specific bactericidal activity against *S. aureus*, was immobilized on the surface of cellulose, cellulose/chitosan, and cellulose/poly(methyl methacrylate) (PMMA) electrospun fiber mats.[158] In addition to cleaving the pentaglycine cross-bridges in the peptidoglycan layer of the cell walls of *S. aureus*, lysostaphin loaded nanofibers also displayed low toxicity towards keratinocytes, which are cells imperative in the proliferative phase of wound healing.

CHAPTER 2
DISSERTATION OBJECTIVES

2.1 Broad Scope

In this dissertation, nanofiber mats electrospun from biopolymers will be engineered for the prevention and treatment of bacterial infection or the removal of bacteria. Natural agents such as essential oils are an alternative class of antibiotics that have large potential, but are currently underexplored. I will be one of the first to incorporate essential oils into electrospun nanofiber mats. As an alternative method to preventing bacterial infections, I will assess the ability of electrospun nanofiber mats to uptake bacteria to potentially remove bacteria from hospital surfaces and open wounds. Thus, I can further the use of electrospun mats by quantifying their capacity to uptake bacteria.

In order to achieve these overarching goals, I will design and assemble an electrospinning apparatus which will provide a better understanding of the electrospinning process and allow for the learning and production of electrospun nanofibers from a variety of polymers. I will focus primarily on two natural polymers, chitosan and cellulose, due to their intrinsic biocompatibility and added functionalities such as hemostatic activity. In order to use minimally harsh solvents, polymeric derivatives of chitosan and cellulose will be considered. In addition to the polymers, I will optimize the process parameters, solvents, and method of antibacterial agent incorporation. I will characterize the chemistry and morphology of the as-spun soft materials utilizing a variety of instruments, including, scanning electron microscopy (SEM), solid and liquid state nuclear magnetic resonance (NMR), Fourier transform infrared spectroscopy (FTIR) and X-ray photoelectron spectroscopy (XPS). To demonstrate antibacterial efficacy, I will show the successful incorporation of an antibacterial agent into electrospun fibers along with the subsequent

release and/or antibacterial activity of the agent against bacteria. As another method to prevent infection, I will examine the ability of nanofiber mats to remove potentially detrimental bacteria. I will utilize florescence microscopy, confocal microscopy, plate counting and plate reading to examine the collection and inactivation of bacteria along with the minimum inhibitory concentration protocol to determine the necessary quantity of an agent to inhibit bacteria growth.

The specific objectives for each project are laid out in the following sections of this chapter. The following chapter provides a detailed list of chemicals and materials used throughout this dissertation. Subsequent chapters provide detailed methods, results, discussion, conclusion and future work for each objective. In each objective below, the specific subsequent chapter containing the work relevant to that objective is stated.

2.2 Utilization of Alternative Antibiotics

2.2.1 Incorporation of an Essential Oil into Electrospun Mats

Electrospinning hydrophilic nanofiber mats that deliver hydrophobic agents, such as, essential oils would enable the development of new therapeutic wound dressings or protective surface coatings that could reduce overall infection and potentially prevent the spread of resistance. We are specifically interested in chitosan-based electrospun nanofibers due to its unique antibacterial and hemostatic properties, which are advantageous to biomedical uses.

The use of essential oils, specifically cinnamaldehyde (CIN) as an alternative for commercial antibiotics is a promising solution as essential oils do not promote resistance.[17] Due to the volatility of essential oils, incorporation within a polymer is imperative for their wide spread use as an antibiotic.[159] While essential oils have been delivered via carrier-

solutions, polymer derivatives, or encapsulated in solid particles/films,[16,17,160–163] the incorporation of essential oils into a porous and permeable scaffold such as electrospun nanofiber mats has not yet been demonstrated.

To complete this objective: synthesis and characterization of novel antibacterial nanofiber mats composed of the renewable biopolymer, chitosan, and the essential oil, cinnamaldehyde (CIN), will yield a broad spectrum biocidal material. Based on previous research[142,164], one way to avoid the use of harsh organic solvents when synthesizing chitosan fibers is to add PEO to the system. Two primary methods will be used to incorporate the immiscible essential oil: chemical attachment to chitosan via a Schiff base reaction and physical incorporation into the precursor solution stabilized by chitosan. The two blocks of chitosan allow the biopolymer to act as a stabilizer.[165–168] Both the release of the CIN and the charged amino groups of chitosan will provide antibacterial activity. The corresponding work relevant to this objective can be found in Chapter 4.

2.2.2 Understanding Electrospinning of Hydrophobic Oils

In Section 2.2.1 (details in Chapter 4), we have demonstrated the ability to deliver a hydrophobic essential oil, CIN, from hydrophilic chitosan-based electrospun nanofiber mats. Investigating a synthetic "analogue" that will not chemically attach to chitosan provides insight into the parameters that enable the electrospinning of hydrophobic molecules stabilized by chitosan-containing solutions and provides a platform to broaden the potential biomedical applications of electrospun nanofiber mats.

Limited research has been conducted on electrospinning nanofibers from polymer solutions that contain immiscible phase liquids. Previously, only six studies have spun two immiscible phases by utilizing a surfactant to stabilize drops of one phase against

coalescence.[101,103,104,107–109] These previous works focus on emulsion electrospinning of water-soluble biological cargo and hydrophobic polymers showing the need to explore the incorporation of hydrophobic agents within electrospun fibers.

To complete this objective: a base solution containing chitosan and PEO dissolved in aqueous acetic acid will be utilized. As a function of chitosan molecular weight and degree of acetylation (DA), correlation between precursor solution properties such as chain entanglement (C_e) and nanofiber morphology will be investigated both with and without an essential oil. In addition to CIN, a second analogous essential oil, hydrocinnamic alcohol (H-CIN, Figure 20) will provide insight into the use of a Schiff base reaction as a means to incorporate essential oils as only CIN can react with chitosan to form a Schiff base.[169–172]

Collaboration with Schiffman lab member, Nate Birch for rheology will be essential in providing insight into precursor electrospinning properties. In particular, viscosity stress sweeps determined how the oils affects solution viscosity and C_e concentration. The corresponding work relevant to this objective is in Chapter 5.

2.2.3 Expansion of an Essential Oil to Spin Coated Thin Films

Translation of the incorporation and subsequent delivery of CIN using the biopolymer chitosan into thin films could broaden the use of these antibacterial agents to additional surfaces where a less porous, more rigid coating is ideal. Furthermore, films also provide an easier platform to study due to short fabrication time and could be used to understand how the introduction of a surfactant changes incorporation and subsequent release of the oil. Overall, chitosan coatings containing CIN could potentially be applied to a variety of indwelling medical devices to deliver therapeutic, hydrophobic components.

Currently, there is a poor understanding of the major factors that influence the incorporation, delivery, and stability of therapeutic hydrophobic components into spin-coated biopolymer thin films. To date, only one paper by Zodrow, Schiffman, and Elimelech[162] has demonstrated that thin films of poly(lactic-*co*-glycolic acid) (PLGA) with 0.1% and 1.0% essential oils demonstrate heightened antimicrobial properties. However, this work did not optimize film properties (t > 500 nm) or characterize the release profile of the essential oils from the films. Additionally, no work on optimizing the quantity of oil incorporated was done.

To complete this objective: chitosan films with and without CIN will be fabricated using spin-coating technique. Systematically, the influence of the surfactant Span®80 on the maximum amount of CIN incorporated into chitosan ultrathin films along with their subsequent release profiles will be determined. Film thickness in correlation to CIN concentration both with and without a surfactant will be investigated by holding the processing parameters and chitosan concentration constant. Release studies will provide insight into if the increased incorporation of CIN in the absence and presence of a surfactant results in subsequently higher release. This project will be done in collaboration with Schiffman undergraduate member, Nat Eagan. The corresponding work relevant to this objective can be found in Chapter 6.

2.3 Assessing the Uptake of Bacteria using Cellulose Electrospun Mats

2.3.1 Quantification of the Ability of Electrospun Mats to Uptake of Bacteria

Nanofiber mats hold potential in numerous applications that interface with microorganisms, specifically as a green platform technology to remove detrimental microorganisms from wounds, trap bacteria within a protective military textile, or

remediate contaminated water. Insight gained from the performance of nanofiber mats in collecting bacteria would benefit the use of nanofiber mats in bacterial applications. Additionally, a variety of antibacterial agents incorporated into materials need direct contact with the bacteria to be effective. Thus, the ability to quantify the uptake of bacteria is imperative to better measure a material's antibacterial efficacy.

A fundamental study that quantifies the transport of microorganisms into three-dimensional microenvironments, such as, nanofiber mats, has not yet been conducted. The only work related to this objective that has been previously conducted is by Abrigo et al.[173], who qualitatively reported that the average diameter of polystyrene fibers influences the ability of microbes to proliferate and colonize within nanofiber mats.

To complete this objective: microbial uptake capacity will be evaluated for three hydrophilic cellulose sorbents, a high surface area electrospun nanofiber mat, as well as two commercial products, a macrofibrous Fisherbrand fabric and an adsorptive Sartorius membrane. A method to quantifying the uptake bacteria into a material will be developed as it is essential to test the performance of nanofiber mats in comparison to other fibrous material. Changing bacterial culture parameters such as concentration, number of different strains and incubation time as well as nanofiber mat size will elucidate to the advantages and disadvantages of nanofiber mats for bacteria capture. In addition to *E. coli*, we studied the cellulose nanofiber mats uptake of two additional medically relevant and distinct microorganisms, Gram-negative *P. aeruginosa* PA01 and Gram-positive *S. aureus* MW2, to probe whether microorganism removal is bacterial specific or adhesive mechanism specific. Experiments will be carried out with an ICE REU student, Maureen Hoen.

Collaboration with Dr. David Ford and Raghu Thyagarajan will be essential in order to develop models to quantify the quasi-equilibrium and dynamic behavior of bacteria uptake using a three-dimensional nanofiber environment specifically because previous modeling of the transport of bacteria into porous media has been limited to soil components. [174–176] An adsorption coefficient (K_{eq}) that relates the concentration of cells in the sorbent to the concentration of cells remaining in solution will also be determined. The corresponding work relevant to this objective can be found in Chapter 7.

2.3.2 Impact of Electrospun Mats' Surface Properties on the Uptake of Bacteria

The physical and chemical properties of electrospun nanofiber mats have been readily modified by encapsulating and/or immobilizing bioactive species to elicit specific biological responses. For example, it has been reported that fiber diameter,[177] alignment[178,179] porosity,[180] and surface functionalization,[178,179,181] all significantly affect the ability of mammalian cells to adhere and proliferate. When considering the interface between nanofiber mats and microbiology, the majority of literature has focused on inhibiting the attachment and growth of bacterial cells[41] by encapsulating antibiotics[182,183] or nanoparticles[184] into the nanofiber mats.

However, probing the materials properties of electrospun nanofibers to elicit specific interacts with microorganisms is limited. Previously, Abrigo et al.[173] qualitatively explored the influence of fiber surface chemistry on microbial behavior by plasma polymerization of four monomers (acrylic acid, allylamine, 1,7-octadiene, and 1,8-cineole) onto the polystyrene fibers.[185] These limited reports demonstrate the potential of strategically tuning fiber diameter and surface chemistry to control bacterial behavior. However, further fundamental studies that quantify the interactions between nanofiber

mats and microorganisms are needed. However, quantifying microorganism behavior with nanofiber mat surface chemistry and hydrophilicity has not yet been demonstrated.

To complete this objective, the collection and inactivation of *E. coli* K12 as a function of nanofiber mat surface charge and hydrophilicity will be quantified. An ultra-thin layer of cationic or anionic polymer will be physically absorbed onto cellulose nanofibers hydrolyzed from electrospun cellulose acetate nanofibers. Changes in surface chemistry and hydrophilicity of the nanofiber mats will be a direct result of dip-coating different polyelectrolytes. Charcterization of the resultant nanofiber mats along with their ability to collect and inactivate bacteria will be performed. This project will be carried out with an ICE REU student, Michael Porter. The corresponding work relevant to this objective can be found in Chapter 8.

2.4. Utilization of Zeolites as Cargo Carriers with Electrospun Mats

2.4.1 Direct Attachment and Growth of Zeolites onto Electrospun Mats

Further modification of cellulose nanofiber mats by the addition of a cargo carrier that can be loaded and regenerated with an antibacterial agent would result in nanofiber mats capable of collecting high quantities of bacteria, inactivating the bacteria and then subsequent regeneration of the nanofiber mats for continued antibacterial efficacy.

Zeolites, microporous, crystalline solids with well-defined structures consisting of a three dimensional arrangement of tetrahedrally coordinated Si and Al (SiO_4^{4-} and AlO_4^{5-}), are optimal cargo carriers. Previous studies have electrospun fiber-zeolite composites by using an electrospinning solution to "carry" pre-synthesized zeolites through the electrospinning process.[186,187] Both of these studies utilized electrospinning to form nanofiber mats, which provided a greater surface area and potentially, accessibility to the

zeolites for toxin removal than if they encased their zeolites inside of solid polymer films. However, the zeolites were buried within the fibers, which would yield diffusion limitations especially if there was interest in unloading and reusing the composite materials.

Therefore to complete this objective: "large" zeolites will be grown on the surface of the cellulose nanofiber mats, as well as post-synthesis attachment of "small" and three-dimensionally ordered mesoporous-imprinted "meso" zeolites to the surface of the cellulose nanofiber mats to maximize the accessibility and functionality of the molecular carriers will be investigated. By controlling the morphology of the LTA zeolites from a nanometer to micrometer scale, as well as their surface area-to-volume ratio, the release profile of the cargo can be tailored.[188] Ag^+ ions will be the model agent loaded as Linde Type A (LTA) zeolites have low Si/Al ratio (Si/Al = 1), which enables them to have a high Ag^+ ion-exchange capability correlating to a strong antibacterial activity.[189–194]. The high cation exchange results from the substitution of Al^{3+} for Si^{4+} leading to a negatively charged aluminosilicate frameworks, which needs to be counterbalanced by the positive charges of cations, such as, Na^+, K^+, Ca^{2+}, Mg^{2+}, and Ag^+.

Collaboration with Dr. Wei Fan and Hong-Je Cho will be essential due to their expertise in the synthesis and characterization of zeolites. The corresponding work relevant to this objective can be found in Chapter 9.

CHAPTER 3
MATERIALS AND CHEMICALS

All compounds were used as received. Low molecular weight chitosan (LMW chitosan, poly(D-glucosamine), Mw=460,000 Da), medium molecular weight chitosan (MMW chitosan, poly(D-glucosamine), Mw=1,000,000 Da), poly(ethylene oxide) (PEO, Mw = 600,000 Da), cellulose acetate (M_w =30,000 Da), low molecular weight polydiallyldimethylammonium chloride (LMW pDADMAC, 20 wt% in water, Mw = 100–200 Da), poly(acrylic acid) (PAA, 35 wt% in water, Mw = 250,000 Da), glycerol (1, 2, 3 Propanetriol Glycerin, ≥99% (GC)), cinnamaldehyde (CIN, ≥ 93%, FG, Mw = 132.16 g/mol), hydrocinnamic alcohol (H-CIN, ≥ 98%, FCC, Mw= 136.19 g/mol), diiodomethane (≥99.0%), analytical reagent grade acetic acid (AA, ≥99.0%), sorbitan monooleate (Span®80, HLB=4.3), sodium chloride (NaCl), acetone, glutaraldehyde (GA, 50 wt% aqueous solution), calcofluor white stain, deuterium oxide (D_2O), deuterium acetic acid-d_4 (AA-d_4), sodium silicate solution (~26.5% SiO_2 and ~10.6% Na_2O), tetramethylammonium hydroxide (TMAOH, 25 wt%), silicic acid (98%), aluminum isopropoxide (98%), sodium nitrate ($NaNO_3$, 99%), sodium aluminate (~53% Al_2O_3 and ~42.5% Na_2O), potassium chloride (KCl), sodium phosphate dibasic anhydrous (Na_2HPO_4), phosphate buffered saline (PBS, 1× sterile biograde) and sodium phosphate monobasic anhydrous ($Na_2H_2PO_4$) were obtained from Sigma-Aldrich (St. Louis, MO). Sodium hydroxide (NaOH, 98%), sulfuric acid (H_2SO_4, 98%), ammonium hydroxide (NH_4OH, 29%) and Fisherbrand Cellulose Paper (09-801C, Fisherbrand control) was obtained from Fisher Scientific (Fair Lawn, NJ). A commercially available regenerated cellulose adsorptive membrane (1401213, Sartorius control) was purchased from Sartorius Stedim Biotech, Germany. Difco Luria-Bertani (LB) broth was purchased

from BD Life Sciences (Franklin Lakes, NJ). Propidium iodide (PI, 1.0 mg/mL in water) and 4′,6-diamidino-2-phenylindole (DAPI) were purchased from Invitrogen (Carlsbad, CA). SYTO 9 green fluorescent nucleic acid stain (S34854, 5 mM solution in dimethyl sulfoxide) was purchased from Life Technologies (Grand Island, NY). Deionized (DI) water was obtained from a Barnstead Nanopure Infinity water purification system (Thermo Fisher Scientific, Waltham, MA).

CHAPTER 4
BACTERIAL INACTIVATION VIA CHITOSAN/PEO/CIN NANOFIBERS

Adapted from: Rieger, K.A.; Schiffman, J.D., Electrospinning an essential oil: Cinnamaldehyde enhances the antimicrobial efficacy of chitosan/poly(ethylene oxide) nanofibers. *Carbohydrate Polymers*, 2014, 113, 561-568.

4.1 Summary

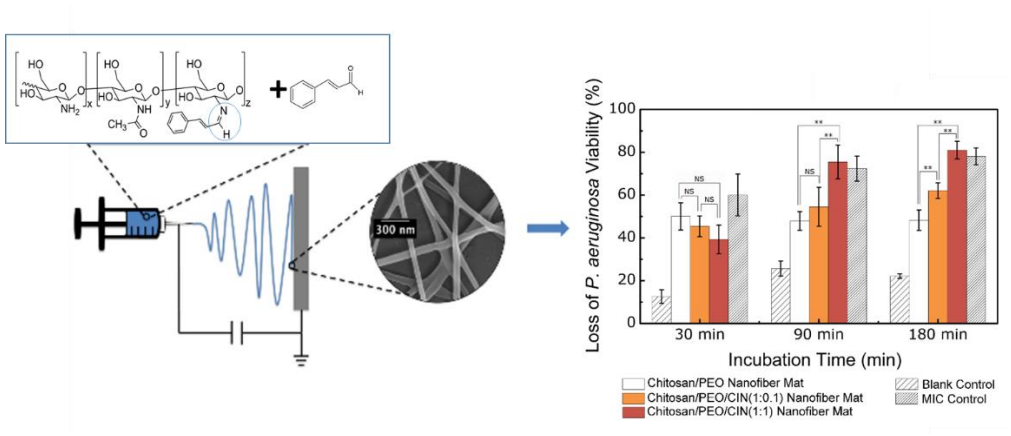

Figure 12**:** Nanofiber mats composed of chitosan/PEO/CIN inactivate microorganisms via environmentally friendly mechanisms, which do not promote antibiotic resistance.

Due to the persistent spread of antibiotic resistance, commercial antibiotic treatments are proving ineffective. CIN, a volatile essential oil, eradicates pathogens non-specifically. However, the ability to incorporate essential oils into nanofiber mats has not yet been demonstrated, and, only six studies have electrospun two immiscible phases. Here, CIN was incorporated into chitosan/PEO solutions at total polymer:oil (p:o) mass ratios of 1:0.1 and 1:1 that were successfully electrospun into mats with ~50 nm fiber diameters, Figure 12. Solid-state NMR results corroborated with release studies wherein the chitosan/PEO/CIN(1:1) mats released a statistically higher amount of CIN-liquid (545% more) and CIN-vapor (279% more) than the chitosan/PEO/CIN(1:0.1) mats. In time

dependent cytotoxicity studies, the intrinsic antibacterial activity of chitosan along with the quick release of CIN enabled high inactivation rates against *E. coli* and *P. aeruginosa*. For the first time we have demonstrated chitosan/PEO/CIN nanofiber mats can serve as CIN delivery vehicles that potentially eradicating pseudomonas infections.

4.2 Methods

4.2.1 Chitosan/PEO/CIN Synthesis and Quantification

A 1:1 ratio of chitosan to PEO (0.5 g:0.5 g) in 0.5 M AA (20 mL) corresponding to a 5.0 w/v% solution was mixed for 24 hr at 20 rpm using an Arma-Rotator A-1 (Bethesda, MA). Various amounts of CIN (0 mL, 0.1 mL, and 1.0 mL corresponding to 1:0, 1:0.1, and 1:1 p:o mass ratios, respectively) were added to the pH 4 solution and allowed to mix for an additional 24 hr at which point, the solution changed from transparent to white. The pH of solutions throughout this process (addition of CIN and mixing) were monitored and it was noted that they remained at a pH of 4. Proton nuclear magnetic resonance (^{1}H NMR) (Bruker Avance 400) along with SpinWorks3, an NMR analysis software, was employed to quantitatively determine the degree of acetylation (DA) and degree of substitution (DS) of the chitosan. Solutions for ^{1}H NMR consisted of p:o mass ratios of 1:0, 1:0.1 and 1:1 of chitosan/CIN using 2.5 w/v% chitosan dissolved in 0.5 M AA-d4 (500 μL).

4.2.2 Chitosan/PEO/CIN Nanofiber Mat Fabrication

Each chitosan/PEO/CIN solution was loaded into a 5 mL Luer-Lock tip syringe capped with a Precision Glide 18 gauge needle (Becton, Dickinson & Co. Franklin Lakes, NJ), which was secured to a PHD Ultra syringe pump (Harvard Apparatus, Plymouth Meeting, PA). Alligator clips were used to connect the positive anode of a high-voltage supply (Gamma High Voltage Research Inc., Ormond Beach, FL) to the needle and the

negative anode to a copper plate wrapped in aluminum foil. A constant feed rate of 60 μL/min, an applied voltage of 25 kV, and a separation distance of 120, 160, and 140 mm were used to spin chitosan/PEO solutions prepared with CIN at p:o mass ratios of 1:0, 1:0.1, and 1:1, respectively. The assembled electrospinning apparatus was housed in an environmental chamber (CleaTech, Santa Ana, CA) with a desiccant unit (Drierite, Xenia, OH) to maintain a temperature of 22 ± 1 ºC and a relative humidity of 24-28%. All nanofiber mats used in release and bacterial studies were spun for 1 hr. As-spun chitosan/PEO/CIN mats were crosslinked using GA vapor as previously described.[139] Briefly, mats were placed in a vapor chamber (122 mm × 98 mm × 78 mm, Biohit Inc, Neptune, NJ) containing 1.0 mL of GA liquid. At room temperature (23 °C), the GA liquid vaporized and was allowed to crosslink the fibers for 4 hr. This ensured the chemical stability of the nanofiber mats for release studies and antibacterial evaluation.

4.2.3 Chitosan/PEO/CIN Nanofiber Mat Characterization

Micrographs were acquired using a FEI-Magellan 400 scanning electron microscope (SEM). A sputter coating machine (Gatan high resolution ion beam coater model 681) was used to coat samples for 4 min with platinum. Fiber diameter distribution was determined by Image J 1.45 software (NIH, Bethesda, MD) by measuring 50 random fibers from 5 micrographs. By following the parameters suggested by previous literature[169,195], carbon-13 NMR (^{13}C NMR, DSX300) and SpinWorks3 were employed to confirm the presence of chitosan, PEO, and CIN within the as-spun mats. Approximately 50 mg of chitosan/PEO/CIN (1:0, 1:0.1, and 1:1) nanofiber mat, as well as a 100 mg powder sample of chitosan/PEO at a 1:1 mass ratio were analyzed.

Changes in surface hydrophobicity were evaluated using a drop shape analysis system (model DSA 100, KRÜSS, Hamburg, Germany). A drop (5 μL DI water) was advanced at 25 μL/min on the surface of a film and then subsequently receded at the same rate to obtain the advance and receding contact angles, respectively. Contact angle hysteresis defined as the difference between the advancing and receding contact angles was also determined.[196] Nanofiber mats were tested in triplicate.

4.2.4 Liquid and Vapor State Release of CIN from Nanofiber Mat

The release characteristics of CIN as a liquid (CIN-liquid) and as a vapor (CIN-vapor) from the nanofiber mats were quantified at times relevant to antibacterial activity experiments. Consistent chitosan/PEO/CIN nanofiber mats (10 mm × 20 mm) were placed into 1.5 mL centrifuge tubes containing 1.0 mL of an isotonic solution (0.9% NaCl, pH 5.7) with virtually no headspace. The samples were maintained at 37 °C and shaken at 100 rpm. As a function of time, 1.0 mL of the isotonic solution was removed for analysis. The CIN amount present in the isotonic solution was determined using UV-Visible spectroscopy (UV-Vis, Agilent Diode Array) at an absorbance of 293 nm, as previously reported for CIN.[197,198] The solution was placed back into the sample to maintain the same gradient flux.

As a function of time, quantification of the CIN-vapor released from the mat into the headspace of the vial was performed using gas chromatography, GC (Agilent/HP 6890 equipped with Flame Ionization Detector FID).[199] Nanofiber mats (10 mm × 20 mm) were placed in 10 mL of isotonic solution with 10 mL of headspace in the vial for the CIN-vapor to accumulate. The sealed vials were kept at 37 °C and shaken at 100 rpm. Manual samples containing 1 mL of gas were injected into the GC at 30, 90, and 180 min intervals. Standard

calibration curves were determined for both UV-Vis and GC to quantify the amount of CIN in each sample. Chitosan/PEO mats were used as controls.

4.2.5 Antibacterial Activity of Chitosan, CIN and Chitosan/CIN

Minimum inhibitory concentration (MIC), was determined for chitosan, CIN and chitosan/CIN at mass ratios of 1:0.1 and 1:1 based on a previously outlined procedure [200]. An overnight culture of *E. coli* K12 and *P. aeruginosa* PA01, purchased from Leibniz Institute DSMZ (Germany) was prepared in Mueller Hinton Broth (MHB, Sigma Aldrich). A Fisherbrand polypropylene 96 well plate was filled with an increasing concentration gradient of the testing solutions, along with a Gentamycin antibiotic control. The starting chitosan/CIN solutions (1:0.1 and 1:1 p:o mass ratios) each had 0.12 v/v% and 0.25 v/v% CIN in each solution, respectively. The overall concentrations of each solution started at 12.5 µg/ml and doubled at each well until it reached 6400 µg/ml. The Gentamycin control started from 0.03 µg/mL and doubled until 16 µg/mL. Two columns of the well plate remained controls: the growth control contained MHB and bacteria and the sterile control contained only MHB. After the well plate incubated (37 °C) for 20 hr, the bacteria concentrations in each well were measured using a BioTek ELx800 Absorbance Reader at an absorbance of 600 nm.

4.2.6 Evaluation of Antibacterial Activity of Electrospun Mat

The bacteria were grown in LB at 37 °C and harvested at a cell concentration of 10^8 cells/mL. To remove residual macromolecules and other growth medium constituents, cells were washed twice and then resuspended in an isotonic solution (0.9% NaCl, pH 5.7). Two control samples were run in parallel to each experiment, (i) no nanofiber mat and (ii)

a chitosan/PEO nanofiber mat to determine the contribution of chitosan towards microbial inactivation. No external forces were applied during incubation.

The contact-killing capacity of nanofiber mats was assayed according to a modified ASTM E2149-01 shake flask method.[201] Nanofiber mats (10 mm × 20 mm) were placed into culture tubes (16 mm × 125 mm) along with 4 mL suspensions of *E. coli* K12 or *P. aeruginosa* PA01 (5×10^6 cells/mL) in an isotonic solution. The suspensions were shaken at 200 rpm in an orbital shaker maintained at 37 °C. At 30, 90, and 180 min, 100 μL were pipetted out from the tubes and serial dilutions were plated onto LB plates using the spread plate method.[29,201,202] After 24 hr incubation on agar plates, the number of viable bacteria was counted. The number of viable cells was multiplied by the dilution factor and expressed as the mean colony forming unit (CFU) per mL. The percent reduction of bacteria resulting from contact with the nanofiber mats was determined using Equation 1, where A represents the mean log10 density of bacteria for the flask containing the treated substrate after the specified contact time and B represents the untreated substrate after the specified contact time.

Equation 1

$$\text{Reduction of Bacteria (\%)} = \frac{B-A}{B} \times 100$$

Viability loss was also determined using a previously described fluorescence assay.[111] Electrospun mats (20 mm × 10 mm) were placed at the bottom of 35 mm × 10 mm petri dishes (Becton, Dickinson & Co., Franklin Lakes, NJ) to which the cells (10^7 cells/mL) resuspended in an isotonic solution were added and diluted by a factor of 2. The cells were incubated at 37 °C for various times (30, 90, and 180 min). At each time point, cells were stained in the dark with PI (excitation/emission at 535 nm/617 nm) for 15 min and then

counter-stained with DAPI (excitation/emission at 358 nm/461 nm). Fluorescence images were acquired to detect the cells utilizing an epifluorescence microscope (Olympus) with a Chroma cube filter. Five representative images were taken at 20× magnification at various locations for each specimen. Dead cells and the total number of cells were determined by direct cell counting. The loss of viability (percentage of dead cells) was determined from the ratio of the number of cells stained with PI divided by the number of cells stained with PI plus DAPI, Equation 2 .

Equation 2

$$Loss\ of\ viability\ (\%) = \frac{Number\ of\ dead\ cells}{Number\ of\ total\ cells} \times 100$$

Throughout the Results and Discussion section, all statistical differences were determined using an unpaired t-test with values of $p \leq 0.05$ considered to be statistically significant.

4.3 Results and Discussion

4.3.1 Chitosan/CIN Characteristics

Using ^{1}H NMR, the DA of chitosan was determined to be 13%[203–205]. We blended all chitosan-based solutions in aqueous AA maintained at a pH value of 4, which is known to enhance Schiff base reactions[170,206]. The degree of substitution (DS)—the ratio of amines reacted with CIN over the total amount of amines[207] was characterized using the ^{1}H NMR peaks at 9.0 ppm and 9.5 ppm[208], which correspond to the presence of unreacted and reacted CIN, respectively (Figure 13). DS values were calculated from the ratio of the integrated resonances of reacted CIN (9.25–9.6 ppm) over glucosamine residues on chitosan (2.7–4.4 ppm). It was determined that chitosan/CIN(1:0.1 and 1:1) solutions yielded comparable DS values, 15% and 16%, respectively. While chitosan initially had 87% free amines, the chitosan/CIN(1:0.1 and 1:1) derivative solutions had ~70% free amines remaining.

Importantly, the ^{1}H NMR spectra revealed that unreacted CIN is also present indicating that chitosan is physically entrapping the volatile oil. The chitosan/CIN(1:0.1) derivative contains 28% unreacted CIN, while the chitosan/CIN(1:1) derivative contains a statistically higher, 89% unreacted CIN.

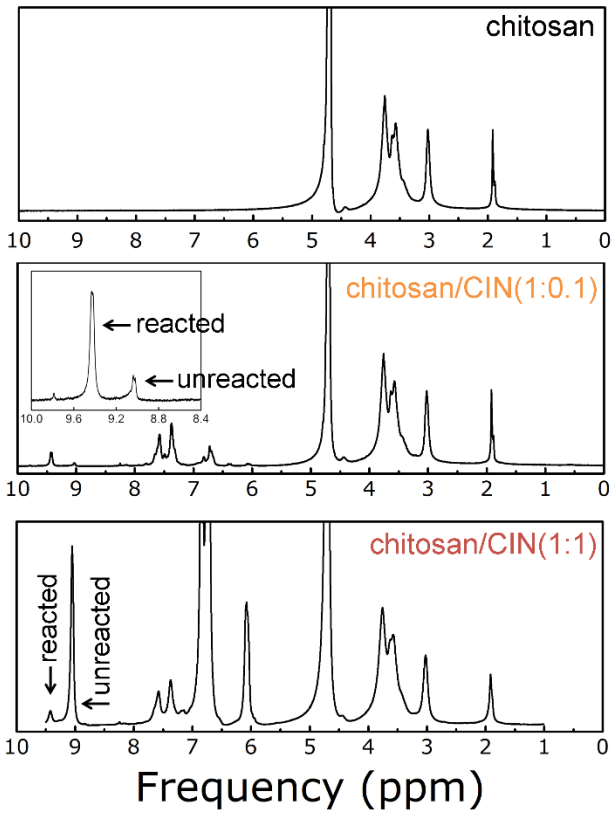

Figure 13: The ^{1}H NMR spectra of the chitosan derivatives synthesized with CIN (top to bottom) at p:o mass ratios of 1:0, 1:0.1, and 1:1 were determined to have 0, 15, and 16% degrees of substitution (DS), respectively. In addition to the CIN that is conjugated to the backbone of chitosan, the spectra revealed that unreacted CIN is also present. The enlarged inset plot is provided to clarify that reacted and unreacted CIN is present in the chitosan/CIN solution at a 1:0.1 p:o mass ratio. PEO was not included in the NMR solutions.

4.3.2 Chitosan/PEO/CIN Nanofiber Mat Physical Characteristics

Chitosan/PEO/CIN nanofiber mats were successfully electrospun from a 5.0 w/v% solution containing an equal mass ratio of the two polymers. As displayed on Figure 14A, the chitosan/PEO nanofiber mats were composed of continuous, fine, cylindrical fibers,

consistent with the morphology previously reported[142,209]. Nanofiber mats were also effectively electrospun from solutions containing the two different p:o mass ratios, chitosan/PEO/CIN(1:0.1 and 1:1) with the polymers at a 1:1 mass ratio (Figure 14C and E). Average fiber diameters (n = 50) for the electrospun chitosan/PEO/CIN(1:0, 1:0.1, and 1:1) nanofiber mats are displayed in Figure 14. The chitosan/PEO/CIN(1:0, 1:0.1, and 1:1) nanofiber mats had average fiber diameters of 55 ± 8 nm, 52 ± 9 nm, and 38 ± 9 nm, respectively, which was similar to the chitosan/PEO nanofiber mats previously spun in literature. An unpaired t-test between the chitosan/PEO and the chitosan/PEO/CIN(1:0.1 and 1:1) mats determined that the variation in fiber diameter was not statistically significant. Simply put, on average, by slight modification to our electrospinning parameters, we were able to produce fiber diameters that did not change due to the presence of CIN.

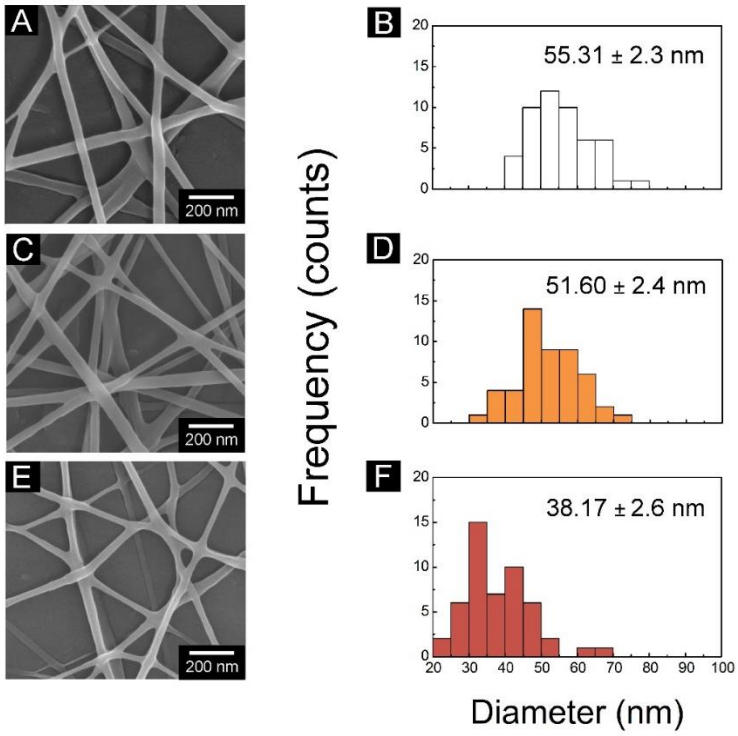

Figure 14: Chitosan/PEO/CIN nanofiber mats' at p:o mass ratios of (A, B) 1:0, (C, D) 1:0.1, and (E, F) 1:1 morphology and fiber diameter distribution are shown. SEM micrographs all have a 200 nm scale bar. Fiber diameter distribution determined using *ImageJ* software. The average fiber diameter and standard deviation (n=50) are also displayed and are statistically equivalent based on an unpaired student *t*-test.

It is important to note that attempts to electrospin solutions containing only PEO and CIN (no chitosan) phase separated: a homogeneous solution appropriate for electrospinning could not be obtained. This suggests that in our system the chitosan is (i) chemically reacting with CIN[170,206] as observed in ^{1}H NMR and (ii) acts as a stabilizer[165,166,168] to physically incorporate the CIN into the precurser solution. In order for release studies and antibacterial testing to be conducted, increased chemical stability of chitosan/PEO/CIN(1:0, 1:0.1, and 1:1) nanofiber mats was achieved using a slightly modified glutaraldehyde crosslinking protocol[210]. The carbonyl groups of glutaraldehyde can form a Schiff base reaction with the free amino groups at the C-2 position of chitosan and an acetalization reaction with the hydroxyl groups at the C-6 position of chitosan[210].

Based on our ^{1}H NMR results, all chitosan/PEO/CIN(1:0, 1:0.1, and 1:1) derivative solutions have an abundant quantity of free amine groups ranging from 84–71% for both crosslinking and antibacterial activity. After crosslinking for 4 h, the average fiber diameter for the crosslinked chitosan/PEO/CIN(1:0, 1:0.1, and 1:1) nanofiber mats were statistically the same as the as-spun chitosan/PEO/CIN(1:0, 1:0.1, and 1:1) mats: 53 ± 8 nm, 56 ± 11 nm, and 41 ± 6 nm, respectively. SEM micrographs of the crosslinked nanofiber mats 72 h post-submersion in acidic, neutral, and basic solutions (not shown) confirmed that the nanofibrous morphology of the mats was retained. Additionally, after the release studies and antibacterial evaluation described below, acquired SEM micrographs confirmed that the nanofiber morphology remained intact (not shown).

Advancing and receding water contact angle measurements for the resultant nanofiber mats are displayed in Table 1. All mats are hydrophilic which would be expected due to the polymer selection and quantity of polymer vs essential oil. Chitosan/PEO/CIN (1:0 and 1:0.1) nanofiber mats have statistically higher advancing and receding contact angles than chitosan/PEO/CIN(1:1) nanofiber mats suggesting that the nanofiber mats containing the most CIN are most hydrophilic. One potential explanation is that as more CIN is added, the resulting polymer/essential oil composition on the surface of the nanofiber is altered. Thus, the addition of more CIN results in a more hydrophobic core with a more hydrophilic shell is suggested by the contact angle data.

Table 1: DI Water Advancing and Receding Contact Angle of Nanofiber Mats

Polymer/Oil (p:o[1] mass ratio)	**Advancing Contact Angle (°)**	**Receding Contact Angle (°)**
Chitosan/PEO(1:0)	28.1±4.4	15.2±5.7
Chitosan/PEO/CIN (1:0.1)	28.6±3.0	16.1±3.3
Chitosan/PEO/CIN (1:1)	23±2.45	12.3±4.2

1 p:o represents polymer:oil mass ratio

4.3.3 Chitosan/PEO/CIN Nanofiber Mat Chemical Characteristics

To qualitatively ensure that attached and unattached CIN were present in the as-spun nanofiber mats, solid state ^{13}C NMR was conducted, Figure 15. The spectra suggests that due to the presence of CIN (i) the height of the aromatic peak[195] is greater for chitosan/PEO/CIN(1:1) nanofiber mats than chitosan/PEO/CIN(1:0.1) nanofiber mats, while (ii) the imine peak at 170 ppm[195] is smaller than that observed for the aromatic peaks. This corroborates the solution NMR data: the majority of CIN within the nanofiber mat is physically entrapped, unreacted CIN. These peaks are absent from the control spectra acquired on chitosan/PEO nanofiber mats and chitosan:PEO powder. "Control" chitosan/PEO nanofiber mats electrospun from the same solvent system with only unreacted CIN could not be obtained as the Schiff base is pH dependent. Further increasing the pH (beyond where Schiff bases are encouraged) resulted in chitosan that was not fully dissolved.

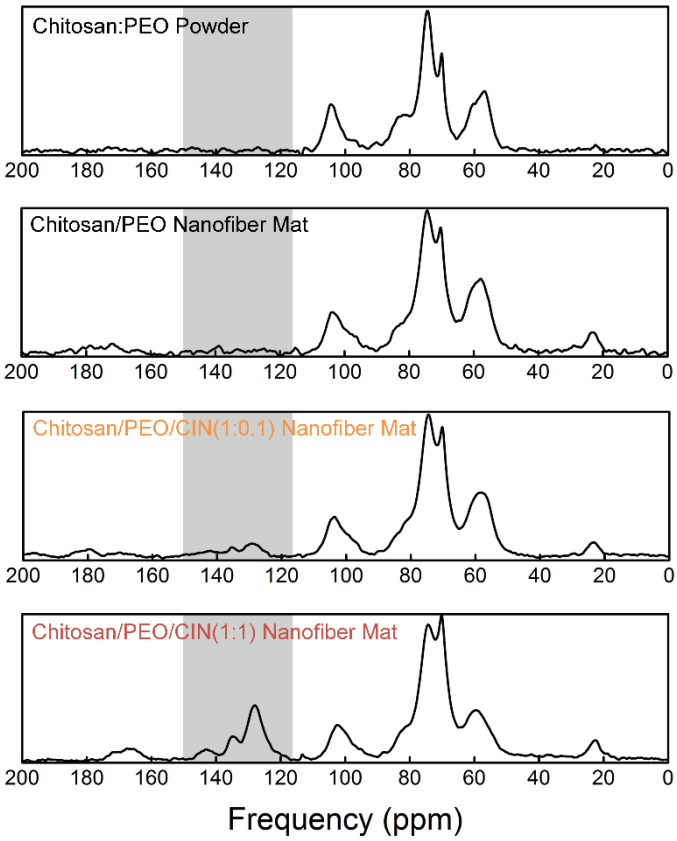

Figure 15: Displayed is the solid state ^{13}C NMR spectra of (top-to-bottom) chitosan:PEO powder (control) and electrospun chitosan/PEO/CIN(1:0, 1:0.1, and 1:1) nanofiber mats. Peaks between 120 and 150, as well as at 170 ppm confirm the presence of CIN in the chitosan/PEO/CIN(1:0.1 and 1:1) nanofiber mats.

4.3.4 Release Characteristics of Chitosan/PEO/CIN Nanofiber Mats

The release characteristics of CIN-liquid and CIN-vapor from the nanofiber mats were quantified using UV–vis, Figure 16A and B, respectively. Experiments were conducted at physiological temperature (37 ◦C) at times relevant to antibacterial activity tests. Preliminary experiments determined that using small, 1.5 mL vials, minimized the vapor space and kept the CIN-liquid highly concentrated, thus enabling the acquisition of the most accurate UV–vis data. Figure 16A displays that as a function of time, the release of CIN continues to gradually increase from the chitosan/PEO/CIN(1:0.1 and 1:1) nanofiber mats. After 15 min, the chitosan/PEO/CIN(1:0.1 and 1:1) nanofiber mats

demonstrated an initial CIN-liquid release of $2.0 \times 10^{-3} \pm 3 \times 10^{-4}$ g and $1.9 \times 10^{-3} \pm 1 \times 10^{-4}$ g, respectively. At longer times (90 and 180 min), the amount of CIN released started to level off indicating that equilibrium has been reached[211,212]. Specifically, CIN-liquid release reached quantities of $2.7 \times 10^{-3} \pm 9 \times 10^{-4}$ g and $1.5 \times 10^{-2} \pm 4 \times 10^{-3}$ g after 180 min for the chitosan/PEO/CIN(1:0.1 and 1:1) nanofiber mats, respectively. Between 30 and 180 min, the cumulative amount of CIN-liquid released from the chitosan/PEO/CIN(1:1) nanofiber mats is statistically higher than the CIN-liquid released from the chitosan/PEO/CIN(1:0.1) nanofiber mats. Overall, 545% more CIN was released from the mats spun with a higher CIN concentration.

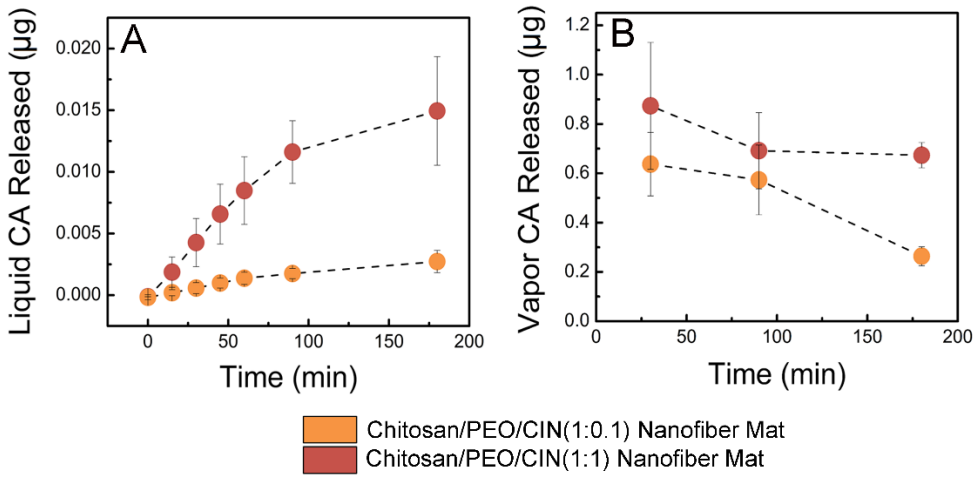

Figure 16: (A) The cumulative quantity of CA-liquid released from chitosan/PEO/CIN(1:0.1 and 1:1) nanofiber mats was determined through UV–vis spectroscopy.(B) Using gas chromatography GC, the amount of CA-vapor released from the chitosan/PEO/CIN(1:0.1 and 1:1) nanofiber mats was determined. Error bars indicate one standard deviation.

In addition to the CIN-liquid release, due to the volatility of the essential oil, it is likely that a significant amount of CIN-vapor will occupy the surrounding air space[159]. GC was employed to quantify the CIN-vapor released into the vial headspace (Figure 16B). In contrast to the UV–vis, larger vials (20 mL) were used for accurate GC data to gain more

air space to increase the sampling volume. From samples acquired after 30 min it was determined that 0.6 ± 0.1 g of CIN-vapor was released from the chitosan/PEO/CIN(1:0.1) nanofiber mats and that a statistically equivalent amount of CIN-vapor, 0.9 ± 0.3 g, was released from the chitosan/PEO/CIN(1:1) nanofiber mats. At 90 min, the CIN-vapor released from chitosan/PEO/CIN(1:0.1) (0.6 ± 0.1 g) and from the chitosan/PEO/CIN(1:1) (0.7 ± 0.2 g) nanofiber mats were statistically equivalent. After 180 min, the quantity of CIN-vapor released from the chitosan/PEO/CIN(1:1) nanofiber mats was statistically higher than the quantity released from the chitosan/PEO/CIN(1:0.1) mats, 0.7 ± 0.1 g versus 0.3 ± 0.1 g. Statistically, the same quantity of CIN occupies the vapor headspace at all three time points investigated for each chitosan/PEO/CIN(1:0.1 and 1:1) nanofiber mats, thus indicating that the CIN-vapor releases quickly. The chitosan/PEO/CIN(1:1) nanofiber mats released 279% more CIN-vapor after 180 min than chitosan/PEO/CIN(1:0.1) nanofiber mats. The use of different collection set-ups for liquid and vapor release means that we cannot plot a reliable total release curve. However, we can state that more vapor-CIN is released than liquid-CIN, which further emphasizes the importance of characterizing the vapor phase release even though most previous studies only quantify release into the liquid phase[197].

Literature reports three potential mechanisms for release: swelling-controlled, diffusion-controlled, and reaction-controlled, all of which are highly pH dependent[211,212]. The governing mechanism of release depends on whether the CIN is attached or unattached to the chitosan. Solid-state ^{13}C NMR informs that the majority of CIN in our chitosan/PEO/CIN(1:0.1 and 1:1) nanofiber mats is physically incorporated and therefore swelling controlled. Unreacted CIN is likely to be released by the swelling of the chitosan

and PEO once the nanofiber mats are submerged in the isotonic solution. Initial release testing at a range of pHs indicated that minimal release of CIN occurred in basic conditions (pH of 8 or greater) where the nanofibers would have minimal swelling (not shown). Based on previous literature, we hypothesize that the CIN diffuses through the mixed polymer network following Fickian diffusion[213].

4.3.5 Minimum Inhibitory Concentrations of Chitosan, Chitosan/CIN and CIN

In Table 2, the minimum concentrations to inhibit the grow of *E. coli* K12 and *P. aeruginosa* PA01 are shown for chitosan, chitosan/CIN(1:0.1 and 1:1) and CIN. The inactivation concentrations shown are after a 24 hr bacteria/antibacterial agent incubation.

Table 2: Minimum Inhibitory Concentrations of Chitosan, Chitosan/CIN and CIN

Polymer/Oil (p:o[1] mass ratio)	***E. coli* K12 (μg/mL)**	***P. aeruginosa* PA01 (μg/mL)**
Chitosan(1:0)	800	3200
Chitosan/CIN (1:0.1)	1600	3200
Chitosan/ CIN (1:1)	1600	3200
CIN	400	400

1 p:o represents polymer:oil mass ratio

The concentration of chitosan needed to be effective against was *P. aeruginosa* PA01 4 × higher than the concentration needed for *E. coli* K12. Additionally, once CIN was introduced, the same concentration of 3200 μg/mL of chitosan/CIN(1:0.1 and 1:1) was needed for *P. aeruginosa* PA01. This would imply the decreased in the amine groups of chitosan due to the attachment of CIN is accounted for by the increase in CIN leading to the same ability to inactive *P. aeruginosa* PA01. However, 2 × increase in concentration is needed after the addition of CIN to inactivate *E. coli* K12 implying that the added CIN is not as effective against *E. coli* K12 as the amine groups on chitosan. Lastly, the

concentration of CIN needed to inactivate *E. coli* K12 or *P. aeruginosa* PA01 is the same (400 µg/mL) suggesting that if used alone, a certain quantity of CIN is needed before being effective against either bacteria strain.

4.3.6 Antibacterial Activity of Nanofiber Mats against *E. coli*

After only 30 min of nanofiber-bacteria contact, a high level of inactivation against *E. coli* is achieved, Figure 17. Statistically, all three of our nanofiber mats demonstrated a complete inactivation at all incubation times evaluated (30, 90, and 180 min). Observed inactivation values for mats incubated for 180 min were at the limit of the accuracy or range of the bacterial viability assay. As displayed on Figure 17, any value greater than 99% must be considered only as >99%[111]. These results are consistent with previous research[209], where nanofiber mats electrospun from a 5.0 wt% solution of chitosan/PEO (1/1) exhibited increased cytotoxicity against *E. coli* for 4 h. A low, statistically smaller loss of viability occurred in the blank control experiment (no nanofiber mat or antibacterial agent present).

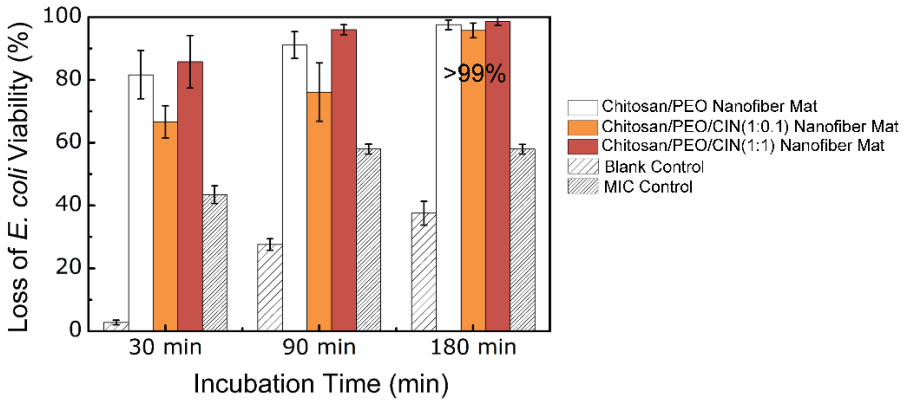

Figure 17: A complete inactivation of *E. coli* was achieved by chitosan/PEO/CIN(1:0, 1:0.1, and 1:1) nanofiber mats at all incubation times. The MIC control (~400 µg/mL CIN) was always statistically higher than the blank control (no nanofiber mat). Experiments were performed in triplicates and error bars indicate one standard error.

The MIC control consisted of 3 mM (396 µg/mL) of CIN solution and no nanofiber mat. It allows for a comparison of the effect of CIN has on *E. coli* inactivation over time.[162]

The MIC control statistically inactivated more *E. coli* than the blank control confirming previous reports that CIN displays antibacterial activity against *E. coli*. Interestingly, after 30 and 180 min, the MIC control displayed a statistically lower level of antibacterial activity than chitosan/PEO/CIN(1:0, 1:0.1 and 1:1) nanofiber mats. At 90 min, the MIC control was statistically equivalent to the chitosan/PEO/CIN(1:0.1) nanofiber mats. The MIC results (Table 2) demonstrate the necessary concentration to completely inactivate *E. coli* after 24 hr. These results suggest that at shorter times, CIN alone may be less effective than the nanofiber mats containing both chitosan and CIN. The chitosan in the chitosan/PEO nanofiber mats offer positively charged free amine groups, which damages the bacterial membrane's ability to function as a barrier[214–218].

Chitosan/PEO/CIN(1:0.1 and 1:1) nanofiber mats offer an additional mechanism to inactivate bacteria: direct contact between microbes and the CIN[219]. While nanofiber mats containing attached CIN offer less free amines to interact with microbes, the statistical equivalence of antibacterial efficacy achieved by all three chitosan/PEO/CIN nanofiber systems confirms that this combination of chitosan and CIN killing mechanisms, a complete inactivation of *E. coli* can be achieved.

4.3.7 Antibacterial Activity of Nanofiber Mats against *P. aeruginosa*

The efficacy of any chitosan-based nanofiber mats against *P. aeruginosa* has not yet been reported. Notably, fewer antibiotics are effective against this strain of microbe[7]. Figure 18 displays that after 30 min, statistically equal levels of *P. aeruginosa* inactivation were demonstrated by all three nanofiber mats. An initial efficacy of 50 ± 6% against *P. aeruginosa* was demonstrated by the chitosan/PEO nanofiber mats confirming the strong intrinsic cytotoxicity of chitosan, which was statistically equivalent to the CIN MIC

control. Once 90 min of incubation was reached, the chitosan/PEO/CIN(1:0.1) nanofiber mats achieved a higher rate of inactivation (76 ± 8%) compared to the chitosan/PEO/CIN(1:0 and 1:0.1) nanofiber mats (48 ± 4% and 54 ± 9%). The higher antibacterial activity of chitosan/PEO/CIN(1:1) nanofiber mats is most likely due to the higher release of CIN. The MIC control at 90 min inactivated *P. aeruginosa* at a statistically equivalent level as the chitosan/PEO/CIN(1:0.1 and 1:1) nanofiber mats, thus validating the contribution of CIN to the increased antibacterial activity exhibited by the chitosan/PEO/CIN(1:1) nanofiber mats. After 180 min, chitosan/PEO/CIN(1:0, 1:0.1, and 1:1) nanofiber mats exhibited statistically different rates of inactivation. Inactivation of *P. aeruginosa* increased with increasing CIN content. These results are in agreement with the MIC values found in Table 2, where higher concentrations are needed of chitosan to inactivate *P. aeruginosa* over *E. coli*. The chitosan/PEO/CIN(1:0, 1:0.1, and 1:1) nanofiber mats inactivated 48 ± 5%,62 ± 4%, and 81 ± 4% of *P. aeruginosa*, respectively. The CIN MIC control (at 180 min) statistically inactivated the same level of bacteria as the chitosan/PEO/CIN(1:1) nanofiber mats. The statistically higher inactivation parallels the statistical increase in CIN release (liquid and vapor) from the nanofiber mats over the 180 min (Figure 16). Additionally, this result would imply CIN has a faster inactivation time against *P. aeruginosa* over *E. coli* because the MIC values needed to inactivate each bacteria type over 24 hr are both 400 µg/mL, Table 2. At all times, the blank control exhibited a statistically lower loss of viability. While literature supports that higher concentrations of CIN released as vapor should increase microbial inactivation,[220] there is a limit to the desired CIN incorporation. The amount of CIN within our nanofiber mats is

under the level toxic to mammalian cells yet high enough to achieve a strong level of *P. aeruginosa* inactivation.

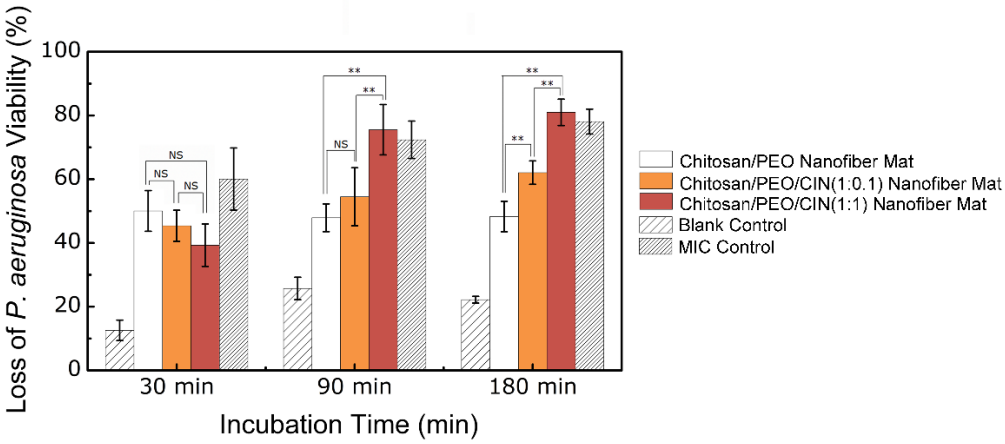

Figure 18: The loss of *P. aeruginosa* viability as a function of incubation time for chitosan/PEO/CIN(1:0, 1:0.1, and 1:1) nanofiber mats. Also displayed is the blank control (no nanofiber mat) and an MIC control (~400 µg/mL CIN). Experiments were performed in triplicate, NS denotes not significant, and error bars indicate one standard error.

4.4 Conclusions and Future Work

An essential oil, CIN, was successfully electrospun and delivered from chitosan/PEO nanofiber mats, without the use of a surfactant. An intrinsically antibacterial biopolymer, chitosan aided in CIN incorporation acting as a stabilizing agent while PEO allowed access to spinnable solutions at a pH value of 4. Solution and solid state NMR on precursor solutions and as-spun mats respectively determined that the attached-CIN and unattached-CIN were present in both. Resultant nanofiber mats were hydrophilic with smooth cylindrical morphology and had on average ~50 nm diameter. At physiological conditions, the polymer nanofiber mats released the CIN-liquid and CIN-vapor. Over 180 min, the quantity of CIN-vapor was two orders of magnitude greater than CIN-liquid with statistically higher levels of release from chitosan/PEO/CIN(1:1) nanofiber mats in both phases. More detailed release studies along with modeling should remain a goal for future work. To capture release profiles without saturating the surrounding solution remained

problematic as these concentrations were too low to be detected in either UV-Vis or Gas chromatography. Additionally, long term storage testing is needed to ensure the nanofiber mats would remain effective.

Within 30 min, chitosan/PEO nanofiber mats achieved a full inactivation of *E. coli*. Exploration into the cytotoxicity of the chitosan/PEO nanofiber mats towards *P. aeruginosa* had not yet been demonstrated, and was determined to have a strong effect, inactivating ~50% of the microbe. The release of CIN from the chitosan/PEO/CIN(1:0.1 and 1:1) nanofiber mats directly influenced their cytotoxicity against *P. aeruginosa*. After 180 min, 81 ± 4% of the *P. aeruginosa*, was inactivated by the chitosan/PEO/CIN(1:1) nanofiber mats. This work is the first demonstration that an essential oil can be incorporated into and successfully delivered from nanofiber mats. The release of CIN from the chitosan/PEO nanofiber mats offers potential as a flexible scaffold that can alleviate nosocomial infections by delivering a broad-spectrum natural antimicrobial agent. Thus, it would be interesting to explore the use of these nanofiber mats against additional bacteria strains, fungus and parasites.

The utilization of these two antibacterial agents, chitosan and CIN, could also be applied to nanofiber mats through post functionalization, Appendix A. This potentially useful method demonstrated that cellulose nanofiber mats coated in chitosan/CIN releaseed 10 × more liquid CIN compared to electrospun chitosan/PEO/CIN nanofiber mats. The release study highlighted the need for chitosan to control quantity of CIN within the coating because the CIN only coatings had very high standard deviations. Further investigation into long term storage would provide more insight on the use to encapsulate CIN.

While the quantity of CIN released in any of the chitosan/CIN coating should be efficient to achieve antibacterial activity, all chitosan/CIN nanofiber mats were hydrophobic and demonstrated low bacterial adhesion. Depending on the application, the placement of chitosan/CIN within or on a nanofiber mats is imperative if certain surface properties are desired. An only CIN coating was specifically interesting because it demonstrated the highest on average bacteria uptake but had very large standard deviation, which suggests that as the CIN coating was released, bacteria collected onto the underlying hydrophilic cellulose nanofiber mats. Thus, a goal of future work would be to utilize the antibacterial activity of CIN while simultaneously use a hydrophilic nanofiber mat to remove potentially harmful bacteria. Overall, chitosan/CIN can be incorporated through either electrospinning or post functionalization. The most optimal method might be a combination especially if there is a need to regenerate the antibacterial activity of the nanofiber mats. Further antibacterial testing should be completed on used nanofiber mats regenerated via post functionalization of cellulose and chitosan/PEO/CIN nanofiber mats with a chitosan/CIN or CIN coating.

CHAPTER 5
FUNDAMENTAL STUDY INTO THE ELECTROSPINNING OF CHITOSAN/PEO NANOFIBERS TO CARRY OILS

Adapted from: Rieger, K. A.; Birch, N. P.; Schiffman, J. D., Electrospinning chitosan/poly(ethylene oxide) solutions with essential oils: Correlating solution rheology to nanofiber formation. *Carbohydrate Polymers*, 2016, 139, 131-138.

5.1 Summary

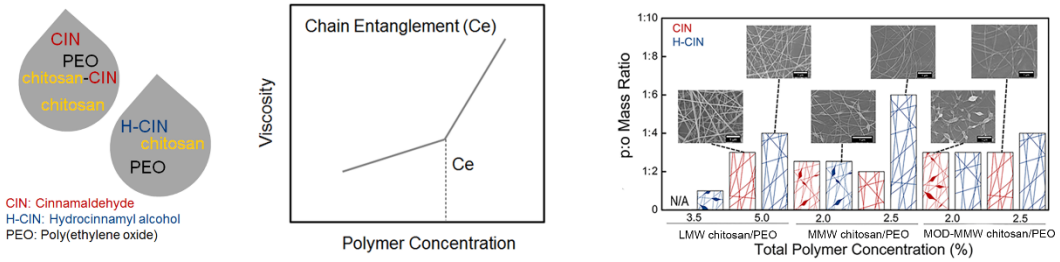

Figure 19: Through the optimization of solution and electrospinning parameters along with rheological analysis, nanofiber mats composed of chitosan/PEO can carry hydrophobic oils that Schiff base such as CIN and do not Schiff base such as H-CIN.

Electrospinning hydrophilic nanofiber mats that deliver hydrophobic agents would enable the development of new therapeutic wound dressings. Previously, strong antimicrobial activity resulted from chitosan/PEO nanofiber mats that released CIN, an essential oil. However, the correlation between precursor solution properties and nanofiber morphology for polymer solutions electrospun with or without hydrophobic oils has not yet been demonstrated. Here, CIN and hydrocinnamic alcohol (H-CIN) were electrospun in chitosan/PEO nanofiber mats as a function of chitosan MW and DA. Viscosity stress sweeps determined how the oils affected solution viscosity and chain entanglement (Ce) concentration. Experimentally, the maximum p:o mass ratio electrospun was 1:3 and 1:6 for chitosan/PEO/(CIN and H-CIN), respectively; a higher chitosan DA increased the incorporation of H-CIN only. The correlations determined for electrospinning plant-

derived oils could potentially be applied to other hydrophobic molecules, thus broadening the delivery of therapeutics from electrospun nanofiber mats.

5.2 Methods

5.2.1 Modification and Characterization of Chitosan

A modified medium molecular weight chitosan (MOD-MMW chitosan, M_w=1,000,000 Da) was synthesized to provide a direct comparison of molecular weight and DA. MOD-MMW chitosan was produced through the deacetylation of the MMW chitosan by suspending 5.0 g of MMW chitosan in 100 mL of 45 w/w% NaOH. The solution was heated at 70 °C for 45 min. The MMW chitosan was then filtered and washed with DI water until a neutral pH was achieved [221]. The resultant powder was then dried for 12 hr in a vacuum oven at 25 °C.

Proton nuclear magnetic resonance (^{1}H NMR, Bruker Avance 400) along with SpinWorks3, an NMR analysis software, were employed to quantitatively determine the DA of the LMW, MMW, and MOD-MMW chitosan. Solutions for ^{1}H NMR containing 1.0 w/v% LMW, MMW, or MOD-MMW chitosan were dissolved in 0.5 M AA-d4 (500 μL). To analyze the interactions between chitosan and CIN or H-CIN, new ^{1}H NMR solutions at the previously mentioned solution parameters and p:o mass ratios of 1:0.2 and 1:0.4 were prepared.

5.2.2 Preparation of Chitosan/PEO and Oil Loaded Chitosan/PEO Solutions

A 1:1 weight ratio of LMW, MMW, or MOD-MMW chitosan/PEO (0.5 g/0.5 g) in 0.5 M AA (20 mL) corresponding to total polymer concentrations ranging from 0.25 to 5.0 w/v% solutions were mixed for 24 hr at 20 rpm using an Arma-Rotator A-1 (Bethesda, MA). CIN or H-CIN (Figure 20), was added to a LMW, MMW, or MOD-MMW

chitosan/PEO solution to form an oil loaded solution ranging from 1:0.2 to 1:12 p:o mass ratio. These solutions were mixed for an additional 24 hr, at which point, the solution changed from transparent to opaque. Throughout the mixing process, the solution had a pH value of 4. Within this manuscript, all solutions were prepared in a similar manner using a 1/1 weight ratio of chitosan/PEO.

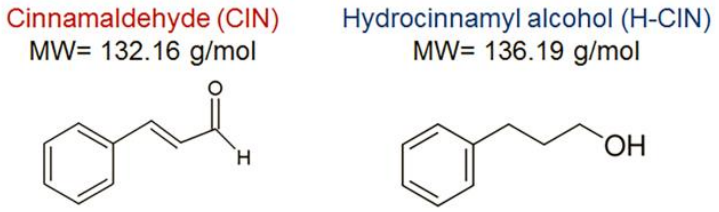

Figure 20: Cinnamaldehyde (CIN) is an essential oil, which has shown to be effective against *P. aeruginosa*. Hydrocinnamyl alcohol (H-CIN), also shown, is an analogous structure that will be used in this thesis for comparative purposes.

5.2.3 Characterization of Chitosan/PEO and Chitosan/PEO/(CIN or H-CIN)

Oil-loaded solutions with and without PEO were imaged using a Zeiss Optical Microscope (Axio Imager A2) to qualitatively examine (i) the polydisperisty of the oil droplets and (ii) the effect of PEO addition on oil droplet size for 1:0.5, 1:1, 1:2 and 1:5 p:o mass ratios. The contact angle of the chitosan/PEO and oil-loaded chitosan/PEO solutions were determined using a home-built digital Olympus camera imaging setup to capture solution droplets. Solutions for contact angle analysis had a total polymer concentration of 2.5 w/v% for MMW and MOD-MMW chitosan/PEO, and a total polymer concentration of 5.0 w/v% for LMW chitosan/PEO. All oil loaded solutions were mixed with a 1:1 p:o mass ratio. *Image J* 1.45 software (NIH, Bethesda, MD) was used to measure the contact angle. The average contact angle along with the standard deviation for each solution was obtained by measuring three droplets.

LMW, MMW, and MOD-MMW chitosan/PEO solutions with total polymer concentrations ranging from 0.25 – 5.0 w/v% were used for rheology. The oil (CIN or H-CIN) was added at a 1:1 p:o mass ratio. Viscosity measurements were performed using a Kinexus Pro rheometer (Malvern, UK) using a concentric cylinder geometry with a diameter of 25 mm, horizontal gap of 1 mm, run with a vertical gap of 1 mm. A viscosity stress sweep was conducted from 0.1 to 10 Pa; there were no signs of phase separation over the course of measurement. Measurements were conducted at 25 ºC. A Newtonian plateau was observed within this range, and the average value of the plateau was reported. The resulting data was fit using a two-phase power regression to determine the change from the untangled regime to the entangled regime [164,222]. Viscosity stress sweeps were conducted from 0.1 to 1,000 Pa. Solutions contained a fixed total polymer concentration of 2.5 w/v% MMW chitosan/PEO and were loaded with CIN and H-CIN p:o mass ratios ranging from 1:0 to 1:12. A Carreau-Yasuda model was fit to the data and plotted to compare both the raw and fitted data.

5.2.4 Electrospinning of Chitosan/PEO/(No Oil, CIN or H-CIN) Solutions

LMW, MMW, and MOD-MMW chitosan/PEO solutions were electrospun at total polymer concentrations ranging from 0.25 - 5.0 w/v% to determine the total polymer concentration needed to electrospin defect-free fibers. CIN or H-CIN was added to the LMW, MMW, and MOD-MMW chitosan/PEO solutions at p:o mass ratios between 1:1 and 1:12. If CIN or H-CIN was fully incorporated into the chitosan/PEO solution (i.e., no large bubbles/macrophase separation was observed), then the solution was electrospun.

Detailed electrospinning apparatus setup can be found in Chapter 4 Section 4.2.2. All solutions were electrospun at a constant feed rate of 60 μL/min, a separation distance of 120 mm and an applied voltage of 35 kV.

5.2.5 Characterization of Electrospun Chitosan/PEO and Chitosan/PEO/(CIN or H-CIN) Nanofiber Mats

Micrographs of electrospun nanofibers were acquired using a FEI-Magellan 400 scanning electron microscope (SEM). A Gatan high resolution ion beam coater model 681 was used to sputter coat samples with ~5 nm of platinum. To confirm that the electrospun nanofiber mats released the oils, LMW chitosan/PEO solutions containing either CIN or H-CIN at a 1:0.2 p:o mass ratio were spun for 60 min. Nanofiber mats were then punched into circles with a 0.9525 cm diameter using a Spearhead® 130 Power Punch MAXiset before being submerged in a 1.5 mL centrifuge vial containing 1 mL of DI water. The vials were mixed for 48 hrs at 20 rpm using an Arma-Rotator A-1. At 3, 24, and 48 hr, 1 mL of solution from each nanofiber mat was tested via UV-Vis spectroscopy (Model 8453, Agilent Diode Array, Santa Clara, CA) at an absorbance of 293 and 288 nm for CIN and H-CIN, respectively[197,198,223]. The absorbance of each aliquot was averaged and related to a concentration based on a standard calibration curve. Total CIN or H-CIN release (μg per nanofiber mat) is reported based on triplicate tests.

5.3 Results and Discussion

5.3.1 Characteristics of Chitosan, CIN, and H-CIN Solutions

5.3.1.1 Chitosan Characteristics

The ^{1}H-NMR spectra of LMW chitosan is displayed on Figure 21 and is representative of the spectra acquired for LMW, MMW, and our in-house modified MOD-

MMW chitosan. By taking the relative integrals of 1.7 – 2.4 ppm over 2.7 – 4.4 ppm, we calculated the degree of acetylation (DA) values for the three chitosans[203–205]. The MMW chitosan had a molecular weight of 1,000,000 Da and a DA of 23%. The LMW and our MOD-MMW chitosan had molecular weights of 460,000 and 1,000,000 Da, respectively, and an identical DA value of 13%. Thus, we can directly study the role that the molecular weight and DA of chitosan have on electrospinning immiscible phase oils.

5.3.1.2 Chitosan/CIN and Chitosan/H-CIN Characteristics

The interactions between chitosan and each oil, CIN and H-CIN, were also characterized using ^{1}H NMR, Figure 21. Peaks at ~7 ppm correspond to aromatics, which are present for both CIN and H-CIN. Highlighted in grey are peaks at 9.0 ppm from unreacted aldehydes present on CIN and a peak at 9.5 ppm from reacted CIN, which is indicative of a Schiff base reaction [169–172]. The imine proton is present at 8.2 ppm as a small peak. No peaks are present at 9.0 or 9.5 ppm in the ^{1}H NMR spectra of chitosan/H-CIN because there is no aldehyde within the H-CIN chemical structure and thus, no Schiff base or substitution reactions. The degree of substitution (DS) values were calculated from the ratio of the integrated resonances of reacted CIN (9.25 - 9.6 ppm) over glucosamine residues on chitosan (2.7 - 4.4 ppm)[169,208]. The DSs for chitosan/CIN at 1:0.2 and 1:0.4 p:o mass ratios for the LMW, MMW, and MOD-MMW chitosans were determined and are compiled in Figure 21B. The DS for the MMW and MOD-MMW chitosans are approximately equivalent and are two times greater than the DS of LMW chitosan.

A

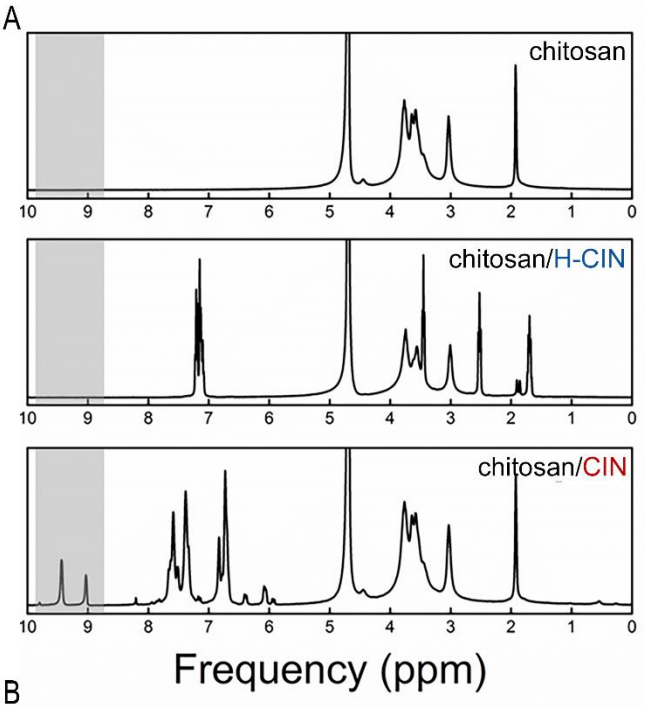

B

chitosan	MW (Da)	DA (%)	DS (%) 1:0.2 p:o CIN	DS (%) 1:0.4 p:o CIN
LMW	460,000	13	15	16
MMW	1,000,000	23	34	32
MOD-MMW	1,000,000	13	30	30

Figure 21: (A) ^{1}H NMR spectra of (top-to-bottom) chitosan, as well as chitosan/H-CIN and chitosan/CIN at a 1:0.2 p:o mass ratio. Sections in grey highlight peaks due to CIN. (B) Summary of the molecular weight (MW), degree of acetylation (DA), and degree of substitution (DS) for chitosan/CIN solutions at 1:0.2 and 1:0.4 p:o mass ratios. H-CIN does not react with chitosan and therefore, no DS values are provided.

5.3.1.3 Chitosan/PEO/(CIN or H-CIN) Solution Characteristics

Chitosan has been suggested to act as a stabilizer[165–168] because it is composed of two blocks, 1,4-linked 2-amino-2-deoxy-β-*D*-glucan and 1,4 linked 2-acetamido-2-deoxy-β-*D*-glucan. To better understand how CIN and H-CIN were stabilized by chitosan within the electrospinning precursor solutions, images of the solutions with and without PEO were acquired. Qualitatively, the addition of PEO had little effect on the dispersion of oil, Figure 22. Due to the challenges of capturing enough representative images containing a statistically relevant number of oil droplets, we offer these images only as a qualitative

characterization of the oil dispersion. CIN droplets were larger and more polydispersed, while H-CIN droplets had a bimodal distribution featuring two smaller droplet sizes. As the mass ratio increased, both types of oil droplets appeared to increase in size and CIN became more polydispersed, consistent with literature[224].

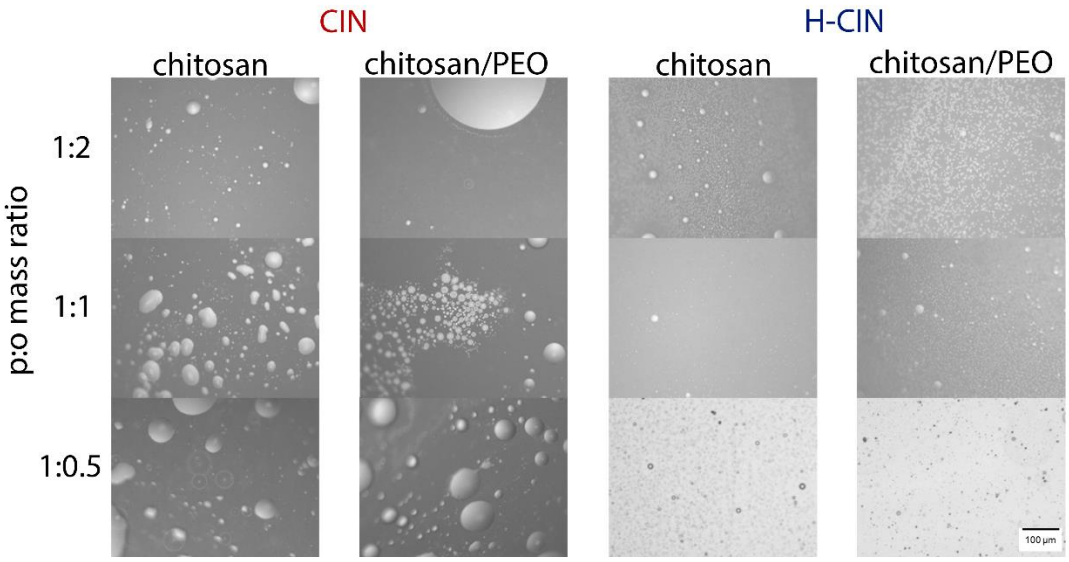

Figure 22: Optical images of electrospinning precursor solutions. Solutions are composed of MMW CS or MMW chitosan/PEO (1/1 wt ratio) mixed with p:o mass ratios of 1:0.5, 1:1, and 1:2 CIN and H-CIN. All images have a 100 µm scale bar.

Contact angle measurements were obtained for 5.0 w/v% LMW chitosan/PEO solutions, as well as for 2.5 w/v% MMW and MOD-MMW chitosan/PEO solutions, Table 3. These polymer concentrations were chosen because when electrospun, they yielded defect-free nanofibers (Chapter 5 Section 5.3.2.1). MMW and MOD-MMW chitosan/PEO had similar contact angles of 28° and 31°, respectively, while LMW chitosan/PEO had a much higher contact angle of 37°. The difference in contact angle is likely due to the polymer concentration difference between the testing solutions. MMW and MOD-MMW chitosan/PEO solutions could not be prepared at 5.0 w/v% because they were too viscous. The contact angle for the LMW, MMW, MOD-MMW chitosan/PEO solutions after the

addition of CIN and H-CIN at a 1:1 p:o mass ratio was also measured. Notably, the addition of CIN and H-CIN at a 1:1 p:o mass ratio significantly decreased the contact angle to 20-25° for all chitosan/PEO solutions.

Table 3: Summary of chitosan/PEO/(No Oil, CIN or H-CIN) solution characteristics.

Chitosan	Contact Angle (°)			Viscosity (Pa s)			C_e (%)		
	No Oil	CIN	H-CIN	No Oil	CIN	H-CIN	No Oil	CIN	H-CIN
LMW Chitosan	37.2±2.3	23.7±0.8	25.8±0.7	0.14	0.10	0.18	3.0	1.8	2.2
MMW Chitosan	31.5±2.4	25.3±1.9	25.4±0.3	3.31	3.35	3.16	0.8	0.8	1.2
MOD-MMW Chitosan	28.2±2.2	20.4±3.0	23.6±0.7	1.92	2.11	1.70	1.3	1.0	1.1

*All solutions were prepared at a 1/1 chitosan/PEO mass ratio. For solutions containing an oil, a 1:1 p:o mass ratio was used. The viscosity measurements were taken using 2.5 w/v% solutions. Chain entanglement is denoted as C_e.

5.3.2 Characteristics of Chitosan/PEO(No Oil, CIN or H-CIN) Nanofibers

5.3.2.1 Electrospinning of chitosan/PEO Nanofibers and Solution Rheology

Chitosan (LMW, MMW, and MOD-MMW) solutions as a function of total polymer concentration, molecular weight, and DA were successfully electrospun at a 1/1 weight ratio with PEO. As the total polymer concentration increased, the resulting nanofibers changed from exhibiting a bead-on-string morphology to a defect-free nanofiber morphology, Figure 23. The MMW and MOD-MMW chitosan/PEO solutions, which have the same chitosan molecular weight but different DAs produced defect-free nanofibers at the same total polymer concentration of 2.0 w/v%. The LMW chitosan/PEO solution, which has a lower chitosan molecular weight but the same DA as the MOD-MMW chitosan needed a higher polymer concentration of 3.5 w/v% to electrospin into defect-free nanofibers.

While chitosan/PEO solutions have previously been electrospun, the polymer chain entanglement concentration (C_e) of the solutions has not yet been reported, Figure 23 and Table 3. This is surprising seeing how the use of PEO enables chitosan to be electrospun using greener solvents[20,164]. The C_e predicts the "spinnability" of a precursor solution and the minimal polymer concentration needed to electrospin fibers with a bead-on-string morphology [70,225,226]. Using rheology, the C_e was determined to be 3.0 w/v% for the LMW chitosan/PEO solution, which was a slightly lower concentration than where defect free fibers were experimentally observed. The MMW chitosan/PEO and MOD-MMW chitosan/PEO solutions had C_e's of 0.8 and 1.3 w/v%, respectively. Molecular weight had a strong impact on C_e because chain entanglement is directly correlated with the length of the polymer backbone [227]. However, DA of the chitosan did not affect the C_e; this is an encouraging finding. This may suggest that despite the batch-to-batch variation that biopolymers experience[20], electrospinning chitosan-containing solutions does offer some flexibility in terms of operational space. Experimentally, for LMW, MMW, and MOD-MMW chitosan/PEO solutions, defect free nanofibers were observed at 1.2-2.5 times C_e which corroborates well with previous rheological studies that have electrospun biopolymer solutions [70,142,164,228]. It has been previously reported[164] that the C_e of chitosan (148,000 Da, DA:15-25%) in aqueous acetic acid was 2.9 wt%. However, this chitosan concentration was notably too viscous to be electrospun[164]. Another study examined how PEO improves the "spinnability" of chitosan, however, they explored the C_e of the polymers separately but found results similar to our MMW and MOD-MMW chitosan/PEO mixtures[142].

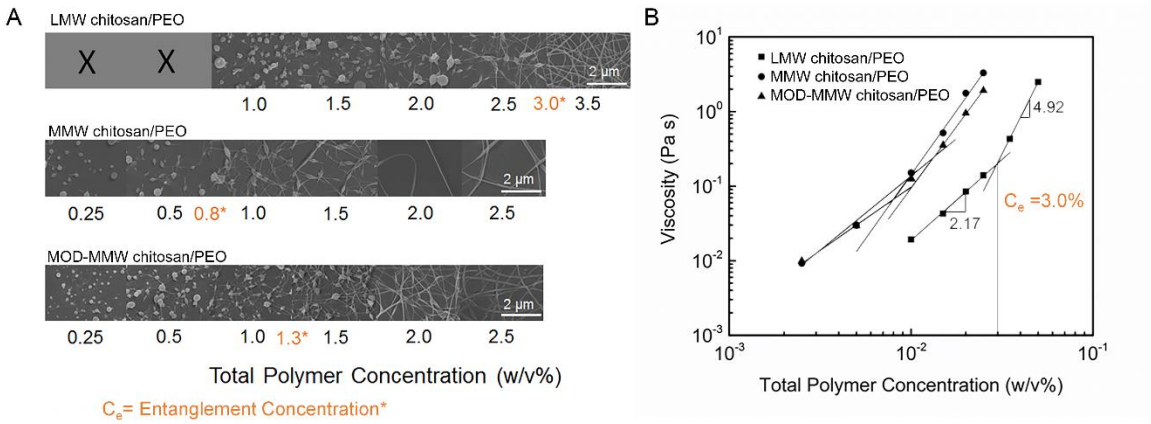

Figure 23: (A) SEM micrographs display the morphology of LMW, MMW, and MOD-MMW chitosan/PEO nanofibers electrospun with increasing total polymer concentration (left to right). On the LMW chitosan/PEO samples, an "X" indicates that there was no observable collection during electrospinning. The entanglement concentrations that were estimated using rheology are also provided. All scale bars are 2 μm. (B) Solution viscosity versus total polymer concentration for LMW, MMW, and MOD-MMW chitosan/PEO solutions. A representative extrapolation of the entanglement concentration (C_e) is provided for LMW chitosan/PEO.

5.3.2.2 Chitosan/PEO/(CIN or H-CIN) Solution Rheology

The addition of CIN or H-CIN at a 1:1 p:o mass ratio to the LMW chitosan/PEO solution had a strong impact on the C_e, Figure 24 and Table 3. The addition of CIN and H-CIN reduced the C_e from 3.0 to 1.8 and 2.2 w/v%, respectively. The C_e of the MMW and MOD-MMW chitosan/PEO solutions remained relatively constant regardless of oil addition, varying overall from 0.8-1.2 and 1.0-1.3 w/v%, respectively. The type of oil had little effect on the C_e for all chitosan/PEO solutions.

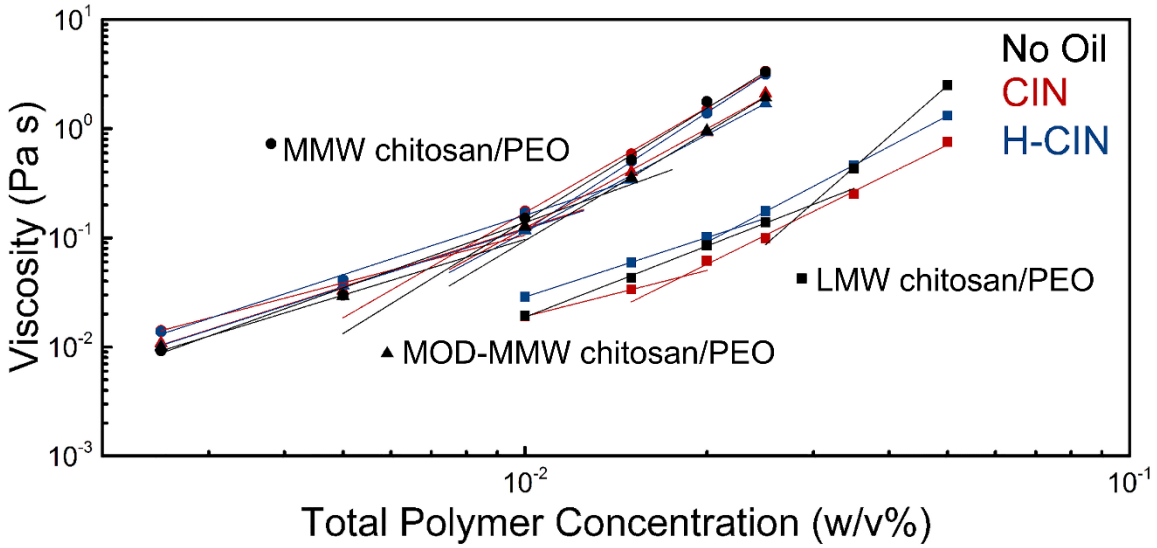

Figure 24: Solution viscosity versus total polymer concentration for LMW, MMW, and MOD-MMW chitosan/PEO solutions, with and without CIN and H-CIN. The data is shown with a two-phase power regression. CIN and H-CIN were added at a 1:1 p:o mass ratio.

Chitosan/PEO solution viscosity with and without CIN or H-CIN at a 1:1 p:o mass ratio was determined, Table 3. The viscosity of the LMW, MMW, and MOD-MMW chitosan/PEO solutions at 2.5 w/v% remained ~0.14, 3.3, and 1.9 Pa s, respectively, regardless of oil loading. The similar behavior between MMW and MOD-MMW chitosan/PEO solutions loaded with CIN or H-CIN suggests that the effect of DA on solution viscosity was small. A similar observation on viscosity was previously reported by the addition of surfactants to chitosan/PEO solutions [134]. As the polymer concentration of the LMW chitosan/PEO solution increased above its C_e (3.0 w/v%), the addition of oil strongly decreased the solution viscosity. At 5.0 w/v% the LMW chitosan/PEO solution viscosity decreased from 2.5 Pa s to 0.8 Pa s with CIN addition, and to 1.3 Pa s with the addition of H-CIN. Similar to C_e, the solution viscosity was only oil sensitive for the LMW chitosan/PEO solution.

Figure 25 displays how the MMW chitosan/PEO solution behavior changed due to the addition of CIN and H-CIN at p:o mass ratios from 1:0 to 1:10 and 1:12, respectively. A Carraeu-Yasuda fit (Equation 3) was applied to further analyze the data.

Equation 3

$$\eta = \eta_\infty + (\eta_0 - \eta_\infty)[1 + (\lambda\dot{\gamma})^a]^{\frac{n-1}{a}} \qquad (2)$$

Wherein the apparent viscosity (η) is described by an infinite shear viscosity (η_∞), a zero shear viscosity (η_0), a relaxation time (λ), a transition width (a), and a power law index (n) [229].

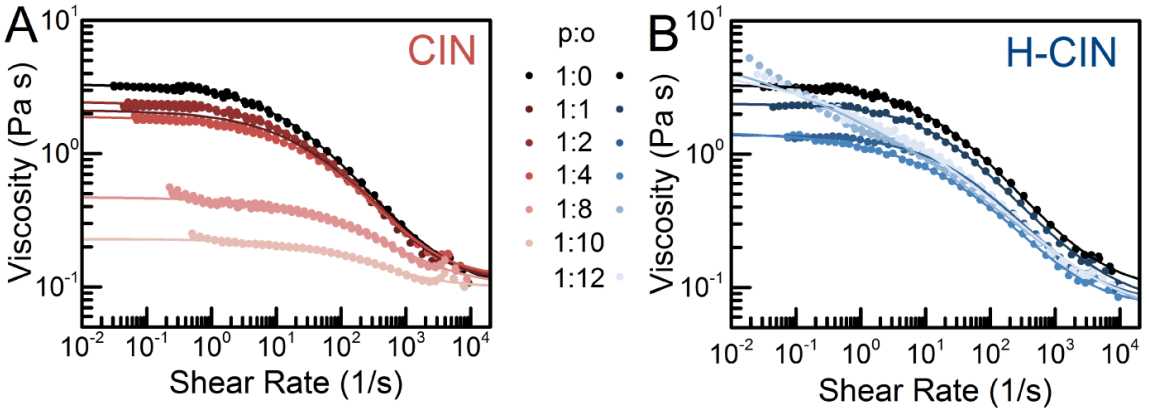

Figure 25: Viscosity curves of MMW chitosan/PEO solutions with increasing p:o mass ratios from 1:0 to 1:12 for (**A**) CIN and (**B**) H-CIN. A p:o mass ratio above 1:10 for CIN was not possible due to phase separation.

Both the infinite shear viscosity and the zero shear viscosity decreased as the amount of CIN or H-CIN increased, which was expected based on the LMW chitosan results from Figure 24. At the 1:1 p:o mass ratio, the viscosity curves are almost identical, but as the amount of oil increased the behavior of CIN and H-CIN started to diverge. At the middle oil loadings (1:2 and 1:4 p:o mass ratios), CIN has a slightly weaker negative effect on the viscosities. At the highest two oil loadings (1:8 and 1:12 p:o mass ratios), H-CIN begins to thicken again and the zero shear viscosity shifts far to the left. By contrast, at the two highest CIN loadings (1:8 and 1:10 mass ratios), the zero shear viscosity drops

substantially and by a p:o mass ratio of 1:10, the curve is nearly flat. When a higher loading of CIN at p:o mass ratio of 1:12 was attempted, we observed severe phase splitting. Additionally, loadings of CIN above a 1:12 p:o mass ratio resulted in the formation of a dynagel, which has been previously reported[171]. Within Marin et al.'s work, the minimum CIN:amine group ratio needed to obtain chitosan gelation was a 22:1 molar ratio, which matches well with our findings of a 21:1 molar ratio. The abnormal behavior of the CIN-loaded solutions can be attributed to the chemical bonding that takes place with chitosan, which shifts the behavior away from that of a non-interacting oil, like H-CIN.

5.3.2.3 Chitosan/PEO/(CIN or H-CIN) Nanofiber Characteristics

Nanofiber mats containing CIN or H-CIN were successfully electrospun from LMW, MMW, and MOD-MMW chitosan/PEO solutions as a function of the chitosan molecular weight, DA, polymer concentration, and p:o mass ratio, Figure 26. The polymer concentrations 3.5 and 5.0 w/v% for LMW chitosan/PEO solutions, as well as 2 and 2.5 w/v% for MMW and MOD-MMW chitosan/PEO were chosen because when electrospun they formed smooth cylindrical nanofiber mats without any oil addition, Figure 23.

After adding CIN or H-CIN to any chitosan/PEO solution, an increase in polymer concentration was needed to electrospin smooth and cylindrical nanofibers. This was expected as the contact angle of the solutions, Table 3, decreased after the addition of CIN or H-CIN, hence leading to a lower surface tension. Previous studies have reported that a decrease in surface tension leads to nanofibers with bead-on-string morphology[142]. Additionally, as shown in Figure 24, both the infinite shear viscosity and the zero shear viscosity decreased as the amount of CIN or H-CIN increased. While the solution

properties, such as, polymer concentration and surface tension, can be confounding, viscosity has been reported to be a dictating parameter for electrospinning[230].

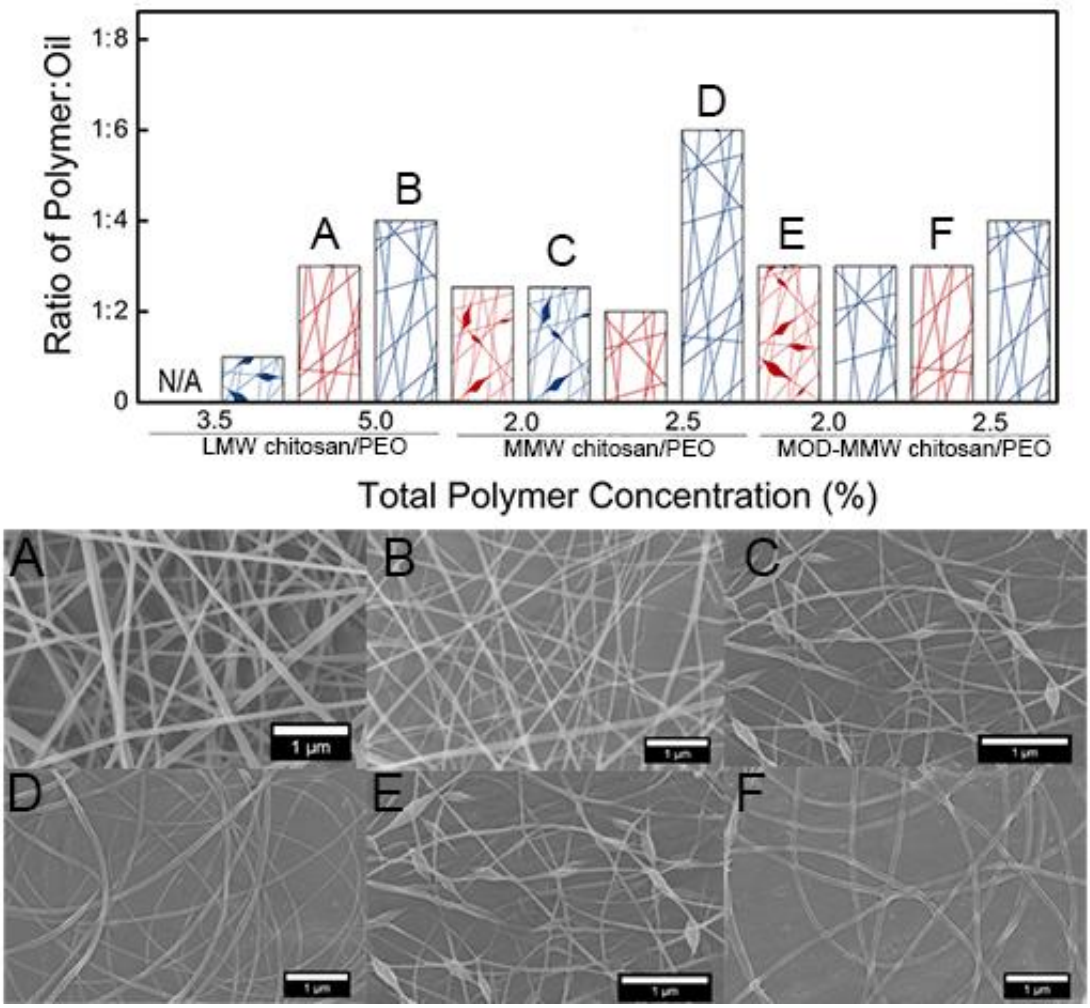

Figure 26: (Top) Cartoon representation of nanofibers electrospun from LMW, MMW, and MOD-MMW chitosan/PEO/(CIN or H-CIN) solutions at various p:o mass ratios. N/A indicates that the solutions did not form nanofibers when electrospun. (Bottom) Corresponding SEM micrographs (A-F) provide representative nanofiber morphology. All scale bars are 1 µm.

A direct comparison of DA was conducted by electrospinning MMW and MOD-MMW chitosan/PEO solutions. The 2.5 w/v% MMW chitosan/PEO solution led to the highest loadings of H-CIN (1:6 p:o mass ratio) suggesting that higher DA improves the stability and electrospinability of H-CIN solutions. A previous report stated that a high DA of 39% increased the stability of carbon nanotubes dispersed in chitosan solutions, as

compared to chitosan DA values of 7 to 29% [165]. The change in DA did not have as large of an effect on CIN solutions. This might be due to the presence of a Schiff base reaction between CIN and chitosan. Additionally, CIN is 10 times less soluble than H-CIN, which could influence the ability of chitosan to disperse the oil. In fact, the highest loading of CIN (1:3 p:o mass ratio) that could be electrospun into defect-free nanofibers was achieved using either a 5.0 w/v% LMW chitosan/PEO solution or a 2.5 w/v% MOD-MMW chitosan/PEO solution. As expected, the effect of molecular weight on the ability to electrospin oil loaded chitosan/PEO solutions appeared to be relatively small because all of the polymer concentrations tested were above the C_e. Overall, for successful electrospinning, the DA and molecular weight of chitosan are parameters that must be tuned based on the oil structure.

5.3.3 Release Characteristics of Chitosan/PEO/(CIN or H-CIN) Nanofiber Mats

As a final proof-of-concept, we confirmed that CIN and H-CIN were incorporated into the electrospun nanofiber mats by examining the release of the oils post-electrospinning. A low, 1:0.2 p:o mass ratio, was chosen because both oils could be electrospun for 1 hr from a 5% LMW chitosan/PEO solution to form robust nanofiber mats that could be handled and tested. UV-Vis quantified that $8.58 \times 10^{-3} \pm 3.8 \times 10^{-3}$ μg of CIN and 1.5 ± 0.5 μg of H-CIN were released from the chitosan/PEO nanofiber mats at a p:o 1:0.2 mass ratio after 3 hr. After 48 hr, there was no further release of CIN or H-CIN. The release of CIN is consistent with the previous work in Chapter 4 Section 4.3.4, where chitosan/PEO/CIN(1:0.1 and 1:1) nanofiber mats demonstrated an initial CIN-liquid release of $2.0 \times 10^{-3} \pm 3 \times 10^{-4}$ μg and $1.9 \times 10^{-3} \pm 1 \times 10^{-4}$ μg, respectively. After a longer duration of time (3 hrs) the CIN-liquid release started to level off indicating that

equilibrium had been reached; namely, $2.73 \times 10^{-3} \pm 9.0 \times 10^{-4}$ µg and $1.49 \times 10^{-2} \pm 4.4 \times 10^{-3}$ µg released from chitosan/PEO/CIN nanofiber mats at 1:0.1 and 1:1 p:o mass ratios, respectively. The cumulative amount of CIN-liquid released from the chitosan/PEO/CIN(p:o mass ratio of 1:1) nanofiber mats was statistically higher than the CIN-liquid released from the chitosan/PEO/CIN(1:0.1) nanofiber mats indicating that an increased loading of CIN correlates with an increased release. In the current work, the difference in release between the two oils is likely due to their unique properties, namely, solubility and/or their chemical interaction with chitosan. For example, the CIN that has Schiff base reacted with chitosan will likely not be released from the nanofiber mats within the timeframe of our experiment.

5.4 Conclusion and Future Work

In this study, the correlation between precursor solution properties and the morphology of CS/PEO and CS/PEO/(CIN or H-CIN)nanofibers was investigated by focusing on CS molecular weight and DA, as well as p:o mass ratio. We have demonstrated that CS/PEO solutions containing a range of CIN and H-CIN p:o mass ratios form nanofibers. A low DA improved the electrospinning of solutions that contained CIN, while the opposite was observed for solutions that contained H-CIN.

An increase in polymer concentration caused a transition from bead-on-string to cylindrical nanofiber morphology, indicating that the addition of oil reduced the solution viscosity; this was corroborated through viscosity stress sweeps. In the future, viscosity stress sweeps should be conducted on solutions that are allowed to age to determine how the solution properties change with time. Additionally, the storage time should be explored by determining the longest time before a solution is not “spinnable.”

When the same p:o mass ratio of CS/PEO to CIN or H-CIN was electrospun into nanofiber mats, there was a 57% higher release of H-CIN than CIN, which was likely a result of oil properties, specifically all H-CIN can theoretically be released as no chemical attachment with chitosan can occur. A complementary future study electrospinning the same hydrophobic oils (CIN and H-CIN) with a hydrophobic polymer would provide insight into how the incorporation, rheological properties and subsequent release of oil found here compare.

Overall, insights gained from electrospinning CIN and H-CIN could be applied to hundreds of additional bioactive essential oils, as well as a variety of small hydrophobic molecules, thus significantly broadening the delivery of therapeutics from electrospun nanofiber mats.

CHAPTER 6
INCORPORATION OF CHITOSAN AND CIN TO SPIN-COATED FILMS

Adapted from: Rieger, K. A.; Eagan, N. M.; Schiffman, J. D., Encapsulation of cinnamaldehyde into nanostructured chitosan films. *Journal of Applied Polymer Science*, 2015, 132 (13).

6.1 Summary

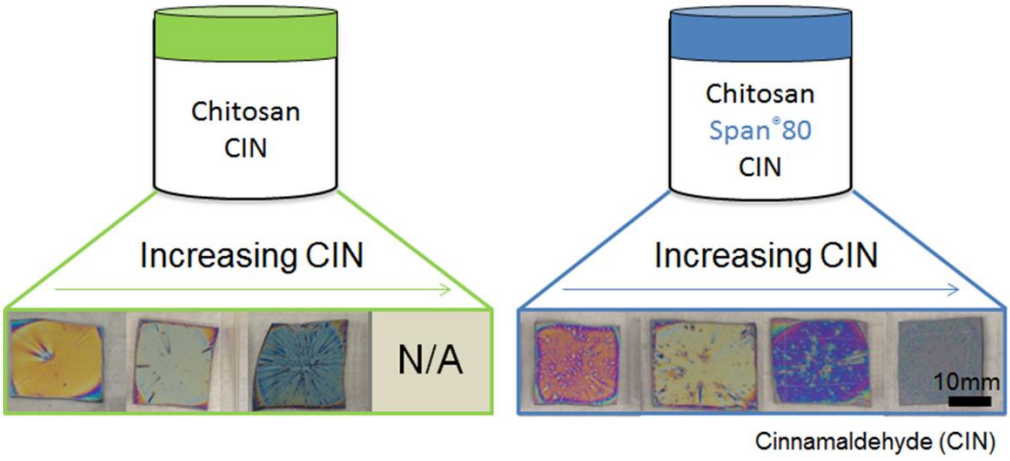

Figure 27: Translation of two antibacterial agents, chitosan and CIN, into thin films via spin coating. An increase in the incorporation of CIN was mediated through the addition of a surfactant.

Chitosan films have attracted much attention due to their intrinsic properties and subsequent versatility in applications ranging from food packaging to wound dressings. However, the ability to incorporate a volatile oil into an ultrathin film remains a challenge. Here, we use the spin-coating technique to fabricate films that incorporate the natural essential oil, CIN, into the renewable biopolymer, chitosan, Figure 27. Systematically, the influence of the surfactant Span®80 on the maximum amount of CIN incorporated into chitosan ultrathin films along with their subsequent release profiles were determined. By

holding the processing parameters and chitosan concentration constant, it was determined that films without Span®80 decreased in thickness with increasing CIN concentration, whereas films with 0.1% Span®80 increased in thickness with increasing CIN concentration. All films were hydrophilic with thicknesses between 145 - 345 nm, which visually exhibited well-defined color. Release studies conducted via UV-visible spectroscopy confirm that higher loadings of CIN only obtained using Span®80 in chitosan films resulted in subsequently higher release. These result indicate that the loading and subsequent release of CIN in chitosan thin films via a surfactant can be tailored to match the release requirements of specific applications.

6.2 Methods

6.2.1 Chitosan/CIN and Chitosan/Span®80/CIN Solution Preparation and Characterization

CIN was incorporated into chitosan or chitosan/Span®80 solutions, Figure 28. A 2.5 w/v% solution of chitosan in 0.5 M AA was mixed until fully dissolved (24 hr at 20 rpm) using an Arma-Rotator A-1 (Bethesda, MA). Emulsions were prepared at organic/aqueous volume ratios of 0, 0.5, 1.0 and 5.0 v/v%, corresponding to CIN/chitosan weight ratios of 0, 0.21, 0.42, and 2.1, respectively. For consistency with the rest of this document, chitosan/CIN solutions will be referred to by p:o (polymer:oil) mass ratios of 1:0, 1:0.1, 1:0.2 and 1:1.

First, Span®80 at 0.1 w/v% was added to the chitosan solution and mixed for 24 hr. CIN was added dropwise to the chitosan/Span®80 solution at a rate of 3 drops every 3 min while the solution was continuously mixed on a stir plate. The chitosan/Span®80/CIN solutions were then mixed for an additional 15 min to ensure a homogeneous solution. Chitosan/CIN solutions (no Span®80) were prepared by adding the various amounts of CIN

to the chitosan solution and mixed for an additional 24 hr. Throughout the mixing process, all solutions had a pH value of 4 and once CIN was added to chitosan, the solutions changed from transparent to white.

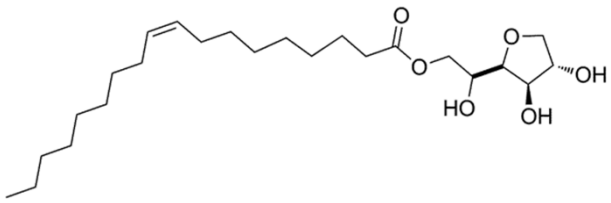

Figure 28: The chemical structure of sorbitan monooleat (Span®80), a surfactant, is shown. In this work, ultrathin films containing chitosan and cinnamaldehyde (CIN) are spin-coated in the presence or absence of Span®80.

Proton nuclear magnetic resonance (^{1}H NMR, Bruker Avance 400) along with SpinWorks3, an NMR analysis software, were employed to quantitatively determine the degree of acetylation (DA) and degree of substitution (DS) of the chitosan. Solutions for ^{1}H NMR consisted of chitosan/Span®80/CIN and chitosan/CIN emulsions containing 1:0, 1:0.1, 1:0.2, and 1:1 p:o mass ratios dissolved in 0.5 M AA-d_4 (600 μL). DA values were determined by taking the relative integrals of 1.7 – 2.4 ppm over 2.7 – 4.4 ppm.[203–205] DS values were calculated from the ratio of the integrated resonances of reacted CIN (9.25 - 9.6 ppm) over glucosamine residues on chitosan (2.7 - 4.4 ppm).[169,208]

6.2.2 Chitosan/CIN and Chitosan/ Span®80/CIN Thin Film Fabrication

Substrates for spin-coating were either silicon wafers (single-sided polished, (100) plane from University Wafer, South Boston, MA) for profilometry or glass coverslips (22 mm × 22 mm × 1.5 mm, Fisherbrand™) for all other characterization. Before spin-coating, silicon wafers were rinsed with water, acetone, and ethanol before 30 min of UV/ozone treatment (UV/Ozone ProCleanerTM, BioForce Nanosciences, Ames, IA) to oxidize the organic material. Cleaned silicon wafers

were cut (25 mm x 25 mm) then rinsed again with water, acetone, and ethanol before being dried under an air stream. Glass coverslip were UV/ozone treated for 30 min to oxidize the organic material then rinsed with water, acetone, and ethanol before being dried under an air stream.

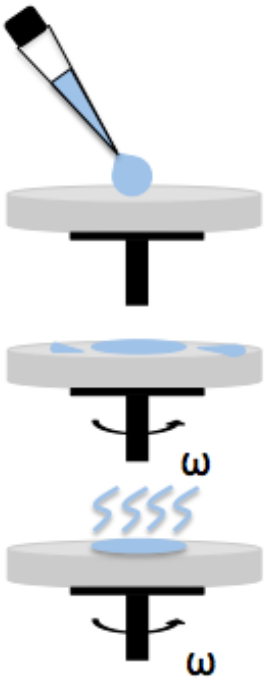

Figure 29**:** The schematic displays the spin-coating process, which is composed of three main phases. Typically, a drop of solution is placed on a substrate on the chuck (Top). The chuck is rotated at a specific angular velocity for a specified amount of time to create a thin film (Middle). The sample is left to dry to remove excess solvents (Bottom).

Chitosan/CIN and chitosan/Span®80/CIN solutions were statically dispensed (0.5 mL) onto a substrates and spin-coated (Spin-Coater model SC-100, Smart Coater, St. Louis, MO) at 4000 rpm for 60 s with an additional 1 s ramp time. Spin coating (Figure 29) is a simple technique used to fabricate uniform thin films via a centrifugal force. The process involves a solution being dispensed and rotated onto a flat substrate held in place by a vacuum pump. Two dispensing methods, static and dynamic, are used to apply the solution either before or during spinning respectively. The substrate

is rotated at an accelerating speed until it reaches an angular speed. This speed is held for duration of time to allow for excess solution to detach from the substrate and the solvent to evaporate.

After spin-coating, remnant AA was allowed to evaporate at room temperature (T = 21 °C) for 24 hr. To ensure their stability for further characterization, films (n = 6) were then crosslinked in a vapor chamber (12.2 cm × 9.8 cm × 7.8 cm, Biohit Inc., Neptune, NJ) containing 1.0 mL of GA liquid at room temperature for 4 hr.

6.2.3 Characterization of Chitosan/CIN and Chitosan/Span®80/CIN Ultra-Thin Spin Coated Film

Film thicknesses of chitosan/Span®80/CIN and chitosan/CIN films spin-coated onto silicon wafers were determined using a stylus profilometer (model Dektak 3, Veeco/Sloan, Santa Barbara, CA). Scratches were made into the film with a razor blade and then scans of 500 point resolution were run perpendicular to the scratches for lengths of 1000 μm at a rate of 80 μm/s.[231] The thickness was determined to be the difference between the surface height and the lowest point of the scratch. Tests were performed on three samples of each type of film with three scratches per sample.

Changes in surface hydrophobicity were evaluated as previously described in Chapter 4 Section 4.2.4. Films were tested in triplicate.

6.2.4 Release of CIN from Chitosan/CIN and Chitosan/ Span®80/CIN Ultra-Thin Films

Films were spin-coated onto glass coverslips, which were cut in half and placed with coated surfaces facing outward into a 10 mL vial filled with 10 mL of DI water. The films were fully submerged. The vials were sealed tightly to prevent evaporation, protected

from light, and shaken at 200 rpm at room temperature. After 7 days or 24 hr, 8×1.0 mL aliquots of release medium (DI water) from each film sample were tested via UV-Vis spectroscopy (Model 8453, Agilent Diode Array, Santa Clara, CA) at an absorbance of 293 nm[197,198]. The absorbance of each aliquot was averaged and related to a CIN concentration based on a standard calibration curve. Total CIN (μg) released per film was calculated based on the 10 mL of release volume. After the 7 day trial, vials were refilled with DI water and retested after another 7 days to determine if there was any further CIN release. Throughout all testing, chitosan and chitosan/ Span®80 films were used as controls. Films were tested in triplicate.

6.3 Results and Discussion

6.3.1 Chitosan/CIN and Chitosan/Span®80/CIN Solution Characteristics

Figure 30 displays the NMR spectra of chitosan, chitosan/CIN and chitosan/Span®80/CIN along with chitosan/Span®80 and Span®80/CIN controls. Span®80 spectra (not shown) has predominant peaks between 0.5-2.5 ppm and 3.4-5.5 ppm, whereas CIN has a characteristic aldehyde peak at 9.0 ppm, which is highlighted in grey on Figure 30.[208] From the chitosan spectra, it was determined[203–205] that the chitosan used throughout this work had a degree of *N*-acetylation of 5-7%. The presence of a peak at 9.5 ppm[208] corresponds to the amine group of chitosan reacting with the aldehyde, CIN. From the ratio of amines reacted with CIN over the total amount of amines, the degree of substitution (DS)[169] was determined to be 13% for chitosan/CIN solutions prepared with either 1:0.1 or 1:0.2 p:o mass ratios (no Span®80). Thus, the solution containing more initial CIN does not increase the DS, but does contain more unattached CIN, which is confirmed by larger peak of unreacted CIN present at 9.0 ppm.

However, when 0.1% Span®80 was incorporated with chitosan/CIN solutions (1:0.1, 1:0.2 and 1:1 p:o mass ratios), the unreacted CIN peak shifted to 9.34 ppm, which has been previously reported.[232] Solutions with Span®80 do not show evidence that a Schiff base has occurred. Span®80 NMR spectra (not shown) displays peaks between 0.5-2.5 ppm and 3.4-5.5 ppm, which would not overlap with the CIN or chitosan-CIN peaks.

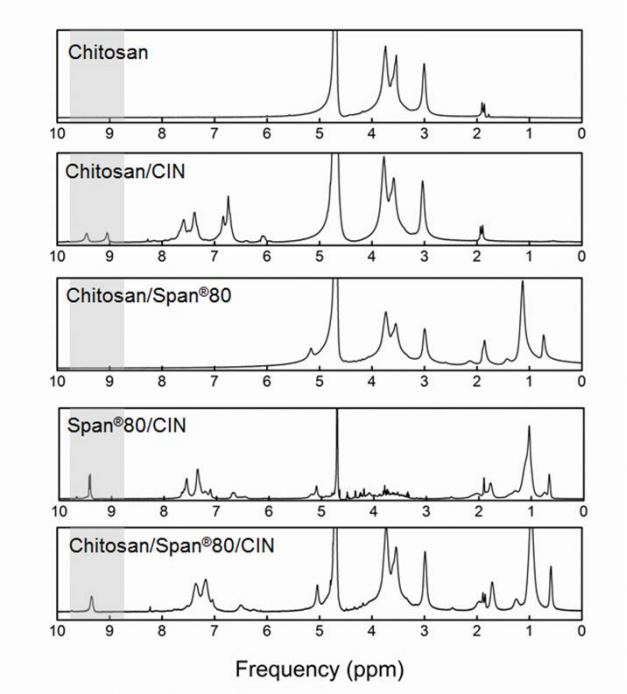

Figure 30: The ^{1}H NMR spectra (top-to-bottom) chitosan, chitosan/CIN, and chitosan/Span®80/CIN, along with control spectra of chitosan/Span®80 and Span®80/CIN. The concentrations utilized were 2.5% chitosan, 0.1% Span®80 and a p:o mass ratio of 1:0.1.

6.3.2 Chitosan/Span®80/CIN and Chitosan/CIN Thin Film Characteristics

Spin-coating successfully produced control chitosan films and films incorporating CIN and Span®80/CIN, (Figure 31). Consistent with the work of Zodrow et al.[162], 1.0% CIN correlating to a 1:0.1 p:o mass ratio was the highest loading of that could be add to the polymer matrix and spin-coated uniformly. However, by introducing 0.1% of the

surfactant, Span®80, the concentration of CIN that could be processed into spin-coated films increased to 5.0% correlating to a 1:1 p:o mass ratio. The digital images displayed in Figure 31 show an apparent change in color, which qualitatively confirms that increasing concentrations of CIN and Span®80/CIN have been incorporated within the films.[233] Initial experiments determined that 0.1% Span®80 was the lowest concentration to produce visually uniform films.

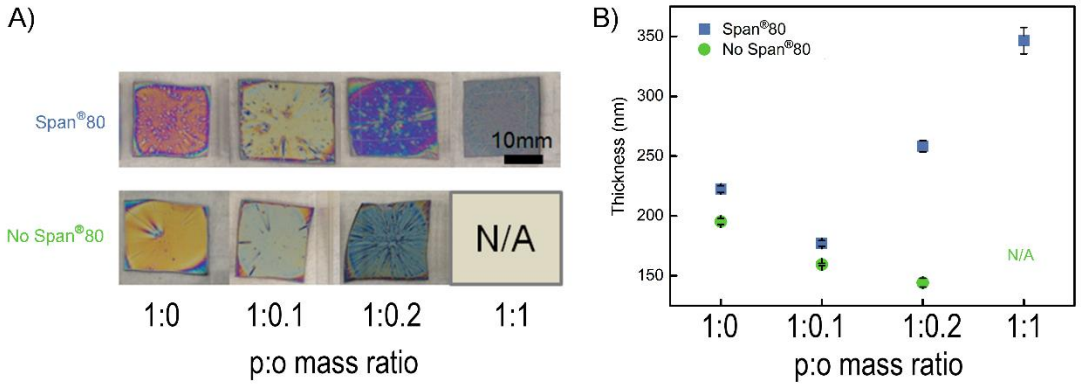

Figure 31: (A) Digital images of spin-coated chitosan films display an apparent change in color, which qualitatively confirms that increasing concentrations of CIN (bottom row) without Span®80 and (top row) with Span®80 have been incorporated within the films. (B) Thicknesses of chitosan films containing CIN without Span®80 and with Span®80 are displayed. A decrease in thickness is observed for chitosan films without Span®80 as CIN increased while with Span®80, the thickness increases after an initial drop in thickness for chitosan/CIN (1:0.1 p:o) films. All solutions were spin-coated from 2.5 w/v% chitosan. Concentrations above chitosan/CIN (1:0.2 p:o) could not be spin-coated without the aid of Span®80, as denoted by "N/A".

Table 4 displays the average thickness of all spin-coated films, which statically were all different. Control chitosan films (no CIN or Span®80) were found to have a thickness of 195.3 ± 2.5 nm (yellow), comparable to Murray and Dutcher's findings.[234] At p;o mass ratios of 1:0.1 and 1:0.2, the average thickness of chitosan/CIN films decreased to 159.5 ± 1.0 nm (green) and 144.3 ± 3.7 nm (aqua), respectively. This decrease is likely

due to phase separation caused by the addition of CIN. Such separation weakens intermolecular forces, thus decreasing the resistance to centrifugal forces during coating, resulting in thinner films.[235] The initial addition of Span®80 (no CIN) to chitosan resulted in the fabrication of films with an average thickness of 222.5 ± 1.0 nm (magenta). For chitosan/Span®80 films, at a p:o mass ratio of 1:0.1 the film thickness initially decreased but further addition of CIN (p:o mass ratios of 1:0.2 and 1:1) continually increased the overall film thickness to 188.1 ± 2.3 (yellow), 258.3 ± 2.8 (aqua), and 246.5 ± 11 (magenta), respectively. The addition of the surfactant should help to stabilize the two phases leading to less separation and stronger intermolecular forces, thus increasing the resistance to centrifugal forces during coating resulting in thicker films.

Table 4: Thickness and Contact Angle of Chitosan/CIN and Chitosan/Span®80/CIN Spin Coated Thin Films.

	p:o mass ratio	Thickness (nm)	θ_A (°)	θ_R (°)	$\theta_{hysteresis}$ (°)
No Span®80	1:0	195.3 ± 2.5	56.5 ± 1.1	31.8 ± 1.2	24.7
	1:0.1	159.5 ± 1.0	60.1 ± 1.0	29.8 ± 0.7	30.3
	1:0.2	144.3 ± 3.7	49.7 ± 0.9	29.3 ± 0.9	20.4
Span®80	1:0	222.5 ± 2.8	73.3 ± 0.4	27.8 ± 0.3	45.5
	1:0.1	177.1 ± 2.3	66.5 ± 1.4	18.2 ± 0.5	48.3
	1:0.2	258.3 ± 4.8	73.0 ± 0.5	19.4 ± 0.7	53.6
	1:1	346.5 ± 11	69.9 ± 1.2	15.9 ± 0.5	54

The thickness, as measured by profilometer, and the advancing (θ_A), receding (θ_R), and hysteresis θ_H contact angles of DI water, are shown as average ± standard deviation.
p:o mass ratio is the polymer:oil ratio, specifically the chitosan:CIN ratio
*All film thicknesses were statistically different from one another.
** Statistically significant increase in advancing and decrease in receding contact angles was observed due to the addition of Span®80. Therefore, the addition of Span®80 results in higher hysteresis, indicating lower heterogeneity and surface roughness.

All films were determined to be hydrophilic from DI water advancing and receding contact angle measurements,

Table 4. This suggests that CIN, a hydrophobic substance, was effectively incorporated rather than being on the surface of the film. The addition of Span®80 to films resulted in a statistically significant increase in the advancing and decrease in receding contact angles. Contact angle hysteresis increases for films with Span®80 when compared to films with no Span®80. Hysteresis has been correlated most strongly with decreases in heterogeneity and/or surface roughness,[196,236] both of which have been reported to increase with a surfactant present[237].

6.3.3 Release Characteristics of Chitosan/Span®80/CIN and Chitosan/CIN Spin Coated Thin Films

The quantity of CIN released from chitosan/CIN and chitosan/Span®80/CIN thin films over a 24 hr and a 7 day period was determined using UV-Vis (Figure 32). After 24 hr, chitosan/CIN (1:0.1 and 1:0.2 mass ratios) films containing released approximately 4-5 μg with no statistical difference. Thus, increasing past p:o 1:0.1 mass ratio in chitosan/CIN films did not result in additional CIN release. There was no increase in release after 7 days indicating that all "releasable CIN" was released in the first 24 hr. Films containing Span®80 demonstrated increased release for increased CIN incorporation. After 24 hr, chitosan/Span®80/CIN films at p:o mass ratios of 1:0.1, 1:0.2 and 1:1 released 8.8 ± 0.3, 17.6 ± 0.6, 29.0 ± 1μg, respectively. No appreciable changes in CIN released during a 7 day release period were observed. Thus, Span®80 can effectively be used to incorporate and release higher levels of CIN. To ensure all "releasable" CIN was released, all 7 day period samples were drained and refilled with 10 mL of fresh DI water. After 7 more days, no CIN was found to be release from any of the films. The governing mechanism of CIN release from both chitosan and chitosan/ Span®80 is swelling-controlled, which is highly pH dependent.[211,212] As the majority of CIN in all films is physically incorporated, the

swelling of chitosan will allow CIN to diffuse through the polymer network following Fickian diffusion.[213]

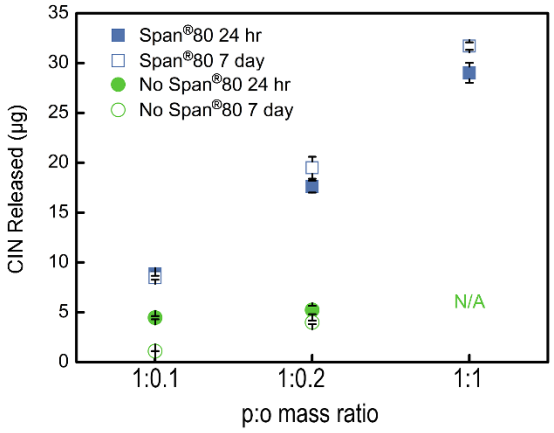

Figure 32: The quantity of CIN released from chitosan/CIN and chitosan/Span®80/CIN thin films over a 24 hr and 7 day period was determined through UV-Visible spectroscopy. Chitosan and chitosan/Span®80 films were utilized as controls. P:o mass ratios above 1:0.2 could only be spin-coated with the aid of Span®80 and is denoted by the N/A placeholder.

6.4 Conclusion and Future Work

We have demonstrated that spin-coating can be used to incorporate and deliver high-loadings of a model essential oil, cinnamaldehyde (CIN), from ultrathin chitosan films. When facilitated by the surfactant, Span®80, up to a 1:1 chitosan/CIN p:o mass ratio can be encapsulated within chitosan films. Because of the different loadings of CIN, all films fabricated had statistically different thickness, but remained under 350 nm with well-defined structural color. NMR indicated that a majority of the CIN was physically incorporated into the hydrophilic chitosan films. A 6 × higher release of CIN was enabled using Span®80. These natural plant and polysaccharide based bioactive films hold potential for use as bioactive coatings in food packaging and on indwelling medical devices.

A comparison of the aging and storage of these thin films with and without the addition of Span®80 should be an objective of future work to highlight the role of the

surfactant in encapsulating the volatile oil. In particular, it would be also interesting to compare the storage of thin films with electrospun nanofibers to determine which fabrication method best encapsulates volatile oils. Due to the higher release that was enabled by the addition of a surfactant, chitosan/PEO/CIN nanofiber mats should be electrospun with a surfactant to determine if the properties from thin films translate directly to electrospun mats. Additional experiments that could further elucidate the surfactant's role on solution viscosity and C_e concentration would be viscosity stress sweeps. These should be performed on the precursor electrospun solutions to be able to compare to the work within this document.

CHAPTER 7
UPTAKE OF BACTERIA INTO ELECTROSPUN NANOFIBERS

Adapted from: Rieger, K. A.; Thyagarajan, R.; Hoen, M. E.; Yeung, H. F.; Ford, D. M.; Schiffman, J. D., Transport of Microorganisms into Cellulose Nanofiber Mats. *RSC Advances*, 2016, 6, 24438-24445.

7.1 Summary

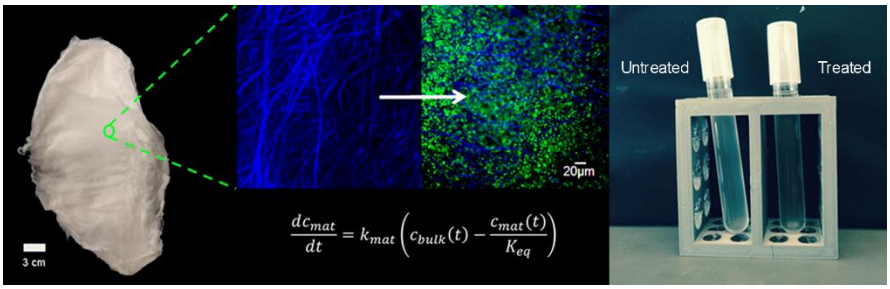

Figure 33: Cellulose nanofiber mat "sponges" are a green platform technology that has the potential to remove detrimental microorganisms from wounds, trap bacteria within a protective military textile, or remediate contaminated water.

Nanofiber mats hold potential in numerous applications that interface with microorganisms. However, a fundamental study that quantifies the transport of microorganisms into three-dimensional microenvironments, such as, nanofiber mats, has not yet been conducted. Here, we evaluate the microbial uptake capacity of three hydrophilic cellulose sorbents, a high surface area electrospun nanofiber mat, as well as two commercial products, a macrofibrous Fisherbrand fabric and an adsorptive Sartorius membrane. The small average fiber diameter (~1.0 μm) and large porosity of the nanofiber mats enabled a 21 times greater collection of *E. coli* K12 per milligram of material than the macrofibrous Fisherbrand controls and 220 times more than the Sartorius controls. In most cases, the exposure time of the nanofiber mats to the microorganisms was sufficient to reach a quasi-equilibrium state of microbial uptake, allowing the calculation of an adsorption coefficient (Keq) that relates the concentration of cells in the sorbent to the

concentration of cells remaining in solution. The Keq of the nanofiber mats was 420, compared to 9.2 and 0.67 for the Fisherbrand and Sartorius controls, respectively. In addition to *E. coli*, we studied the cellulose nanofiber mats uptake of two additional medically relevant and distinct microorganisms, Gram-negative *P. aeruginosa* PA01 and Gram-positive *S. aureus* MW2, to probe whether microorganism removal is bacterial specific. The high uptake capacity of all three bacteria by the nanofiber mats indicates that microbial uptake is independent of the microorganism's adhesion mechanism. This work suggests that cellulose nanofiber mat "sponges" are a green platform technology that has the potential to remove detrimental microorganisms from wounds, trap bacteria within a protective military textile, or remediate contaminated water.

7.2 Methods

7.2.1 Cellulose Fiber Mat Fabrication

A 15% w/v solution of cellulose acetate in acetone[28] was mixed for 24 hr at 20 rpm using an Arma-Rotator A-1 (Bethesda, MA). The solution was loaded into a 5 mL Luer-Lock tip syringe capped with a Precision Glide 18 gauge needle (Becton, Dickinson & Co. Franklin Lakes, NJ), which was secured to a PHD Ultra syringe pump (Harvard Apparatus, Plymouth Meeting, PA). Alligator clips were used to connect the positive anode of a high-voltage supply (Gamma High Voltage Research Inc., Ormond Beach, FL) to the needle and the negative anode to a copper plate wrapped in aluminum foil. A constant feed rate of 3 mL/hr, an applied voltage of 25 kV, and a separation distance of 10 cm were used to spin cellulose acetate nanofiber mats. The assembled electrospinning apparatus was housed in an environmental chamber (CleaTech, Santa Ana, CA) with a desiccant unit (Drierite, Xenia, OH) to

maintain a temperature of 22 ± 1 ºC and a relative humidity of 55%. In this study, all cellulose acetate nanofiber mats were electrospun for 1 hr before being converted to cellulose nanofiber mats. As-spun mats sandwiched between Teflon sheets were thermally treated at 208 °C for 1 hr and then submerged in a 4:1 v/v solution of H_2O/ethanol containing 0.1 M NaOH for 24 hr.[30,238] The mats were then washed using DI water and placed in a desiccator for 24 hr at room temperature (23 °C) to dry.

7.2.2 Characterization of Electrospun Nanofiber Mat, Fisherbrand Control, and Sartorius Control

Micrographs were acquired using a FEI-Magellan 400 scanning electron microscope (SEM). A sputter machine (Gatan high resolution ion beam coater model 681) was used to coat samples with ~5 nm of platinum. Fiber diameter distribution was determined using *Image J 1.45* software (NIH, Bethesda, MD) by measuring 50 random fibers from 5 micrographs. A PerkinElmer Spectrum 100 Fourier transform infrared spectrometer (FTIR) confirmed that cellulose was regenerated after alkaline treatment of the as-spun cellulose acetate nanofiber mats.

A Zeiss Axiovert 4-laser Spinning Disc Confocal microscope (Zeiss confocal, 20× magnification) was used to collect z-stack composite images of cellulose nanofiber mats fluorescently dyed with calcofluor white stain (1 μL/mL). The 3D composite images from Zen software were imported to *Image J 1.45* software from which the average thickness of the nanofiber mats was determined by averaging 50 thickness measurements taken from 5 different nanofiber mats (Figure 34). The thicknesses of the Fisherbrand and Sartorius controls were measured using a Mitutoyo micrometer (Aurora, IL).

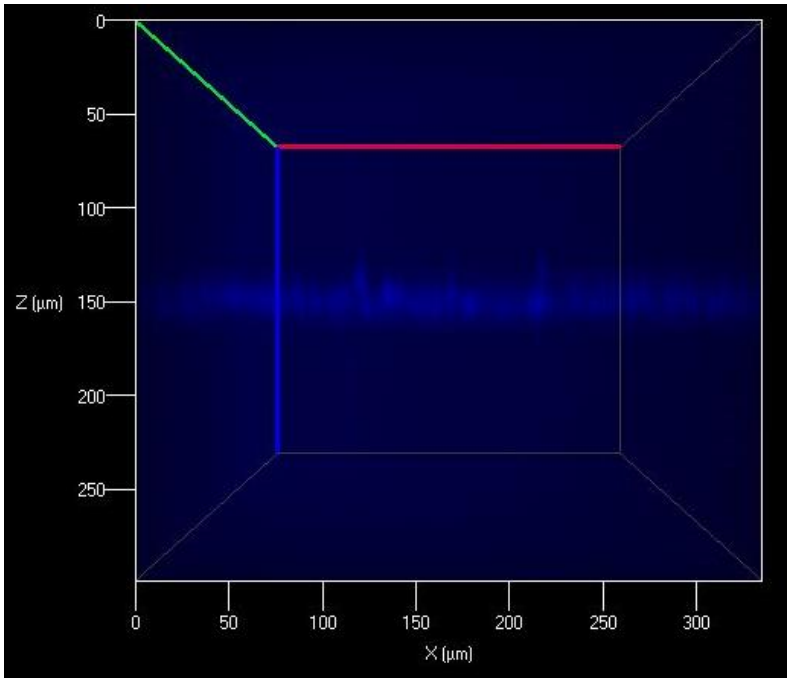

Figure 34: Representative z-stack composite image displays the cross-section of a nanofiber mat. Measurements were utilized to obtain the average thickness of the nanofiber mats, 50 measurements were obtained using 5 different nanofiber mats stained with calcofluor white.

Average thickness was multiplied by surface area to calculate nanofiber mat volume, V_{mat}. The total internal surface area of the nanofiber mats was estimated using an Autosorb®-iQ system (Quantachrome) using 50 mg of nanofiber mat that were degassed for 2 hr at 150 °C. The total surface area was calculated for the nanofiber mat using the Brunauer–Emmett–Teller (BET) method.[239] The surface area of the Fisherbrand and Sartorius controls was too low to be estimated using BET.

7.2.3 Quantification of Bacteria Uptake by the Nanofiber Mat, Fisherbrand Control, and Sartorius Control

E. coli K12 and *P. aeruginosa* PA01 were purchased from Leibniz Institute DSMZ (Germany). *S. aureus* MW2 was a kind gift from Prof. Neil Forbes at the University of Massachusetts Amherst. Bacteria were grown in Luria Broth at 37 °C

and re-suspended in a phosphate buffered saline solution (PBS, pH 7.2) to remove residual macromolecules and other growth medium constituents. Throughout the experiment, no external forces were applied. For experiments where killed bacteria was needed, bacteria were soaked in a 70% ethanol solution for 1 hr prior to use.

Using 6-well plates, each porous sorbent (nanofiber mat, Fisherbrand control, and Sartorius control) was punched into a circle with a diameter of 2.54 cm and incubated in a bacterial solution with an initial concentration of 1.52×10^8 cells/mL (5 mL per well). A control sample (no sorbent, bacteria solution only) was run in parallel to each experiment and six trials for each sorbent were performed. Additional experiments were conducted as a function of nanofiber mat diameter (2.54, 2.22, 1.91, and 1.27 cm) and initial *E. coli* K12 concentration (1.52, 4.46, 6.32 $\times 10^8$ cells/mL). For all experiments, the sorbents were incubated for 2 hr at 37 °C at 150 rpm; over this period of time a portion of the bacteria transferred from the surrounding solution to the sorbent. The optical density of the solution in both the sample and control well were monitored using the McFarland 0.5 standard, which is equal to $1\text{-}2\times10^8$ cells/mL.[200] Concentrations were measured using a BioTek EL×800 Absorbance Microplate Reader at an absorbance of 600 nm. A calibration curve (Figure 35) was developed to convert the microplate reading to optical density, and then to cell concentration. These concentrations were confirmed using plate counting. To calculate the total number of cells removed by the sorbent at time, *t*, we calculated the difference between the concentration of bacteria in the sample well containing a sorbent and the concentration of bacteria in the control well.

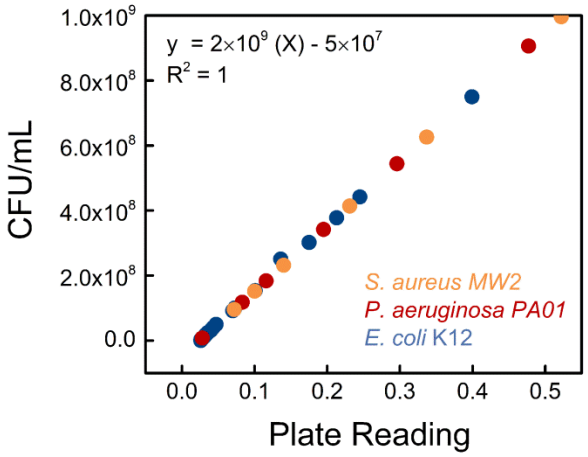

Figure 35: Calibration curve used to convert plate readings (600 nm) to CFU/mL for *S. aureus* MW2, *P. aeruginosa* PA01, and *E. coli* K12.

A Zeiss confocal (20× magnification) was used to (1) collect micrographs that qualitatively confirmed *E. coli* K12 collection by the nanofiber mat, Fisherbrand control, and Sartorius control, and (2) to examine where within the sorbents the bacteria collected. Cellulose was dyed fluorescently with calcofluor white stain (1 μL/mL) and *E. coli* K12 was tagged using a plasmid green fluorescent protein. Zen Software was used to generate 3D composite images.

7.2.4 Modeling of Bacteria Uptake by the Nanofiber Mats

The quantity of *E. coli* K12 collected at the longest time (t = 120 min), for the largest mat (2.54 cm), as a function of initial cell concentration was used to determine a quasi-equilibrium model. The adsorption coefficient, K_{eq}, from the equilibrium model was utilized to build a dynamic model to capture the transient behavior[240,241] of the collection of bacteria into the nanofiber mats of various mat diameters. A first-order kinetics model, with external transport mechanisms assumed to be controlling, was postulated based on observations of the data. The model was fit to time-dependent uptake data for the four different mat diameters, at

one initial concentration. The dependence of the fitted rate constant k_m on mat diameter was examined.

7.3 Results and Discussion

7.3.1 Characteristics of the Electrospun Nanofiber Mat, Fisherbrand Control, and Sartorius Control

Cellulose acetate was successfully electrospun and converted via alkaline treatments to regenerated cellulose nanofiber mats (Figure 39). Consistent with literature,[28,30] the as-spun cellulose acetate nanofibers, as well as the cellulose nanofibers had a ribbon morphology (Figure 36).

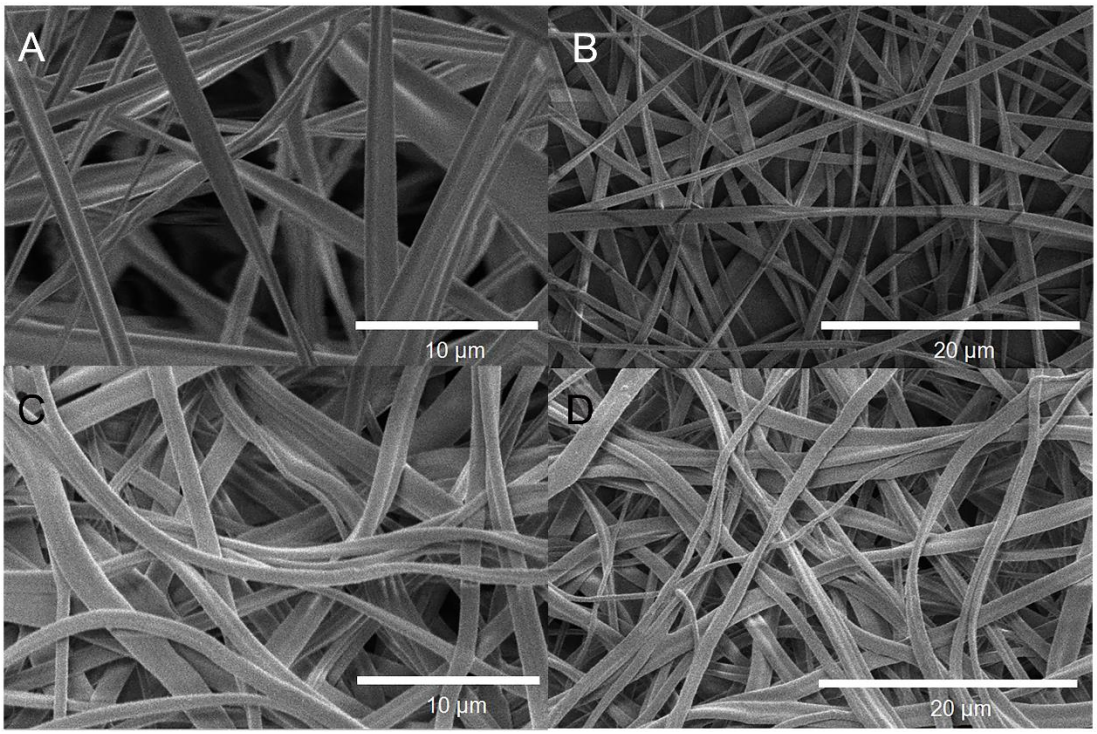

Figure 36: Micrographs of (A and B) as-spun cellulose acetate nanofiber mat, as well as the (C and D) cellulose nanofiber mat.

The materials properties of the nanofiber mats are summarized in Table 5**.** From SEM micrographs, the average fiber diameter of the cellulose nanofiber mats was

determined to be 1.08 ± 0.46 μm. Figure 37 displays the fiber diameter distribution of the electrospun nanofiber mats.

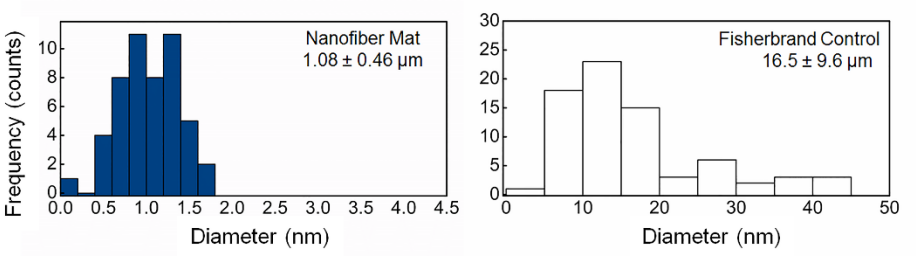

Figure 37: Fiber diameter distribution for the (Left) cellulose nanofiber mat and (Right) the Fisherbrand control as determined using ImageJ software on SEM micrographs. The average fiber diameter and standard deviation of 50 random fiber diameters are also provided.

FTIR spectra of the as-spun cellulose acetate and the cellulose nanofiber mats is displayed on Figure 38. Notably, the disappearance of the 1750 cm^{-1} peak indicates that the acetate groups have been replaced with hydroxyl groups.[238] Detailed description of the characteristics peaks are also shown in Figure 38. The total surface area of the cellulose nanofiber mats was estimated to be 4.5 m^2/g, which is consistent with literature, Figure 38.[242] All nanofiber mats were electrospun for 1 hr; the bulk thickness of the nanofiber mats was determined to be 42.4 ± 12 μm using confocal microscopy. In general, the regenerated cellulose nanofiber mats were consistent with regard to their fiber diameter [28,30,238], morphology [30,243], and surface area [187] to cellulose nanofiber mats previously reported in the literature.

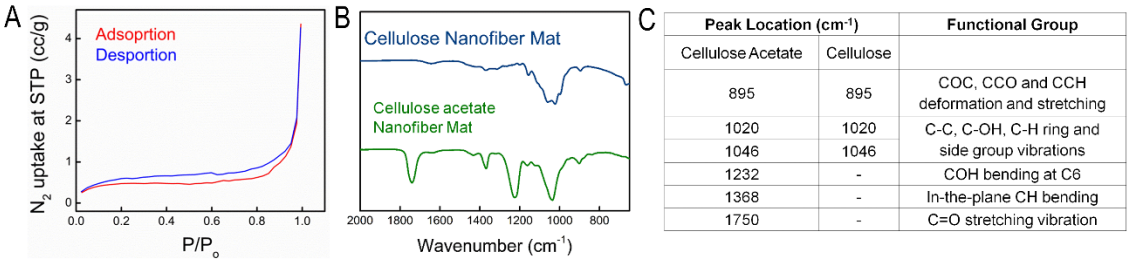

Peak Location (cm^{-1})		Functional Group
Cellulose Acetate	Cellulose	
895	895	COC, CCO and CCH deformation and stretching
1020	1020	C-C, C-OH, C-H ring and side group vibrations
1046	1046	
1232	-	COH bending at C6
1368	-	In-the-plane CH bending
1750	-	C=O stretching vibration

Figure 38: (A) The surface area of the cellulose nanofiber mat was determined to be 4.5 m2/g using an Autosorb®-iQ system. The surface area of the Fisherbrand and Sartorius controls was too low to be estimated using the Autosorb®-iQ system. (B) FTIR spectra of the as-spun cellulose acetate nanofiber mat and the cellulose nanofiber mat are displayed. (C) Characteristic FTIR peaks for cellulose acetate and cellulose nanofiber mat are summarized in the table.

We compared our nanofiber mats to two model commercial controls, Fisherbrand and Sartorius, Figure 39. All three sorbents had the same cellulose chemistry ─ a promising polymer for protective clothing,[244] wound bandages,[245] filtration, and adsorption,[246] as well as a similar fiber morphology (on different length scales). Additionally, the Fisherbrand and Sartorius materials have previously served as controls to electrospun cellulose nanofiber mats in studies that quantified the adsorption of proteins.[247,248]

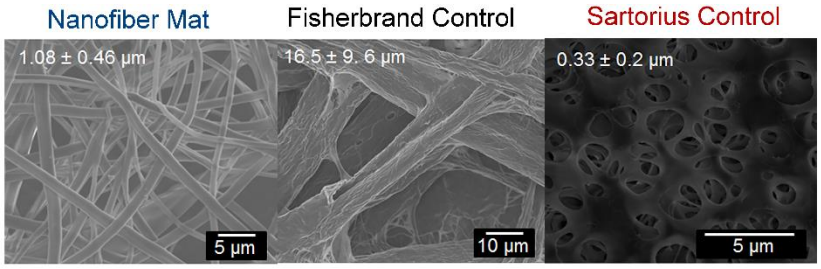

Figure 39: SEM micrographs display the morphology and average fiber diameter of cellulose sorbents: nanofiber mat, Fisherbrand control, and Sartorius control.

Table 5: Summary of the materials properties of cellulose sorbents: electrospun nanofiber mat, Fisherbrand control, and Sartorius control.

		Nanofiber Mat				Fisherbrand	Sartorius
Material Property	Fiber Diameter (µm)	1.08 ± 0.46				16.5 ± 9.6	0.33 ± 0.2
	Total Surface Area (m^2/g)	4.5				N/A	N/A
	Mat Thickness (µm)	42.4 ± 12				151.6 ± 4.9	154.7 ± 5.5
	Mat Diameter (cm)	2.54	2.22	1.91	1.27	2.54	2.54
	Mat Volume (cm^3)	0.0215	0.0164	0.0121	0.0054	0.0765	0.0780
	Mat Weight (mg)	9.3 ± 1.8	6.18 ± 1.0	4.0 ± 0.8	1.8 ± 0.3	35.6 ± 1.0	37.4 ± 0.7
	Density (mg/cm^3)	432.6	376.8	330.6	333.3	465.4	479.5

The materials properties of the Fisherbrand and Sartorius controls are summarized in Table 5. The Fisherbrand control contains cellulose macrofibers with an average fiber diameter of 16.5 ± 9.6 μm, an order of magnitude larger than our electrospun nanofiber diameter. The fiber diameter distribution of the Fisherbrand controls is provided in Figure 37. While individual Fisherbrand control fibers are generally cylindrical and continuous, they appeared less smooth than the electrospun nanofibers. The average thickness of the Fisherbrand control was 151.7 ± 4.9 μm. Analogous to the nanofiber mat, the Sartorius control is regenerated cellulose; micrographs display that it had a webbed-fiber morphology, Figure 39. The average diameter of the webs were 0.33 ± 0.2 μm, the pores had an average diameter of 1.70 ± 0.6 μm, and the overall thickness of the Sartorius control was determined to be 154.7 ± 5.5 μm. The surface area was too low to be estimated for the Fisherbrand and Sartorius controls.

7.3.2 *E. coli* K12 Uptake by the Nanofiber Mat, Fisherbrand Control, and Sartorius Control

While the use of nanofiber mats as effective size selective sieves has been extensively studied,[249–252] the demonstration that nanofiber mats can serve as a simple, inexpensive way to uptake bacteria from a wound is an emerging concept that has not yet been quantified.[185,253] Ideally, a lightweight nanofiber mat could simply be placed within the contaminated area and removed after bacteria have transported into the mat.

The total number of *E. coli* K12 cells collected over 120 min by the electrospun nanofiber mat, Fisherbrand control, and Sartorius control is shown in Figure 40. After 120 min, the nanofiber mat collected 4.2 and 55.3 times more *E. coli* K12 cells than the Fisherbrand and Sartorius controls, respectively. Per milligram, the nanofiber mat collected 21and 220 times more *E. coli* K12 than the Fisherbrand and Sartorius controls,

respectively. When we compare our nanofiber mat to data previously published on activated carbon, our nanofiber mat uptakes approximately 16 times more *E. coli* K12 cells per milligram of material.[254] Digital images taken before and after the nanofiber mats were used as sponges show that the water visually changed from opaque to clear indicating that there was a significant amount of microorganisms removed (Figure 40). The number of *E. coli* K12 cells adsorbed per mass, volume, and surface area are summarized in Table 6.

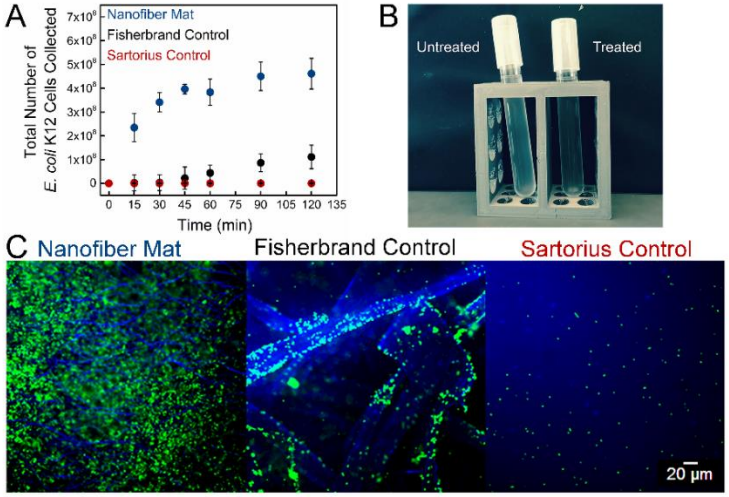

Figure 40: (A) The total number of *E. coli* K12 collected by the nanofiber mat, Fisherbrand control, and Sartorius control over 120 min. Error bars represent the standard deviation of six trials. (B) Digital pictures of the initial cloudy *E. coli* K12 solution (time = 0 min) and the clear solution after 120 min treatment with a nanofiber mat. (C) Fluorescent micrographs of nanofiber mat, Fisherbrand control, and Sartorius control acquired after 120 min of incubation with *E. coli* K12. All cellulose sorbents fluoresce blue, and *E. coli* K12 fluoresce green. The scale bar displayed is 20 µm. For (A, B, and C) The initial concentration of E. coli K12 was 1. 52 × 108 cells/mL and a constant sorbent diameter of 2.54 cm was used.

Fluorescent micrographs in Figure 2C were used to (1) confirm qualitatively that the nanofiber mats collected more bacteria than the controls and to (2) gain insight into where the bacteria physically collected on the cellulose sorbents. Visually, it is evident that many more green fluorescent *E. coli* K12 cells collected on the nanofiber mats than on the Fisherbrand or Sartorius controls. On the nanofiber mat, the bacteria appear to be both attaching to the nanofibers and filling the void space between the nanofibers. Confocal z-

stack images were acquired at three points during the bacteria collection experiments (t = 15, 60, and 120 min), which confirmed that bacteria were always present throughout the entire nanofiber mat; after only 15 min of collection no gradient was observed.

Table 6: Summary of the *E. coli* K12 removal capacity of cellulose sorbents: electrospun nanofiber mat, Fisherbrand control, and Sartorius control.

		Nanofiber Mat				Fisherbrand	Sartorius
	Mat Diameter (cm)	2.54	2.22	1.91	1.27	2.54	2.54
Total *E. coli* K12 at t = 120 min	Adsorption (cells)	4.61×10^8	4.32×10^8	3.59×10^8	1.16×10^8	1.11×10^8	8.34×10^6
	Adsorption (%)	72	52	44	14	12	1
	Adsorption per Weight (cells/mg)	4.98×10^7	6.99×10^7	8.97×10^7	6.43×10^7	3.11×10^6	2.23×10^5
	Adsorption per Volume (cells/cm^3)	2.15×10^{10}	2.63×10^{10}	2.97×10^{10}	2.16×10^{10}	1.45×10^9	1.07×10^8
	Adsorption per Surface Area (cells/m^2)	1.11×10^{10}	1.55×10^{10}	1.99×10^{10}	1.43×10^{10}	N/A	N/A

The Fisherbrand control exhibited poor cell adsorption. Fewer bacteria adsorbed onto the Fisherbrand control than the nanofiber mat and a majority of the *E. coli* K12 appeared to be attached to the macrofibers. The Fisherbrand control had a statistically higher average fiber diameter than our nanofiber mats. This suggests that increasing the fiber diameter of a sorbent does not increase adsorption. The lowest amount of bacteria uptake was achieved by the Sartorius control, where cells did not appear to be preferentially adsorbing onto the webbed-fibers or within the pore voids. This suggests that simply continuing to decrease the fiber diameter alone is not sufficient to increase bacteria uptake into fiber mats. Previous literature reports that higher adhesion of bacteria is possible by using surfaces that conform to their size, offer surface roughness, are porous, or have a higher surface area.[255] Our findings demonstrate that the *E. coli* K12, which are ~0.5 μm in width by 2 μm in length, prefer the high porosity nanofiber mats with a ~1 μm diameter over the Fisherbrand or Sartorius controls.

7.3.3 Equilibrium and Diffusion Kinetics of Bacteria Uptake by the Electrospun Nanofiber Mat.

Adsorption isotherm models, predominantly Langmuir isotherms, have been used to characterize microbial behavior in porous media.[174] To explore the applicability of an isotherm model to our nanofiber mats, we experimentally varied the initial *E. coli* K12 concentration (1.52×10^8, 4.46×10^8, 6.32×10^8 cells/mL) and measured uptake over time for the nanofiber mats with a diameter of 2.54 cm. The experimental data collected (Figure 41B) suggest that an equilibrium state with respect to the removal of cells from the solution is reached by 120 min for each of the initial *E. coli* concentrations.

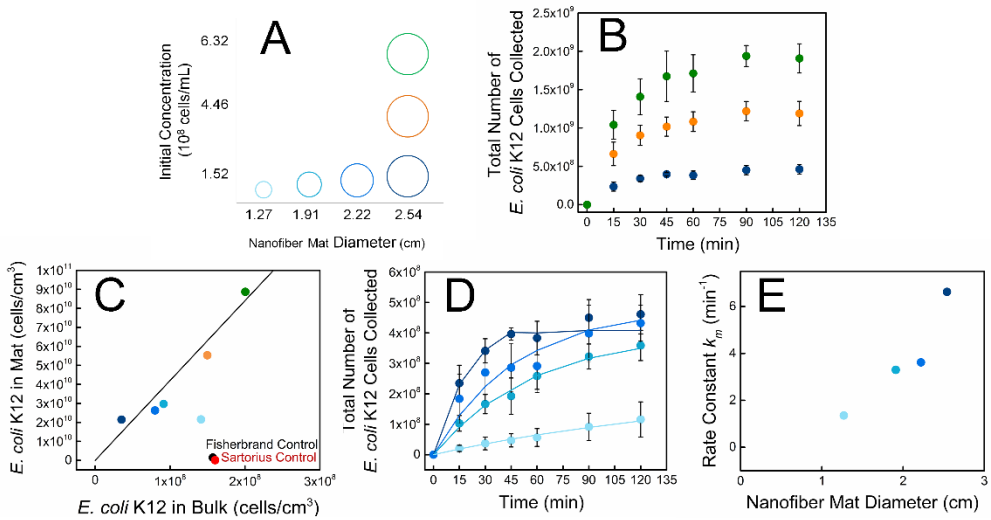

Figure 41: (A) Summary and color representation of the different conditions tested: three initial *E. coli* K12 concentrations (1.52 × 108, 4.46 × 108, 6.32 × 108 cells/mL) and four nanofiber mat diameters (1.27, 1.91, 2.22, 2.54 cm). (B) The total number of *E. coli* K12 collected as a function of initial cell concentration and time are displayed. The diameter of the nanofiber mat (2.54 cm) was held constant. (C) The concentration of *E. coli* K12 collected by the nanofiber mat vs. the concentration remaining in the bulk solution at t = 120 min. The subsequent quasi-equilibrium model (line) is derived from Figure B. The experimental data collected by varying nanofiber mat diameter (from Figure D), as well as the Fisherbrand control (black) and Sartorius control (red) are plotted to benchmark the model. (D) The total number of *E. coli* K12 collected as a function of nanofiber mat diameter and time. The initial concentration of cells was held constant at 1.52 × 108 cells/mL. The dynamic model (solid lines) predicts the uptake of bacteria as a function of nanofiber mat diameter and time. (B and D) Error bars represent the standard deviation of six trials. (E) The rate constants determined from the dynamic model increase with increasing nanofiber mat diameter.

Figure 41C is an adsorption isotherm created from the longest-time data points from Figure 41B. Here, the concentration of bacteria taken up by the 2.54 cm diameter nanofiber mat is plotted as a function of the concentration of bacteria remaining in the bulk solution, at t = 120 min. The three data points (darkest blue, yellow, green) lie on a straight line, suggesting that we are in the Henry's Law or linear regime of adsorption. The slope of a straight line fit of the data is the equilibrium adsorption coefficient, K_{eq}, which indicates the uptake capacity of the nanofiber mats, Equation 4.

Equation 4

$$c_m = K_{eq}\, c_b$$

where c_m is the concentration of bacteria inside the mat and c_b is the concentration of bacteria in the bulk solution. K_{eq} was determined to be 420 ± 82, with 95% confidence bounds; this means that a nanofiber mat will contain ~420 times as many *E. coli* K12 cells as an equal volume of solution at equilibrium. The K_{eq} of the Fisherbrand and Sartorius controls, were determined to be much lower 9.24 and 0.67, respectively. These values are plotted on Figure 41C as black and red points that lie well below the isotherm for the nanofiber mats, thus reiterating the impressive removal capability of the nanofiber mats. The data represented by the lighter-blue symbols in Figure 41C are described next.

To further understand the dynamics of the *E. coli* K12 uptake into the mats, we measured bacterial uptake over time for nanofiber mats of various diameters (1.27, 1.91, 2.22, and 2.54 cm) starting from the same initial concentration of 1.52×10^8 cells/mL, Figure 41D**.** After 120 min, it appeared that all of the nanofiber mats have (at least nearly) reached quasi-equilibrium except for the smallest diameter nanofiber mat (lightest blue circle), for which the data have still not begun to plateau. The overlay of the t = 120 min data for the three smaller-diameter mats onto the quasi-equilibrium model (Figure 41C)

confirms that all mats have reach quasi-equilibrium except the smallest nanofiber mat (lightest blue circle), which lies below the isotherm. The number of *E. coli* K12 removed per mass, volume, and surface area for all nanofiber mats at t = 120 min are provided in Table 6. The total removal capacity increased with increasing nanofiber mat diameter while the mass-, volume-, and area-normalized capacities fluctuate with no clear pattern, as expected.

A dynamic model was developed to describe the behavior seen in the experimental uptake data, under an assumption that transport processes external to the mat are controlling uptake. The data in Figure 41D clearly show that the rate of bacteria removal is greater for physically larger mats, which indicates that bacterial transport within the mat is not the rate-limiting process. Furthermore, z-stack confocal micrographs indicated that bacteria were uniformly distributed throughout the void space of the nanofiber mats at all-time points during adsorption experiments, which further confirmed that transport inside the nanofiber mat was not the rate limiting factor. Under the further assumption that the concentration difference between the mat and the bulk solution is driving the transport, Equation 5 was derived.

Equation 5

$$\frac{c_m(t)}{c_{b0}} = \frac{1}{\emptyset}\left[1 - e^{-\emptyset k_m t}\right]; \quad \emptyset = \frac{1}{K_{eq}}\left[1 + \frac{K_{eq}V_{mat}}{V_{sol}}\right]$$

where k_m is the first-order rate constant and the other symbols have been defined previously.

The solid curves in Figure 41D are the fits of the model to the experimental data. The variable k_m was the only fitted parameter in each case, as the values of all other variables are assumed known (including K_{eq} from the fit in Figure 41C). The overall quality

of the fits support the an apparent first-order kinetics for bacterial removal by the nanofiber mat, consistent with Liu and Ford's report that bacteria may aggregate in a thin layer outside of a porous medium (50 to 500 μm diameter spherical particles) before diffusing in from there.[176]

The values of the rate constant, k_m, as estimated from the dynamic model fits are shown as a function of nanofiber mat diameter in Figure 41E. The geometry of the experiment is such that the mat is a two-dimensional target floating on the surface of the bacterial solution covering only a fraction of that surface. If the *E. coli* K12 removal were controlled by external diffusion or some other process that is limited by the rate at which the cells reach the surface of the mat, then one would expect k_m to scale with the surface area of the mat, i.e., with the square of the mat diameter. Figure 41E displays that the dependence of k_m on the nanofiber mat diameter does indeed appear to have nonlinear, possibly a quadratic character. Overall the results confirm that some external process, which is dependent on the geometry of the mat within the test well, is controlling bacterial uptake in our experiments.

7.3.4 Nanofiber Mat Uptake Additional Microorganisms

High surface-to-volume area nanofiber mats featuring 1 μm diameter fibers hold potential as sponges that can efficiently remove *E. coli* K12 from a contaminated area such as a wound. As a further proof-of-concept we challenged the nanofiber mat with an additional model Gram-negative microbe, *P. aeruginosa* PA01, as well as with the model Gram-positive microbe, *S. aureus* MW2, Figure 42. At t = 120 min, the nanofiber mat collected statistically more *S. aureus* MW2 (6.28×10^8 cells) and *P. aeruginosa* PA01 (5.96×10^8 cells) than *E. coli* K12 (4.61×10^8 cells). Since these microbes have different transport

and adhesion mechanisms, we suggest that the ability of the nanofiber mats to remove microbes is independent of their adhesion mechanisms. *E. coli* have receptor specific binding through organelle, specifically type 1 frimbraie, auto transporter proteins, and aggregative frimbraie, that can permanently bind the bacteria to surfaces.[256] *S. aureus* lack these extracellular organelle and instead rely on protein adhesions through microbial surface components recognizing adhesive matrix molecules (MSCRAMM).[257,258] *P. aeruginosa* PA01 contain two distinct lipopolysaccharide (LPS) O-polysaccharide species, A- and B-band LPS, which control the surface hydrophobicity and surface charge on the bacteria thus dictating its ability to adhere to a material.[259] All of the bacteria strains tested have different adhesion mechanisms and thus, we suggest that the nanofiber morphology and void spaces within the electrospun mat predominantly dictate the removal capacity.

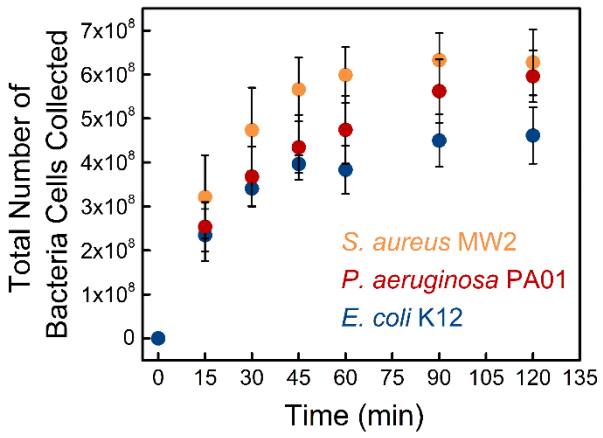

Figure 42: The total number of *S. aureus* MW2, *P. aeruginosa* PA01, and *E. coli* K12 collected as a function of time is displayed. An initial concentration of 1.52×10^8 cells/mL was used and the diameter of the nanofiber mat (2.54 cm) was held constant. Error bars represent the standard deviation of six trials.

7.3.5 Nanofiber Mats Uptake Killed Microorganisms

The uptake of viable *E. coli* K12 cells is compared to the uptake of killed *E. coli* K12 cells over time for cellulose nanofiber mats, Figure 43. At 120 min, nanofiber mats collected $8.9 \times 10^8 \pm 7.3 \times 10^7$ killed cells compared to $4.6 \times 10^8 \pm 6.4 \times 10^7$ viable cells. The higher

collection of dead cells might be due to changes in the surface properties of the bacteria and in particular, the changes in surface properties are related to the method of killing[260]. However, it is important to note the potential of nanofiber mats to uptake and remove both viable and killed cells.

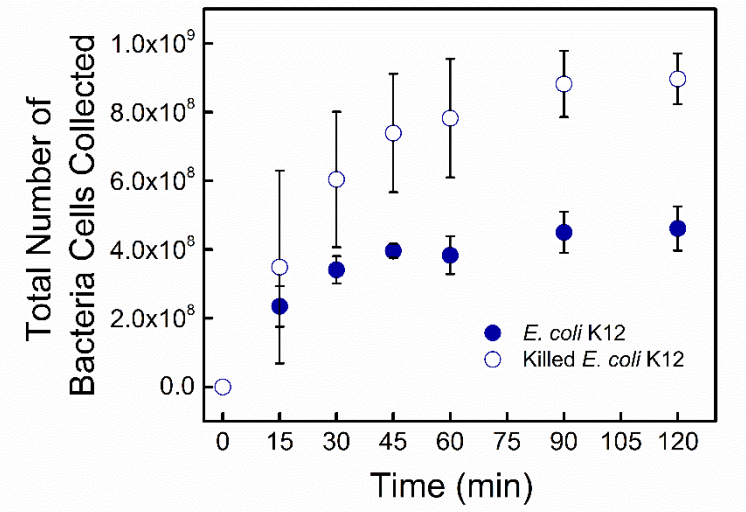

Figure 43: The total number of viable and killed *E. coli* K12 as a function of time is displayed. An initial concentration of 1.52×10^8 cells/mL was used and the diameter of the nanofiber mat (2.54 cm) was held constant. Error bars represent the standard deviation of six trials.

7.4 Conclusion and Future Work

Overall, the high adsorption of multiple microorganisms both viable and killed achieved by the electrospun cellulose nanofiber mats demonstrates their potential application as sponges. On a per milligram basis, the cellulose nanofiber mat collected 21 and 220 times more *E. coli* K12 than the Fisherbrand control and Sartorius control, respectively. While all sorbents had the same surface chemistry, the nanofiber mat demonstrated the best removal efficiency due to their ideal diameter fibers and larger available pore structures. By pairing the experimental data with the quasi-equilibrium model and diffusion kinetics of *E. coli* K12 removal, we provide insight into the properties and parameters that result in high microorganism removal using nanofiber mats.

Future objectives should focus around improving the method to determine the quantity of bacteria collected by a fibrous material. Currently, the bacteria range that can be tested must be within the linear concentration region for a plate reader at 600 nm. Testing the uptake capacity at very low levels of bacteria would provide insight on the usage of nanofibers where there is low contamination levels. Additionally, testing solutions containing multiple microorganisms would also be interesting but first an improved protocol capable of differentiating between strains being collected needs to be produced.

For majority of applications, bacteria are not usually within a pure solution and the presence of other particles could change the uptake profile of bacteria. Understanding and testing the competition between particles and bacteria from the surrounding solution into the nanofiber mat should be examined. While particles have no adhesion mechanism to attach the nanofiber mats, they could get trapped within the fibers depending on the pore and particle sizes. Lastly, another important aspect that should be considered is the ability to remove bacteria from the mat post collection for reusability. The protocols and methods described in this chapter should be able to be adjusted for this purpose.

CHAPTER 8
UPTAKE POLYELECTROLYTE COATED NANOFIBER MATS TO CONTROL COLLECTION AND INACTIVATION OF *E. COLI*

Adapted from: Rieger, K. A.; Porter, M.; Schiffman, J. D., Polyelectrolyte-Functionalized Nanofiber Mats Control the Collection and Inactivation of *Escherichia coli*. *Materials*, 2016, 9(4), 297.

8.1 Summary

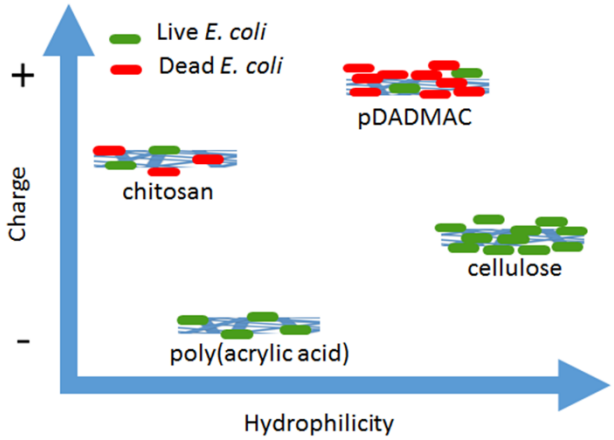

Figure 44: Functionalization of electrospun cellulose nanofiber mats with polyelectrolytes to tailor the collection and inactivation of *E. coli*.

Quantifying the effect that nanofiber mat chemistry and hydrophilicity have on microorganism collection and inactivation is critical in biomedical applications. In this study, the collection and inactivation of *Escherichia coli* K12 was examined using cellulose nanofiber mats that were surface functionalized using three polyelectrolytes: poly(acrylic acid) (PAA), chitosan (CS), and polydiallyldimethylammonium chloride (pDADMAC). The polyelectrolyte functionalized nanofiber mats retained the cylindrical morphology and average fiber diameter (~0.84 µm) of the underlying cellulose nanofibers. X-ray photoelectron spectroscopy and contact angle measurements confirmed the presence of polycations or polyanions on the surface of the nanofiber mats. Both the control cellulose

and pDADMAC-functionalized nanofiber mats exhibited a high collection of *E. coli* K12, which suggests that mat hydrophilicity may play a larger role than surface charge on cell collection. While, the minimum concentration of polycations needed to inhibit *E. coli* K12 was 800 µg/mL for both CS and pDADMAC, once immobilized, pDADMAC-functionalized nanofiber mats exhibited a higher inactivation of *E. coli* K12, ~97%. This effect may be due to a higher functionalization of pDADMAC vs CS on cellulose nanofiber mats. Here, we demonstrate that the collection and inactivation of microorganisms by electrospun cellulose nanofiber mats can be tailored through a facile polyelectrolyte functionalization process conducted on.

8.2 Methods

8.2.1 Cellulose Nanofiber Mat Fabrication

Details are provided in Chapter 7 Section 7.2.1.

8.2.2 Coating Electrospun Cellulose Mats with Polyelectrolytes

A chitosan solution was prepared by first dissolving chitosan in 0.5 M AA at a 2.5% w/v and then diluting to a 0.5 % w/v chitosan solution in 0.5 M AA. PAA and pDADMAC solutions were prepared by diluting the as-received stock solution to 0.5 w/v% in DI water. Before use, each diluted solution was first vortexed using a Fisher Scientific Analog Vortex Mixer (02215365). To coat, first an electrospun mat was punched into a circle with a 2.54 cm diameter using a Spearhead® 130 Power Punch MAXiset. Six mats at a time were submerged in a square petri dish containing 20 mL of one of the coating solutions described above. The petri dish was then placed onto a 120 V Lab Line 3-D rotator (model #4630) for 30 min. After rotation, the mats were removed from solution, rinsed with DI water, and dried for 24 hr.

8.2.3 Characterization of Polyelectrolyte Coated Electrospun Mats

The static contact angle was measured using an in-house apparatus and a Nikon camera. Each fiber mat was taped to a glass microscope slide to ensure that the sample was flat when the picture was taken. To form a droplet on the fiber mat sample, a solution of glycerol, obtained from Sigma Aldrich, was dropped from above the sample using a glass pipet. DI water and diiodomethane were also used but the droplets immediately absorbed into the samples. Data was collected in triplicate and analyzed using Image J 1.45 software (NIH, Bethesda, MD).

Micrographs were acquired using a FEI-Magellan 400 SEM. A sputter machine (Gatan high resolution ion beam coater model 681) was used to coat samples with ~5 nm of platinum. Fiber diameter distribution was determined using Image J 1.45 software (NIH Bethesda, MD) by measuring 50 random fibers from 5 micrographs.

High resolution scans were obtained using x-ray photoelectron spectroscopy (XPS, Physical Electronics Quantum 2000 Microprobe) to determine the chemical composition using the known sensitivity factors. A monochromatic Al X-rays at 50 W was used with a spot area of 200 μm and the take-off angle was set to 45°.

8.2.4 Quantification of Bacteria Uptake by Polymer Coated Electrospun Mats

Methods used are previously described in Chapter 7 Section 7.2.3.

8.2.5 Evaluation of Antibacterial Activity of Polyelectrolyte Coated Mats

Minimum inhibitory concentration (MIC), was determined for chitosan and pDADMAC based on a previously outlined procedure [200]. An overnight culture of *E. coli* K12, purchased from Leibniz Institute DSMZ (Germany) was prepared in Mueller Hinton Broth (MHB, Sigma Aldrich). A Fisherbrand polypropylene 96 well plate was filled with

an increasing concentration gradient of the chitosan and pDADMAC coating solutions, along with a Gentamycin antibiotic control. The concentrations of the chitosan and pDADMAC solutions started at 12.5 µg/mL and doubled at each well until 6400 µg/mL. The Gentamycin control started from 0.03 µg/mL and doubled until 16 µg/mL. Two columns of the well plate remained controls: the growth control contained MHB and bacteria and the sterile control contained only MHB. After the well plate incubated (37 °C) for 20 hr, the bacteria concentrations in each well were measured using a BioTek ELx800 Absorbance Reader at an absorbance of 600 nm.

Viability loss was determined using a previously described fluorescence assay described inChapter 4 Section 4.2.6.[111] Electrospun mats (2.54 cm diameter) were individually placed in a 6 well plate (Becton, Dickinson & Co., Franklin Lakes, NJ). Throughout the Results and Discussion section, all statistical differences were determined using an unpaired t-test with values of $p \leq 0.05$ considered to be statistically significant.

8.3 Results and Discussion

8.3.1 Characteristics of Polyelectrolyte Coated Cellulose Nanofiber Mats

Characteristics for cellulose nanofiber mats including fiber diameter, morphology, and surface area can be found in Chapter 7 Section 7.3.1.

Table 7: Summary of the Materials Properties of Polyelectrolyte Functionalized Electrospun Cellulose Nanofiber Mats

Polymer Coating	Average Fiber Diameter (µm)	Contact Angle (°)[1]	XPS (Atomic %)		
			C	N	O
N/A	0.85±0.22	35.9±4.8	56.2±4.3	-	41.6±1.8
PAA	0.75±0.20	54.5±9.7	56.3±5.6	-	42.5±4.6
Chitosan	0.84±0.21	69.2±7.4	62.5±3.3	2.3±1.4	35.2±4.0
pDADMAC	0.89±0.32	42.2±2.8	57.8±1.6	1.3±0.9	40.9±1.8

[1] Glycerol contact angle is reported. The water and diiodomethane contact angles were also tested but the solutions absorbed immediately into all nanofiber mats.

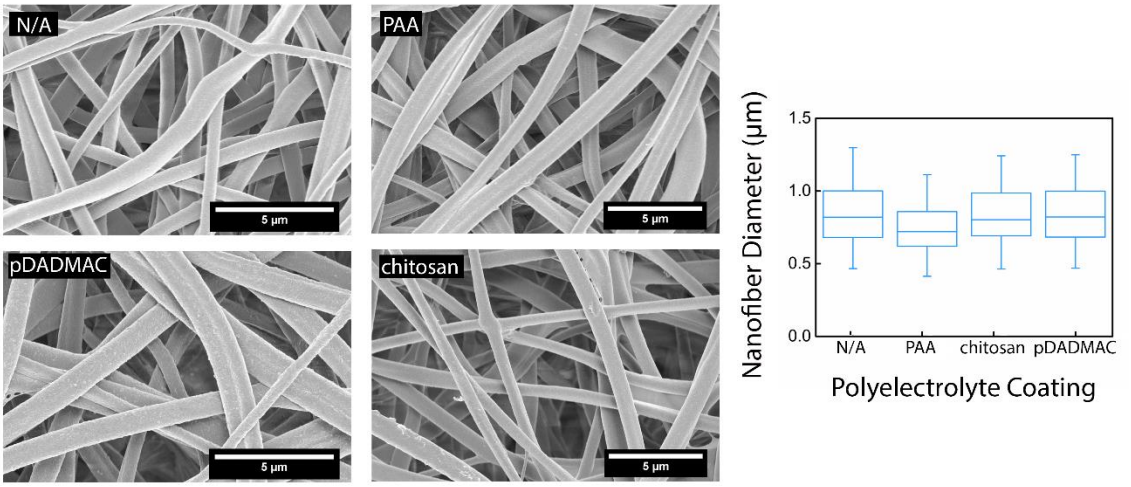

Figure 45: (Left) SEM micrographs of electrospun cellulose nanofiber mats without functionalization (N/A) and functionalized with PAA, CS, and pDADMAC. All scale bars are 5 µm. (Right) A box-and-whisker plot shows the median, lower and upper quartile, and the minimum and maximum value for the nanofiber diameter distribution for the cellulose nanofiber mats without any functionalization (N/A) and functionalized with PAA, CS, and pDADMAC. All nanofiber mats had a statistically equivalent average fiber diameter.

Cellulose nanofiber mats were functionalized with one of three different polyelectrolytes: PAA, an anionic polymer, as well as chitosan and pDADMAC which are cationic polymers. The average fiber diameter for each sample after undergoing the coating process was determined; there was no statistical change in average fiber diameter, Table 7. Based on SEM micrographs (Figure 45), post functionalization with PAA and chitosan, the nanofiber surface appeared smooth and the fiber morphology stayed intact. Nanofiber mats functionalized with pDADMAC appeared to have a textured surface but there was no indication of aggregation or that the coating was uneven.

Elemental data acquired using x-ray photoelectron spectroscopy (XPS) for carbon, nitrogen, and oxygen are summarized in Table 7. Consistent with previous literature [261], there was no statistical difference in the elemental data acquired on the control cellulose nanofiber mats and those functionalized with PAA. Nanofiber mats functionalized with chitosan and pDADMAC showed a statistical increase in nitrogen versus the control

cellulose nanofiber mats that lacked a coating. Functionalization using either pDADMAC or chitosan should result in the adsorption of the positively charged amine groups to negatively charged hydroxyl groups of cellulose due to electrostatic interactions.[262,263] Thus, this statistical difference supports the hypothesis that a surface functionalization with polycations was achieved.

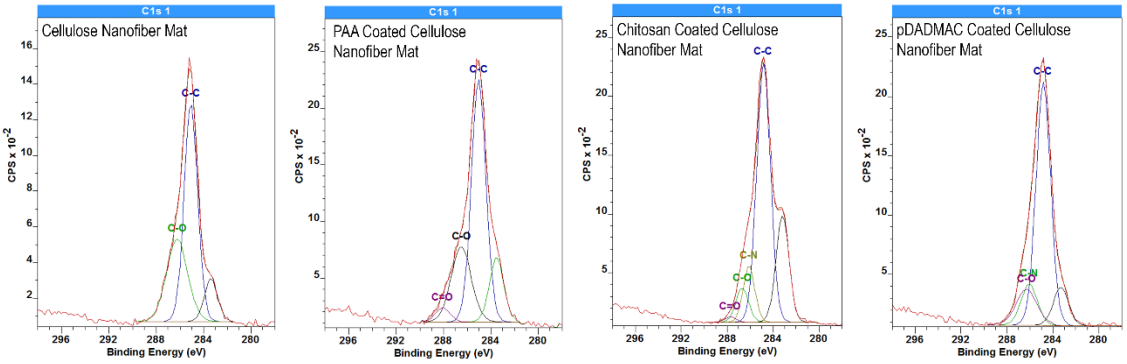

Figure 46: High resolution C 1s XPS spectra for cellulose nanofiber mats and PAA, chitosan and pDADMAC functionalized cellulose nanofiber mats. The individual contributions to the data from different functional groups such as C-C (285.0 eV), C-O (286.6 eV), C-N (287 eV) and C=O (287.9 eV) are provided. The unmarked curve at 283 eV is likely because the nanofiber mats are morphologically heterogeneous.

Figure 46 highlights the presence of PAA on the PAA-functionalized cellulose nanofiber mats; the PAA functionalized C1s spectrum show the presence of C=O component at 287.9 eV, which is absent in the cellulose C1s spectra. C1s spectra for cellulose and PAA functionalized cellulose nanofiber mats both resolve into contributions centered at 285.0 eV from the C-C and C-H functionalities. Additionally, at 286.6 eV, the C-O contribution of hydroxyl groups is present in both spectra. The unmarked curve at 283 eV is likely caused by “loose” nanofibers, which have a different neutralization time scale than bulk material, thus leading to morphologically heterogeneous samples.

Further chemical analysis was performed using FTIR. A comparison of control cellulose nanofiber mats (no coating), to mats functionalized with PAA, and chitosan and

pDADMAC, as well as, bulk PAA, chitosan and pDADMAC polymer controls are shown in Figure 47. No significant changes can be seen in the FTIR spectra after functionalization using chitosan or pDADMAC. However, an additional peak in the 1700 cm^{-1} region that correlates with the C=O of carboxylic acid became present after the cellulose nanofiber mats were functionalized with PAA [264]. The presence of this second peak (Figure 47, highlighted region) confirms that PAA-functionalization on the cellulose nanofiber mats was successful.

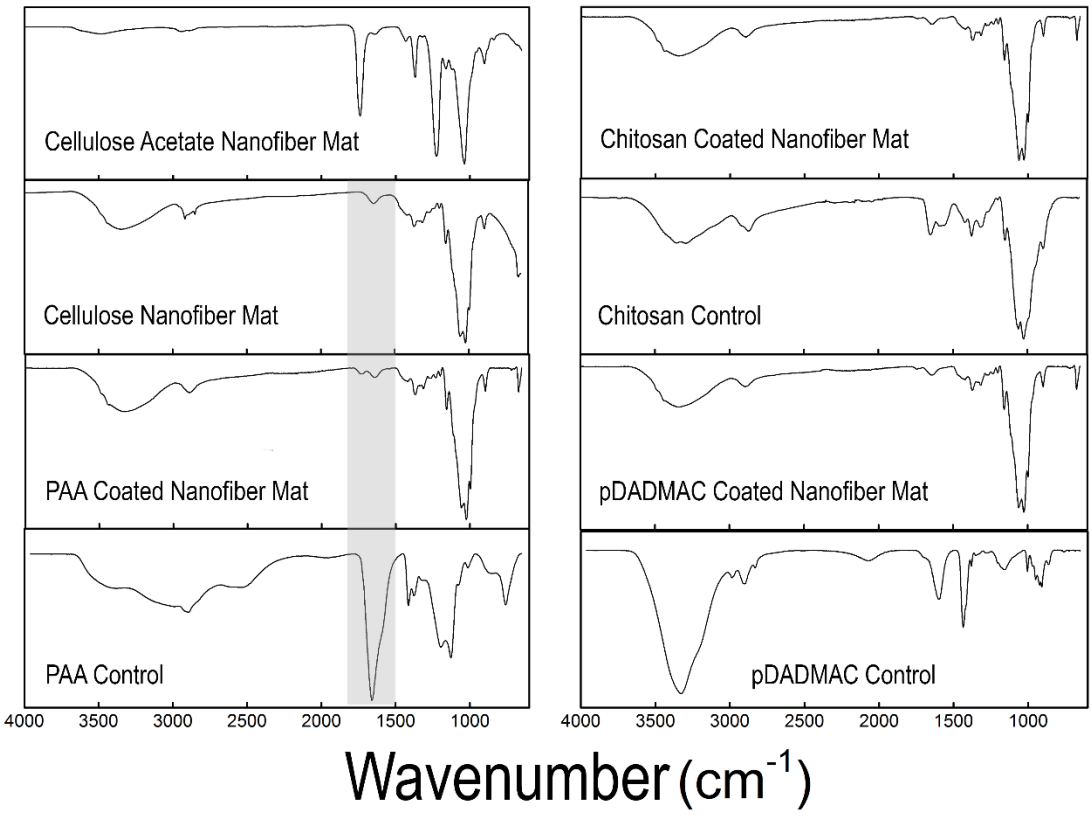

Figure 47: FTIR spectra of the as-spun cellulose acetate nanofiber mat and the regenerated cellulose nanofiber mat are displayed, along with the spectra for cellulose nanofiber mats functionalized with PAA, CS and pDADMAC. Control spectra for PAA, CS and pDADMAC are also provided. The highlighted region shows the addition of a peak in the 1700 cm^{-1} region that correlates with C=O of carboxylic acid for PAA functionalized cellulose nanofiber mats.

Contact angle measurements of the cellulose nanofiber mats with and without polyelectrolyte functionalization are shown in Figure 48 and on Table 7; measurements were performed using three solutions: water, glycerol and diiodomethane. Both water and diiodomethane immediately absorbed into all nanofiber mats, thus prohibiting the acquisition of a measurement. Cellulose nanofiber mats had a glycerol contact angle of 35.9 ± 4.8°, which is consistent with the low contact angle reported by others [265]. The contact angle measurements of cellulose nanofiber mats with PAA were statistically increased over the cellulose nanofiber mat [266,267]. Coating with chitosan resulted in the highest glycerol contact angle of 69.2±7.4° [268]; a statistically higher contact angle than non-functionalized and pDADMAC functionalized cellulose nanofibers. Statistically speaking, the PAA and chitosan functionalized samples had the same contact angle, which could be attributed to the high standard deviation. The high standard deviation could insinuate that less functionalization occurred by these polyelectrolytes than by the pDADMAC. There was no statistical difference in contact angles between uncoated cellulose nanofiber mats and the cellulose nanofiber mats coated with pDADMAC. Overall, all of the nanofiber mats, both non-coated and coated, were hydrophilic as the contact angle was <90 °C.

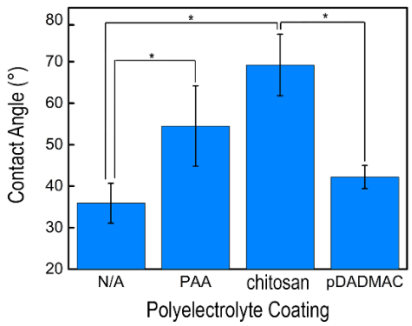

Figure 48: The average glycerol contact angle on cellulose nanofiber mats without coating (N/A) and coated with PAA, chitosan and pDADMAC are shown along with the standard deviation. Statistical significance between samples is shown by *.

Overall, functionalization of cellulose nanofiber mats with different polyelectrolytes provides an effective method to add chemical groups onto the material's surface while keeping the morphology, fiber diameter, and high surface area constant. Additionally, electrospinning polyelectrolytes usually involves co-spinning with a synthetic polymer, harsh solvents, or a post-crosslinking. This simple post-functionalization technique was facile, effective, and avoided these issues.

8.3.2 Collection and Inactivation of *E. coli* K12 by Polyelectrolyte Coated Cellulose Nanofiber Mats

Cellulose nanofiber mats with and without polyelectrolyte functionalization were incubated with *E. coli* K12 for 120 min to demonstrate the effect that surface charge has on microbial collection, Figure 49 (left). The highest *E. coli* K12 collection was achieved by the electrospun cellulose nanofiber mats without a coating (N/A) and functionalized with a pDADMAC coating. After 120 min, the highly hydrophillic mats (Figure 4), cellulose and pDADMAC functionalized cellulose nanofiber mats, removed a statistically equivalent amount of *E. coli* K12: $6.2 \times 10^8 \pm 8.0 \times 10^7$ and $6.5 \times 10^8 \pm 5.5 \times 10^7$ cells, respectively. Despite also having cationic charge groups, nanofiber mats coated with CS collected the lowest number of cells ($2.8 \times 10^8 \pm 7.7 \times 10^7$ cells), which equated to a statistically lower removal than the pDADMAC coated mats and non-coated cellulose mats. Irrespective of whether the bacteria is Gram-positive or Gram-negative, bacterial cells have net negative charges on their surface suggesting that electrastatic interaction increases with increasing positive charges on the material surface leading to higher adsorbption.[269] While both pDADMAC and CS have positive charges, adhesion is also dependent on other interaction such as hydrophoic/phillic interactions[269] and based on the contact angle, pDADMAC functionalized mats are more hydrophilic. Additionally, *E. coli*

K12 contains an LPS in their cell envelope attracting a water layer leading to a high level of hydrophilicity[269], which is likely to enhance cell adhesion to hydrophilic surfaces. The nanofiber mats coated with PAA had a statistically lower amount of *E. coli* K12 cells collected, $4.0 \times 10^8 \pm 1.4 \times 10^7$ cells, than the non-coated or pDADMAC-functionalized cellulose nanofiber mats. The PAA-functionalized nanofiber mats did collect more *E. coli* K12 than the CS-functionalized nanofiber mats likely due to their lower contact angle. Bacteria attachment to a surface is dependent on both bacteria type and material properites, such as, hydrophobicity and surface charge. Additionally, previous studies have concluded that a higher collection was achieved by hydrophilic metals with a positive or neutral surface charge compared to hydrophilic, negatively charged substrates[270]. When taken collectively, the statistical changes in nanofiber mat contact angle and total number of microbial cells collected support that a simple polyelectrolyte functionalization on cellulose nanofiber mats can provide a tailored collection of microorganisms.

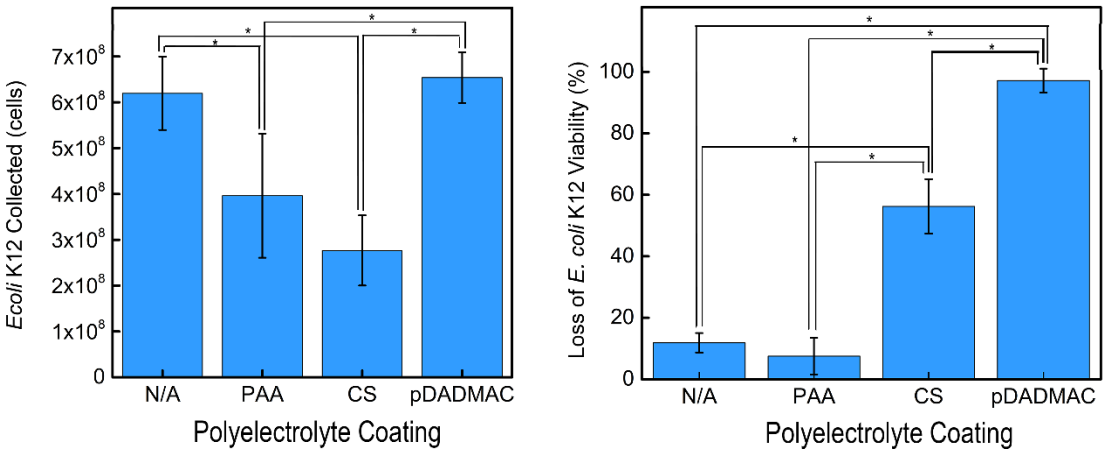

Figure 49: (Left) The average number of *E. coli* K12 cells collected after 120 min using cellulose nanofiber mats not coated (N/A) and coated with PAA, chitosan and pDADMAC. (Right) The average loss of viability for *E. coli* K12 cells after 180 min using cellulose nanofiber mats not coated (N/A) and coated with PAA, chitosan and pDADMAC. Error bars represent standard deviation. All experiments were performed in triplicate. Statistical significance is denoted by *.

In addition to altering the microbial collection rate, the presence of cationic charges should provide innate microbial inactivation. We conducted a solution based minimum inhibitory concentration (MIC) evaluation using *E. coli* K12 for both CS and pDADMAC polymers. Both polymer solutions had an MIC value of 800 µg/mL, which was similar to those reported in the literature [271,272]. MICs are known to vary based on molecular weight, and previously, CS MIC's for *E. coli*, *P. aeruginosa*, and *S. aureus* have been reported to range between 100-1000, 200-1700, 20-1250 µg/mL, respectively [272]. The MIC of pDADMAC was absent from literature but some values have been reported for polymers containing DADMAC monomers [273]. Notably, the antibacterial activity of the polymer in solution does not necessarily correlate to its activity once the polymer is immobilized or processed into a solid material because the interactions between the antibacterial agent and the microorganism change.

The inactivation of *E. coli* K12 by the nanofiber mats was measured after 180 min of incubation, Figure 49 (right). The cellulose nanofiber mats (non-functionalized) and the nanofiber mats functionalized with PAA, exhibited a minimal loss of *E. coli* K12 viability, 11.8 ± 3 % and 7.5 ± 6 %, respectively. This was expected because these polymers do not contain cationic groups that provide antibacterial activity. In applications such as microbial fuel cells, cellulose and PAA functionalized nanofiber mats could provide a platform for tailored biofilm growth. Both mats provide high cell viability and the carboxyl groups of PAA could be used to further functionalize the nanofiber mat.

Both CS and pDADMAC are cationic polymers and have intrinsic antibacterial activity; thus, we expected these two coatings to lead to antimicrobial nanofiber mats. Functionalizing the cellulose nanofiber mats with CS statistically increased the inactivation

activity to 56.3 ± 9%. Our previous report indicated that chitosan-based nanofiber mats inactivated >99% *E. coli* K12 and thus, a higher inactivation might be achieved if the chitosan content on the surface of the nanofibers was increased [223]. The statistically highest inactivation (97.2 ± 4%) was achieved by the electrospun nanofiber mats functionalized with pDADMAC. While the MIC experiment indicated that both CS and pDADMAC have the same solution-based antibacterial activity against *E. coli* K12, the higher level of inactivation demonstrated by the pDADMAC-functionalized nanofiber mats suggests that when immobilized, pDADMAC has a higher inactivation potential than CS. Another hypothesis is that more functionalization occurred using pDADMAC than CS and the overall quantity of cationic polymer on the cellulose nanofiber mats is different. pDADMAC has been used previously to uniformly functionalize cellulose nanofiber mats through electrostatic interactions, which was confirmed by the post attachment of zeolites, which utilize the positive charge of pDADMAC to electrostatically attach to the nanofibers.[263] Additionally, previous literature has shown that minimal chitosan is absorbed on cellulose thin coated films but greatly improved after the oxidation of cellulose providing more anionic sites[262] suggesting that further processing of the cellulose nanofiber mats could improve the CS functionalization. Overall, functionalization with these cationic polymers allows for a tuned collection of microorganisms with the ability to inactivate them as well using cellulose nanofiber mats.

8.3 Conclusion and Future Work

In this study, the correlation between nanofiber mat surface chemistry and hydrophilicity was investigated by functionalizing the surface of cellulose nanofiber mats with PAA, chitosan, and pDADMAC. We have demonstrated that while the polyelectrolyte

coatings did not change the fiber morphology or their average fiber diameter, the surface chemistry and hydrophilicity of the fiber mats were impacted. Hydrophilicity paired with neutral or positive charge improved the collection of *E. coli* K12, whereas hydrophilic cationic nanofiber mats exhibited the highest killing of *E. coli* K12. We suggest that insights gaining from this work could enable the fine-tuning of high porosity nanofiber mat surfaces towards the desired end application. By optimizing the hydrophilicity and surface chemistry, a balance of microorganism collection versus repulsion, as well as microbial viability versus killing can be achieved.

Continuation of this work should focus on expanding the optimization of surface properties of nanofiber mats to collect viruses. Previously, literature has shown that viruses can be filtered using nanofiber mats where the primary means of collection is adsorption[274,275]. However, the uptake of viruses via adsorption using nanofiber mats without filtration has not yet been studied. Additionally, an optimization of surface properties of nanofiber mats to yield the highest adsorption of viruses should also be explored. It would be specifically optimal to develop nanofiber mats optimized to collect both bacteria and viruses through adsorption with the ability to tailor the collection.

CHAPTER 9
ANOTHER MECHANISM TO RELEASE ANTIBACTERIAL AGENT FROM ELECTROSPUN FIBER

Adapted from: Rieger, K. A.; Cho, H. J.; Yeung, H. F.; Fan, W.; Schiffman, J. D., Antimicrobial Activity of Silver Ions Released from Zeolites Immobilized on Cellulose Nanofiber Mats. *ACS Applied Materials and Interfaces*, 2016, 8(5), 3032-3040.

9.1 Summary

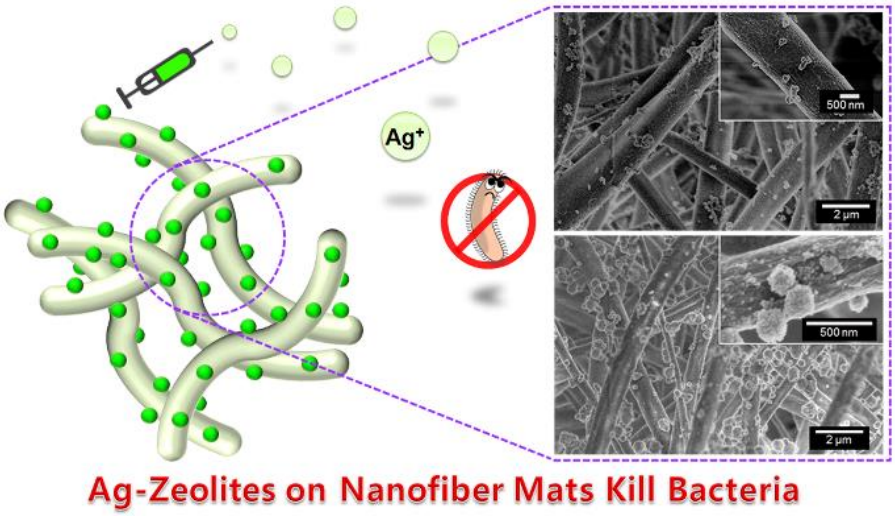

Figure 50: Control release of silver from loaded zeolites either grown or post-attached to cellulose nanofiber mats results in quick effective antibacterial activity.

In this study, we exploit the high silver ion exchange capability of Linde Type A (LTA) zeolites and present, for the first time, electrospun nanofiber mats decorated with in-house synthesized silver (Ag^+) ion exchanged zeolites that function as molecular delivery vehicles. LTA-Large zeolites with a particle size of 6.0 μm were grown on the surface of the cellulose nanofiber mats, while LTA-Small zeolites (0.2 μm) and three-dimensionally ordered mesoporous-imprinted (LTA-Meso) zeolites (0.5 μm) were attached to the surface of the cellulose nanofiber mats post-synthesis. After the three zeolite/nanofiber mat assemblies were ion-exchanged with Ag^+ ions, their ion release

profiles and ability to inactivate *E. coli* K12 were evaluated as a function of time. LTA-Large zeolites immobilized on the nanofiber mats displayed more than an 11× greater *E. coli* K12 inactivation than the Ag-LTA-Large zeolites that were not immobilized on the nanofiber mats. This study demonstrates that by decorating nanometer to micrometer scale Ag^+ ion-exchanged zeolites on the surface of high porosity, hydrophilic cellulose nanofiber mats, we can achieve a tunable release of Ag^+ ions that inactivate bacteria faster and are more practical to use in applications over powder zeolites.

9.2 Methods

9.2.1 Fabrication of Cellulose Nanofiber Mats

Details are provided in Chapter 7 Section 7.2.1.

9.2.2 Synthesis of LTA-Large Zeolites Grown on Cellulose Nanofiber Mats

Cellulose nanofiber mats (3 cm × 6 cm) were secured between two chemically resistant polypropylene meshes (9275T28, McMaster-Carr) and floated in an aqueous 0.5 wt% pDADMAC solution for 30 min at 60 °C to achieve polycation adsorption that ensured a uniform growth of zeolites on the surface of the nanofiber mats.[276] Treated nanofiber mats were rinsed with 0.5 L DI water and then dried for 24 h at 90 °C before being submerged in 30 g of the Na-LTA-Large synthesis solution, which was prepared according to a previously reported method.[277] Briefly, 2 g of NaOH was dissolved in 91.75 g of DI water in a plastic container that was split into two portions of 42.20 g and 49.55 g. To the smaller portion, 12.57 g of sodium silicate solution was added, and 5.35 g of sodium aluminate was added to the larger portion. Both solutions were stirred thoroughly for 10 min at room temperature. A dense gel was formed by pouring the silicate solution into the aluminate solution. The gel was stirred thoroughly until the texture became uniform. Na-

LTA produced from this solution possessed a composition of 2 SiO_2: Al_2O_3: 3 Na_2O: 200 H_2O.[277] The produced Na-LTA nanofiber mats and all residual LTA zeolite were rinsed with 2 L of DI water until the pH value of nanofiber mat surface was less than 8; next, the zeolite/nanofibers composites were dried overnight in an oven at 60 °C. Throughout this manuscript, the LTA zeolites with 6 μm particle size grown on the surface of cellulose nanofiber mats are denoted as LTA-Large zeolites.

9.2.3 Synthesis of LTA-Small Zeolites

Na-LTA with a 150 nm particle size, denoted as LTA-Small, were prepared according to a method previously reported.[278] Briefly, 13.29 g of TMAOH, 7.05 g of NaOH solution (0.1 g of NaOH dissolved in 14.28 g of DI water), and 1.2 g of silicic acid were mixed at 70 °C. After the silicic acid dissolved, 1.0 g of aluminum isopropoxide was added, followed by stirring for 2 h at room temperature. The mixture was filtered using a 200 nm syringe filter to obtain a clear solution with a composition of 11.25 SiO_2: 1.8 Al_2O_3: 13.4 $(TMA)_2O$: 0.6 Na_2O: 700 H_2O. For zeolite crystallization, the solution was heated to 90 °C for 16 h under static conditions. Afterwards, the resulting white precipitate (~0.15 g) was washed 5× by centrifugation with DI water and re-dispersed by sonication in 10 g of DI water that contained 0.5 g of sucrose and 41.8 μL of H_2SO_4 in order to avoid an irreversible aggregation of the LTA nanoparticles. Because of the relatively large molecular size of sucrose (~0.9 nm), sucrose molecules do not readily diffuse into the micropores of LTA (0.41 nm). For the polymerization of sucrose, the mixture was stirred at 60 °C for 3 h and subsequently dried overnight in an oven at 90 °C. The drying temperature was increased to 160 °C for an additional 6 h to induce partial carbonization of the polymerized sucrose.

Subsequently, the sample was subjected to a carbonization process under N_2 flow at 900 °C for 6 h, leading to a composite of LTA and carbon. Finally, LTA-Small was obtained by calcination at 600 °C for 24 h in a furnace with air.

9.2.4 Synthesis of LTA-Meso Zeolites

To synthesize three-dimensionally ordered mesoporous-imprinted (3DOm-i) LTA, denoted as LTA-Meso, first the LTA-Small synthesis solution described above with a composition of 11.25 SiO_2: 1.8 Al_2O_3: 13.4 $(TMA)_2O$: 0.6 Na_2O: 700 H_2O[278] was prepared. In this approach, 3DOm (three-dimensionally ordered mesoporous) carbon with a pore size of 35 nm was used as a hard template to create mesopores in the LTA zeolite. The 3DOm carbon was prepared by replication from colloidal crystals composed of monodispersed 35 nm silica nanoparticles.[279,280]

Here, 0.4 g of 3DOm carbon was immersed in 25 mL of the clear (LTA-Small) synthesis solution and heated for 12 h at 70 °C for zeolite growth. The product was then washed by filtration with DI water before being re-immersed it into a freshly prepared synthesis solution for an additional round of hydrothermal synthesis at 70 °C for 12 h. The growth process was repeated six times. After zeolite growth inside the carbon was complete, the zeolite carbon composite was washed by filtration with DI water and dried overnight at 100 °C. The LTA-Meso was obtained by calcination at 600 °C for 24 h in a furnace with air to remove the carbon and organic structure directing agents.

9.2.5 Attachment of LTA-Small and LTA-Meso Zeolites to Cellulose Electrospun Nanofiber Mats

Cellulose nanofiber mats were punched into circles with a 12.7 mm diameter using a Spearhead® 130 Power Punch MAXiset (Cincinnati, Ohio). Batches of six nanofiber mats were placed into a Fisherbrand™ square petri dish (100 mm × 100 mm × 15 mm)

containing 20 mL of a 0.5 wt% pDADMAC solution and mixed using a 120 V Lab Line 3-D rotator (model #4630) for 30 min before being removed from solution, washed with DI water, and dried overnight at ambient conditions. Next, the mats were mixed with a zeolite solution for various time durations at 20 rpm on Arma-Rotator A-1 (Bethesda, MA).

Zeolite suspensions were prepared at either a 0.06 or 0.1 mg/mL concentration by adding 2.5 mg of the LTA-Small or 1.5 mg of the LTA-Meso zeolites into 25 mL of DI water (pH = 9.3, adjusted by NH_4OH), and then sonicated for 1.5 h. After sonication, the solution was filtered (P5 filter paper, Fisher Scientific) to remove large aggregates. To optimize the attachment of LTA-Small and LTA-Meso zeolites on the surface of the nanofiber mats, solvent pH value, zeolite quantity, and mixing time were systematically varied. For the LTA-Small zeolites, 2.5 mg of zeolites were suspended in DI water (pH = 6.8 or pH = 9.3, adjusted by NH_4OH) for 4 h and 24 h. The cellulose nanofiber mats without a pDADMAC coating served as a control sample. For LTA-Meso zeolites, mixing time (1, 2 and 4 h), and the quantity of zeolites (1.5 and 2.5 mg) were varied using DI water (pH = 9.3, adjusted by NH_4OH) because this was the optimal pH value for the LTA-Small zeolites.

9.2.6 Preparation of Ag-LTA Zeolites on Cellulose Nanofiber Mats

The Na-LTA zeolites or Na-LTA zeolite/nanofiber mats were placed into a 0.05 M aqueous $AgNO_3$ solution for 24 h and stirred at room temperature to exchange sodium ions with silver ions within the zeolites.[281] The zeolite/nanofiber mats were secured between two chemical resistant polypropylene meshes (9275T28, McMaster-Carr) during exchange. The resulting Ag-LTA zeolites or Ag-LTA zeolite/nanofiber mats were dried at room temperature in the dark. Throughout the ion exchange process, the samples were protected from light using aluminum foil to prevent oxidation of $AgNO_3$.

9.2.7 Characterization of Cellulose Nanofiber Mats and LTA Zeolites

Micrographs of zeolites (LTA-Large, -Small and -Meso), as well as cellulose nanofiber mats with and without zeolites were acquired using a FEI-Magellan 400 scanning electron microscope (SEM). A sputter machine (Gatan high resolution ion beam coater model 681) was used to coat samples with ~5 nm of platinum. The average nanofiber diameter was determined by measuring 50 random fibers from 7 micrographs using *Image J 1.45* software (NIH, Bethesda, MD). The distribution size of LTA-Large, LTA-Small and LTA-Meso was determined using *Image J* software by measuring 100 random zeolite crystals from 7 micrographs. To obtain the average thickness of the nanofiber mats, the mats were fluorescently dyed with calcofluor white stain (1 μL/mL). Power x-ray diffraction (XRD) patterns of all LTA zeolites were obtained using a PANalytical X'Pert diffractometer using Cu Kα radiation. XRD data was collected in the 2θ range from 5° to 40° with a step size of 0.04° and a step time of 1 s. The concentration of Na-LTA zeolites on the nanofiber mats was determined by thermogravimetric analysis (TGA, TA instrument Q500) using the following temperature program under 100 mL/min of air: (1) heating from room temperature to 700 ^{o}C, with a rate of 10 ^{o}C/min, (2) holding at 700 ^{o}C for 2 h, and (3) cooling from 700 ^{o}C to 25 ^{o}C, with a rate of 10 ^{o}C/min.

9.2.8 Characterization of Isotherm and Ag^{+} Ions Release from LTA Zeolites

The Ag^{+} ion-exchange capacity was evaluated by submerging the Na-LTA zeolites in an initial 0.005 M-0.05 M $AgNO_3$ solution and stirring for 24 h at room temperature. All samples were prepared in triplicate. The exchanged amount of Ag^{+} ion was calculated Equation 6 where, q_e is the exchanged amount of Ag^{+} ions onto the mass of the Na-LTA at equilibrium (mg Ag^{+}/mg Na-LTA); C_i and C_e correspond to the concentration of Ag^{+} in

the initial solution and in equilibrium solution after the exchange; V, M_{Ag}, and m are the volume of the ion-exchange solution, the atomic weight of silver ion, and the mass of the Na-LTA, respectively.

Equation 6

$$q_e = \left[(C_i - C_e)VM_{Ag}\right]/m$$

The desorption of Ag^+ ion from the LTA samples was determined by fully submerging 4 mg of Ag-LTA zeolite in 2 mL of solution at 37 °C with constant shaking at 150 rpm. Two release solutions were tested: (1) DI water and (2) an aqueous $NaNO_3$ solution that had the same salt concentration (0.1468 M $NaNO_3$) as the PBS solution (0.1468 M Na^+) used in the antibacterial activity studies. Ag^+ ion concentrations were measured at 15 min, 30 min, 45 min, 60 min, 90 min, 120 min, 24 h, and 48 h using an Orion Star A214 Silver ISE probe (Thermo Scientific). Throughout the release experiments, zeolite solution was covered with Parafilm (Fisher Scientific) to prevent evaporation; Ag^+ ion concentrations were reported as the average of 3 repeated measurements.

9.2.9 Antibacterial Activity of Ag-LTA-Zeolites Immobilized on Cellulose Nanofiber Mats

E. coli K12 MG1655 purchased from Leibniz Institute DSMZ (Germany) was used as the model microorganism. The bacteria was grown in LB at 37 °C and re-suspended in a PBS solution (pH = 7.2) to remove residual macromolecules and other growth medium constituents. The antibacterial activity of LTA-Large, LTA-Small, LTA-Meso zeolites immobilized on cellulose nanofiber mats was tested. Controls included (i) cellulose nanofiber mats (ii) residual Na-LTA zeolites, (iii) cellulose nanofiber mats treated at Ag^+ ion-exchange conditions, and (iv) residual Ag-LTA zeolites. Viability loss was determined using a previously described fluorescence assay described in Chapter 4 Section 4.2.6.[223]

Electrospun nanofiber mats (diameter = 1.27 cm) were placed at the bottom of 12 well plates (diameter = 25 mm). Throughout the Results and Discussion section, all statistical differences were determined using an unpaired t-test with values of $p \leq 0.05$ considered to be statistically significant.

9.3 Results and Discussion

9.3.1 Characteristics of Cellulose Nanofiber Mats and LTA-Zeolites

Characteristics for cellulose nanofiber mats including fiber diameter, morphology, and surface area can be found in Chapter 7 Section 7.2.1. Figure 51 displays the SEM micrographs of the three Na-LTA zeolite samples synthesized in this study. LTA-Large particles displayed typical cubic structures with slightly truncated edges and were somewhat agglomerated. The particle size of LTA-Large zeolite ranged between 3.0 and 8.5 μm with an average size of 6.0 μm. In contrast, LTA-Small zeolites were cubic, varying between 120 nm and 170 nm in size. Different from the two conventional zeolites with LTA topology, the LTA-Meso zeolites had an average particle size of ~500 nm, and were composed of ~30 nm spherical primary particles with a close packing arrangement.[278]

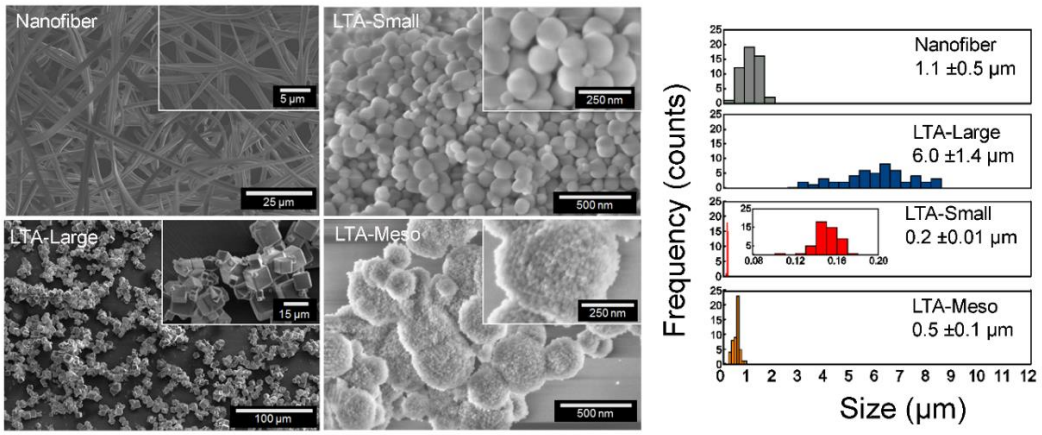

Figure 51: (Left) Micrographs of cellulose nanofiber mats and the zeolites: LTA-Large, LTA-Small and LTA-Meso. (Right) Fiber diameter distribution and zeolite particle size distribution are displayed along with their average size and standard deviation (n = 50 for nanofibers and n= 100 for zeolites).

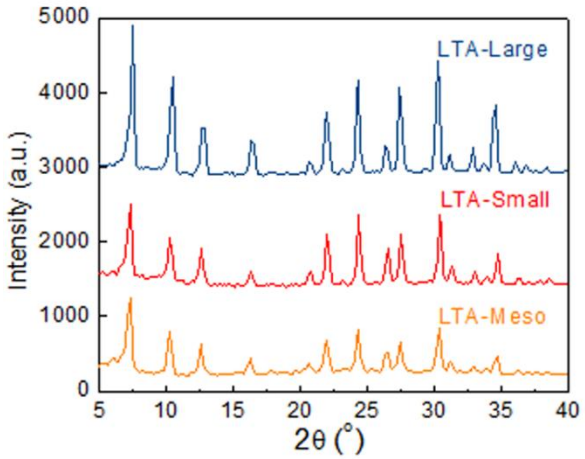

Figure 52: XRD patterns of the LTA-Large, LTA-Small and LTA-Meso zeolites synthesized in this study.

The phase purity of the zeolites was confirmed using XRD analysis as shown in Figure 52. All observed Bragg diffraction peaks in the XRD patterns can be indexed to the LTA topology,[282] indicating that highly crystalline LTA zeolites were synthesized without forming other impurity phases. As a result of the LTA-Meso zeolites being grown inside the 3DOm carbon template, the zeolites had a smaller primary particle size and exhibited relatively broader diffraction peaks than the LTA-Large and LTA-Small zeolites.

9.3.2 Characteristics of LTA-Zeolites Immobilized on Cellulose Mats

LTA-Large zeolites were successfully grown on the surface of cellulose nanofiber mats by an *in-situ* crystal growth method, Figure 53A. By coating the cellulose nanofiber mats with pDADMAC, positive charges were rendered on the surface of the nanofibers, which served as nucleation sites for zeolite growth.[276] During zeolite crystallization, the positive surface charge on the nanofiber mats electrostatically attracted the zeolite precursors, such as $Si(OH)_3O^-$ and $Al(OH)_4^-$, thus promoting the formation of the LTA-Large zeolites on the nanofiber surfaces. The average particle size of the LTA-Large zeolites grown on the cellulose nanofiber mats and the residual zeolites, which were not grown on the mats, were statistically equivalent in size. Growing the LTA-Large zeolites

on the surface of the nanofiber mats increased the weight of the mats by 12.5 ± 3.5%, as determined via TGA, Table 8.

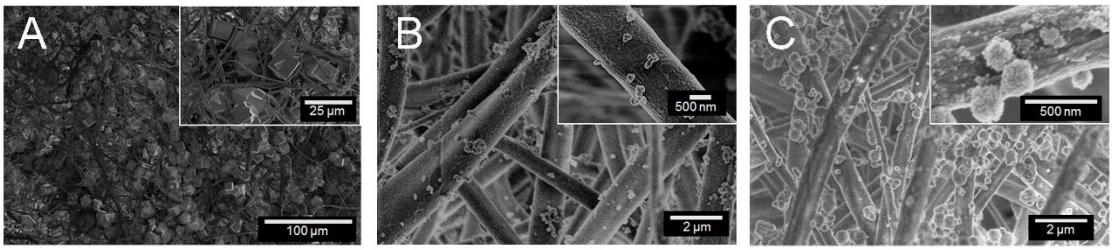

Figure 53: Micrographs of the (A) LTA-Large zeolites grown on the surface of cellulose nanofiber mats. (B) LTA-Small and (C) LTA-Meso zeolites attached to the surface of cellulose nanofiber mats post-synthesis.

Table 8: Weight percent of Na-LTA attached to the surface of cellulose nanofiber mats [a]

	LTA-Large/Fiber	LTA-Small/Fiber	LTA-Meso/Fiber
Na-LTA (wt%) [b]	12.5 (± 3.5)	2.6 (± 0.6)	2.9 (± 0.9)

[a] The average mass of the cellulose nanofiber mats used in these experiment was 1.70 (± 0.39) mg.

[b] 95% confidence interval in parentheses obtained from three repeated tests.

LTA-Small and LTA-Meso zeolites were successfully attached to the cellulose nanofiber mats post-synthesis, Figure 53B and C, respectively. It was observed that the pre-treatment of cellulose nanofiber mats with the polycation pDADMAC facilitated the attachment of LTA-Small and LTA-Meso zeolites to the surface of the nanofiber mats, Figure 54. It was confirmed that exposure of the nanofiber mats to the pDADMAC solution did not change the morphology or the average diameter of the nanofiber mats. The average diameter of cellulose nanofibers coated with pDADMAC solution was 1.15 ± 0.12 µm. The attachment of LTA-Small and LTA-Meso zeolites to the nanofiber mats resulted in a weight increase of 2.6 ± 0.6% and 2.9 ± 0.9%, respectively.

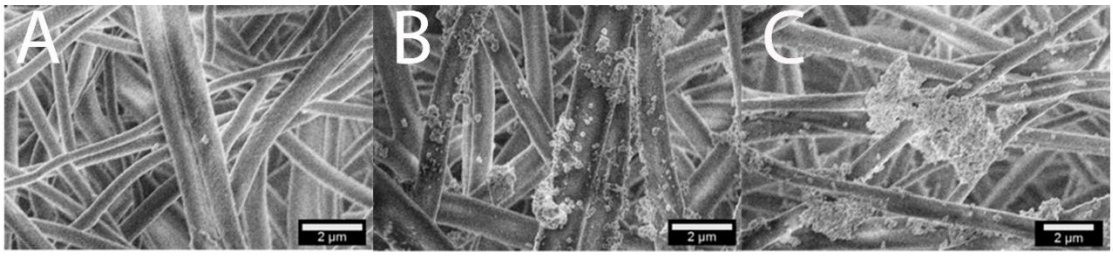

Figure 54: Preliminary experiments were conducted to improve the attachment of LTA-Small zeolites to the surface of cellulose nanofiber mats. Comparison of micrographs show the effect of (A) no pre-coating and (B) pre-coating the cellulose nanofiber mats with pDADMAC solution. The effect of solvent was also explored; in (A) and (B) DI water was used, whereas in (C) DI water (pH = 9.3, adjusted by NH_4OH) was used. (A-C) A constant concentration of 0.1 mg/mL of LTA-Small zeolites and a 24 h mixing time were tested.

To minimize aggregation of zeolites, the parameters for the attachment procedure including time, the pH value of the solvent, and the quantity of the zeolites were investigated, Figure 55. A uniform attachment for both LTA-Small and LTA-Meso zeolites was achieved. For LTA-Small and -Meso zeolites, a 0.1 mg/mL and a 0.06 mg/mL concentration of zeolites in an aqueous solution with a pH value of 9.3 (adjusted using NH_4OH) was reacted with the nanofiber mats for 4 h and 1 h, respectively. It was reported that LTA zeolites have negatively charged surfaces at a pH value of ~9.3 because of their isoelectric point (pH = 5.5).[276] Thus, it was not a surprise that an aqueous solution with a pH value of 9.3 yielded nanofiber mats with the most consistent LTA-Small and LTA-Meso zeolite decoration. At this pH value, the zeolite particles had a negative surface charge, while the pDADMAC coated nanofiber mats had a positive surface charge (isoelectric point of pDADMAC is at a pH value of 12).[283] Thus, we suggest that that zeolites were immobilized onto the nanofiber mats post-synthesis via strong electrostatic attractions.

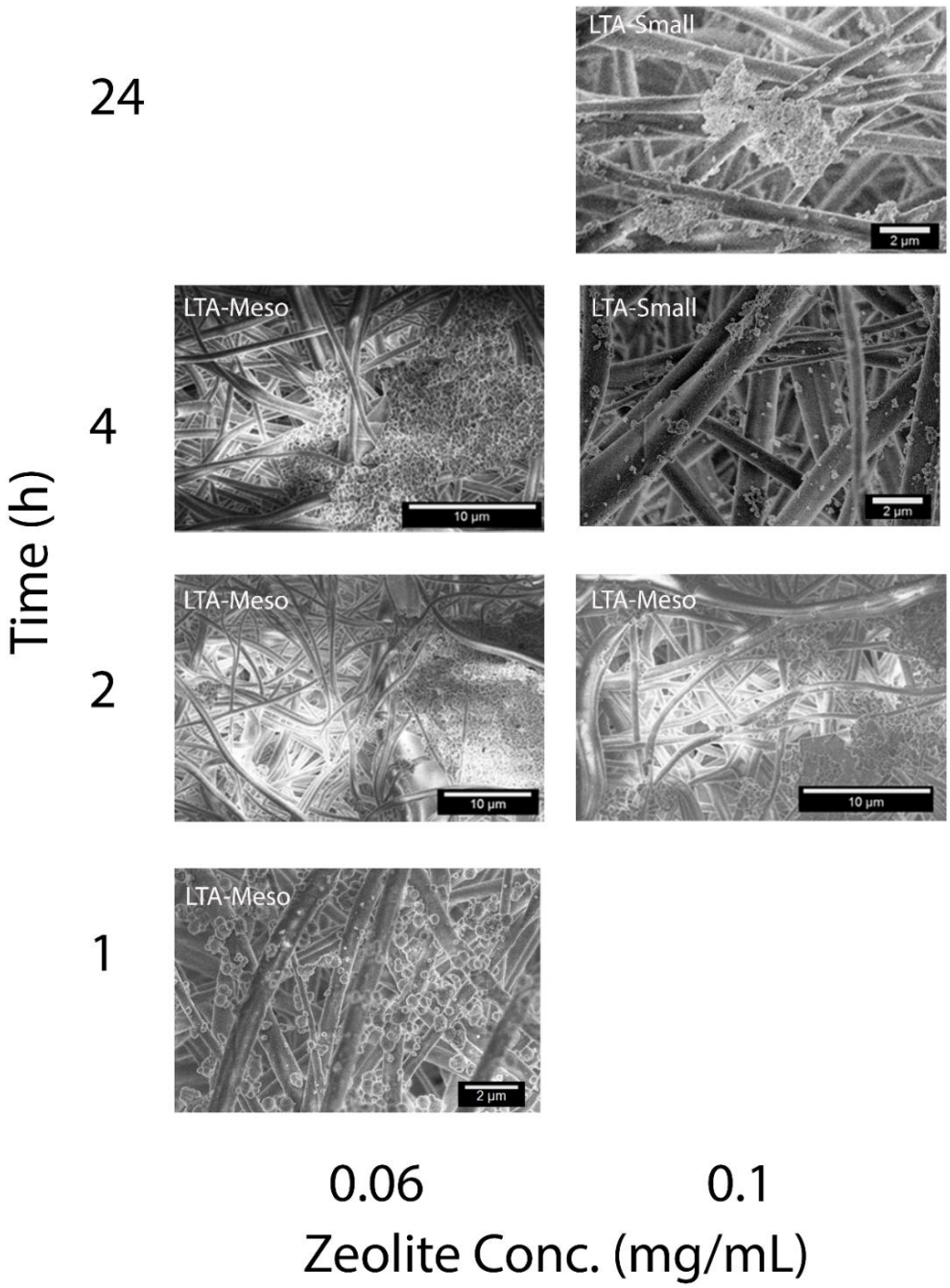

Figure 55: Micrographs display the attachment of LTA-Small and LTA-Meso zeolites as a function of mixing time and zeolite concentration. In general, decreasing time and concentration resulted in less aggregation and a more even coverage of zeolites over the nanofiber mats. The LTA-Meso zeolites needed a shorter mixing time and a lower concentration than the LTA-Small zeolites. All nanofiber mats were pre-coated with pDADMAC before zeolite attachment and the solvent used was DI water (pH = 9.3, adjusted by NH_4OH).

9.3.3 Characteristics of Ag-LTA Zeolites and Ag^+ Ions Release from Zeolites

The ion-exchange isotherms in Figure 56 reveal the adsorption equilibrium between the exchanged amounts of Ag^+ ion within the zeolites and their equilibrium concentration in solution at room temperature. Increasing the initial Ag^+ ion concentration increased the Ag^+ ion content within the zeolites until a 0.03 M concentration of Ag^+ solution was used. The Ag^+ ion-exchange capacity was also estimated using the maximum adsorption capacity divided by the theoretical value under the assumption that 100% Ag^+ ion-exchange occured, Figure 56 right y-axis. The maximum Ag^+ adsorption capacity for Ag-LTA-Large, -Small and -Meso was found to be 0.46, 0.47, and 0.51 mg Ag^+/mg Na-LTA, respectively, implying that the Na^+ was replaced with 60, 62, and 67% of their theoretical ion-exchange capacity. There was no statistically significant difference in the ion-exchange capacity for the three zeolites (95% confidence interval) in Figure 56. This result agrees well with the data from Meyer et al.[284] that experimentally showed that the maximum Ag^+ ion-exchange in Na-LTA zeolites was about 70% at 30 °C because the Ag^+ ion-exchange reached equilibrium.

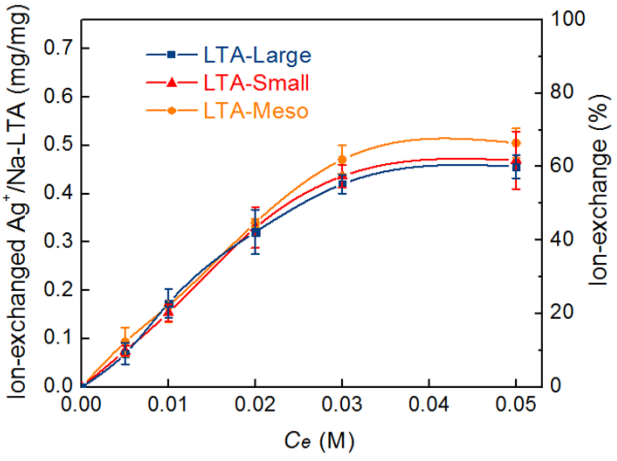

Figure 56: Ag^+ ion-exchange isotherms for the LTA -Large, -Small, and -Meso zeolites. C_e is the Ag^+ equilibrium concentration in an aqueous medium.

The release profile of Ag^+ ions from the three Ag-LTA zeolites into DI water was studied by preparing the zeolites using 0.05 M of $AgNO_3$ thus allowing them to reach a 60% equilibrium, which was the maximum loading achieved during the antibacterial studies. Figure 57 displays that the Ag^+ ion release from the Ag-LTA-Large and -Small zeolites in DI water was fast for the first 15 min, and then the Ag^+ ion concentration leveled out after 1 h. However, in the case of the Ag-LTA-Meso zeolites, there was a slight increase of Ag^+ ion concentration after an initially rapid Ag^+ ion release. The Ag^+ ion release behavior into an aqueous $NaNO_3$ solution was also investigated to simulate the PBS media used in the antibacterial activity experiments. The $NaNO_3$ solution was chosen because chloride anions in the PBS solution can form the insoluble compound, AgCl that rapidly precipitates out of solution. The Ag^+ ion release data summarized in **Error! Reference source not found.** and Figure 57, displays that a higher Ag^+ ion release occurred for all three zeolite samples in $NaNO_3$ than in DI water. Likely, this is because Ag^+ ion release is facilitated by the presence of other cations capable of exchanging with Ag^+ ion sites.[189] Thus, it is inferred that the Na cations in the $NaNO_3$ can occupy exchange sites and pump out Ag^+ ions. The percentage of Ag^+ ion release was also evaluated by dividing the measured value by the Ag^+ ion content in the solution. After two days 21.1%, 25.5%, and 32.2% of the Ag^+ ions present in the Ag-LTA-Large, -Small and –Meso zeolites, respectively, leached into the $NaNO_3$ medium. In both mediums, Ag-LTA-Small and -Meso zeolites released almost the same Ag^+ ion concentration within the first 15 min, which was higher than the concentration of Ag^+ ions released from the Ag-LTA-Large zeolites. This might be due to the lower external surface area and larger particle size of the Ag-LTA-Large zeolites. After 1 h, the Ag-LTA-Meso zeolites released a slightly greater quantity of Ag^+ ions than the

Ag-LTA-Small zeolites. The similar release profile for the three zeolite samples indicates that the release of Ag^+ ions from the LTA zeolites is fast, and reaches an equilibrium in less than 30 min. Due to the limitation of the instrument, we unfortunately could not measure the very quick release of Ag^+ ions accurately; quantification of release at times under 15 min was inaccurate. However, because the antibacterial activity experiments were performed after a 30 min incubation period, the shortest time allowable,[111] the effects from the initial release kinetics might not be as imperative for this study.

Table 9: Concentration of Ag^+ ions released from the Ag-LTA -Large, -Small, and -Meso zeolites into DI water and an aqueous $NaNO_3$ solution.

	Ag^+ ions released from Ag-LTA Zeolites (mg Ag^+/mg Ag-LTA) [a]			
	in DI water		in $NaNO_3$	
	at 15 min	at 2 days	at 15 min	at 2 days
Ag-LTA-Large	0.051 (± 0.011)	0.066 (± 0.008)	0.081 (± 0.004)	0.073 (± 0.010)
Ag-LTA-Small	0.074 (± 0.010)	0.079 (± 0.006)	0.099 (± 0.002)	0.089 (± 0.007)
Ag-LTA-Meso	0.070 (± 0.011)	0.109 (± 0.014)	0.097 (± 0.011)	0.112 (± 0.010)

[a] 95% confidence interval in parentheses, obtained from three repeated tests.

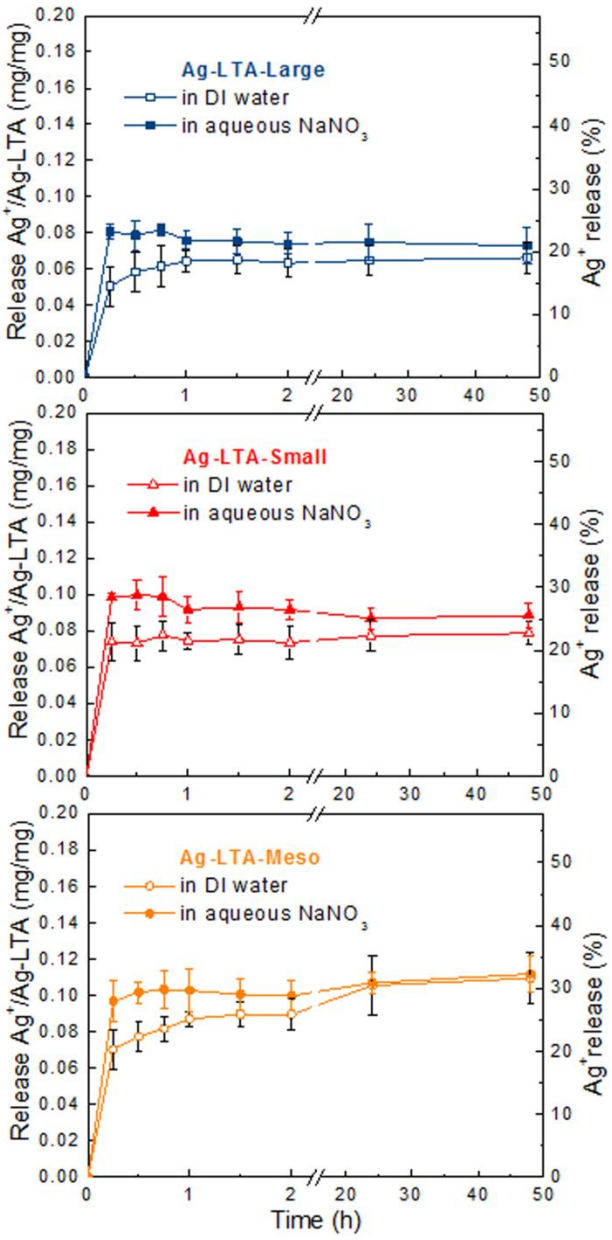

Figure 57: Release profile of Ag^+ ions from the Ag-LTA -Large, -Small, and -Meso zeolites into DI water and an aqueous $NaNO_3$ solution.

10.3.4 Antibacterial Activity of Ag-LTA Zeolites Immobilized on Cellulose Nanofiber Mats

The antibacterial activity of Ag^+ ion exchanged zeolites (Ag-LTA-Large, Ag-LTA-Small, and Ag-LTA-Meso) immobilized on cellulose nanofiber mats against *E. coli* K12 was evaluated, Figure 58. Two negative controls were tested: cellulose nanofiber mats (no

zeolites or silver) and Na-LTA-Large zeolites (~4 mg, without Ag^+ ion exchange). A suspension (~4 mg) of Ag-LTA-Large zeolites that were not immobilized on cellulose nanofiber mats were used as a positive control. Additionally, cellulose nanofiber mats that underwent Ag^+ ion-exchange conditions (without the presence of zeolites) were used to examine the effectiveness of Ag^+ ions absorbed onto the surface of the nanofiber mats. The antibacterial activity of all samples and controls was determined at three different incubation times (30, 60, and 90 min). Additionally, Table 10 compares the quantity of Ag^+ ions released from each zeolite/nanofiber mat sample at each incubation time point.

After a 30 min incubation period, a high level of *E. coli* K12 inactivation (68.7%, 88.5%, and 82.7%) was achieved for Ag-LTA-Large, Ag-LTA-Small, and Ag-LTA-Meso zeolites immobilized on the cellulose nanofiber mats, respectively. The Ag-LTA-Large zeolite/nanofiber mats released approximately four times more Ag^+ ions than Ag-LTA-Small and Ag-LTA-Meso zeolite/nanofiber mats. However, faster bacterial inactivation (after 30 min incubation) was not achieved by the Ag-LTA-Large zeolites that were immobilized on the nanofibers. This finding might be explained by the lower external surface area of the Ag-LTA-Large zeolite due to their larger particle size, thus affecting the interaction between Ag-LTA-Large zeolites and bacteria. Free Ag-LTA-Large (~4 mg) zeolites (in solution) served as a positive control because they released the highest quantity of Ag^+ ions (~0.32 mg, Table 10). After a 30 min incubation period, the suspension of Ag-LTA-Large zeolites killed a statistically lower amount of *E. coli* K12 (52.9%) than the Ag-LTA-Large, Ag-LTA-Small, and Ag-LTA-Meso zeolites that were immobilized on nanofiber mats. Notably, there was a much smaller quantity of zeolites (~0.07-0.35 mg, calculated from Table 8) immobilized on the nanofiber mats than the positive control of

LTA-Large zeolites (~4 mg). One potential mechanism why zeolites immobilized on nanofiber mats initially showed a greater inactivation of *E. coli* K12 (despite the lower concentration of Ag^+ ion) than the suspended zeolite powder is due to the hydrophilic and highly porous nature of the cellulose nanofiber mats. These materials' properties encourage the bacteria to transport quickly throughout the mat thus, potentially, the Ag^+ ion might have faster contact with a microbe. Additionally, by being immobilized on a nanofiber mat scaffold, the zeolites and Ag^+ ions might have been better dispersed than the powder zeolite control. At 30 min, the Ag-LTA-Large zeolites immobilized on the nanofiber mats did show at least an eleven times higher antibacterial efficacy per Ag^+ ion released (mg) than the zeolites that were not immobilized on the nanofibers, suggesting that having a high porosity scaffold that bacteria can freely travel within greatly enhances the inactivation process.

Cellulose nanofiber mats that underwent Ag^+ ion-exchange conditions (without the presence of zeolites) inactivated 16.8%, 49.3%, and 55.1% *E. coli* K12 after 30, 60, and 90 min of incubation. Thus, we hypothesize that a small quantity of Ag^+ ions absorbed onto the surface of the nanofiber mats; however, this quantity was below the detection limit of Ag^+ ions that could be measured in the release study (Figure 57). Two negative controls, cellulose nanofiber mats (no zeolites or silver) and Na-LTA-Large zeolites (~4 mg, without Ag^+ ion-exchange), showed only baseline inactivation levels over all three inactivation times indicating that neither of these materials were cytotoxic to bacteria. Similar inactivation rates were observed after 60 and 90 min incubation of *E. coli* K12 with Ag-LTA-Large, Ag-LTA-Small, and Ag-LTA-Meso zeolites immobilized on the cellulose nanofiber mats, as well as the positive control LTA-Large zeolites (no nanofiber mat). At

90 min, Ag^+ ion loaded zeolites (Ag-LTA-Large, Ag-LTA-Small, and Ag-LTA-Meso) immobilized on the cellulose nanofiber mats effectively inactivated 92.8%, 93.7%, and 93.0% *E. coli* K12, respectively. The Ag-LTA-Small zeolites exhibited the same antibacterial performance as the Ag-LTA-Meso zeolites, which is in good agreement with the release behavior of Ag^+ ions observed after 90 min, as shown in Figure 57. Furthermore, because the same antibacterial effectiveness was demonstrated by each of the zeolite/nanofiber mat composites, we suggest that the lower quantity of Ag^+ ions (~0.0070 mg, Table 10) released by the Ag-LTA-Small and Ag-LTA-Meso zeolites is sufficient for microbial inactivation.

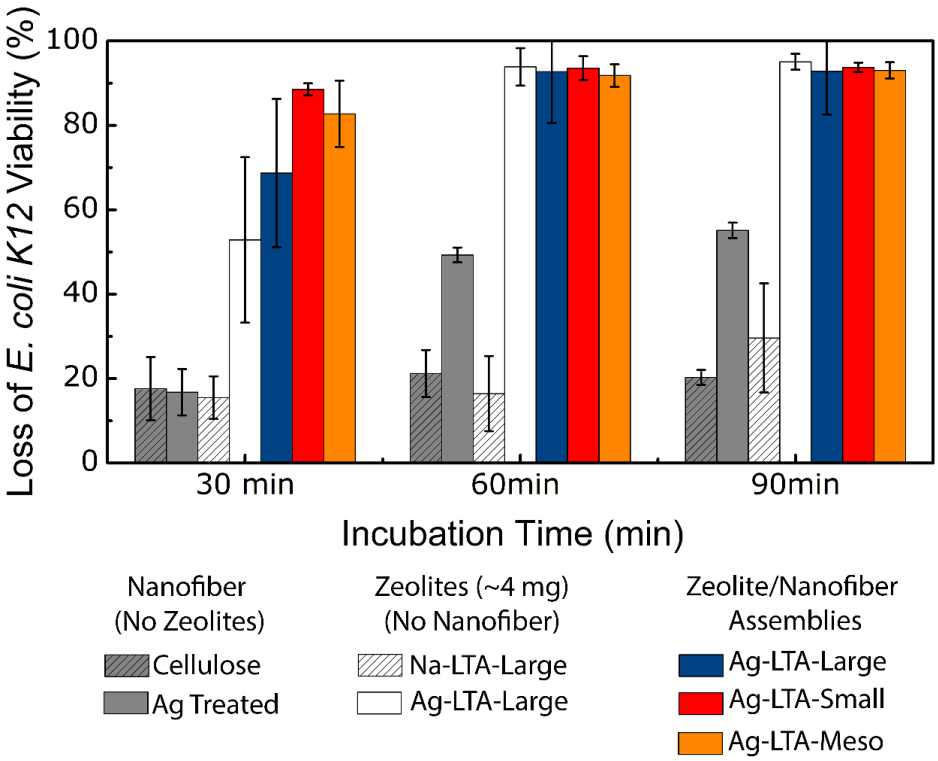

Figure 58: Inactivation of *E. coli* K12 as a function of time was achieved by releasing Ag^+ ions from Ag-LTA-Large, -Small, and -Meso zeolites that were immobilized on the cellulose nanofiber mats. Negative controls included Na-LTA-Large zeolites and untreated cellulose nanofiber mats. Ag-LTA-Large zeolites (no nanofiber mats) served as a positive control. Cellulose nanofiber mats treated in Ag^+ ion-exchange conditions (without zeolites present) were tested as an additional control. Experiments were performed in triplicates and error bars indicate one standard error.

The zeolite particles immobilized on the nanofiber mats, were qualitatively stable throughout the Ag^+ ion-exchange process, release studies, and antibacterial activity testing. The pH value of the ion-exchange $AgNO_3$ solution ranged from 6.8 to 7.2 and the PBS solution used in the antibacterial testing had a pH value of 7.2. Under this pH range (6.8-7.2), the LTA zeolite surface is negatively charged due to the isoelectric point of LTA zeolites (pH = 5.5),[276] whereas the pDADMAC coated nanofiber mats possess a highly positive surface charge (isoelectric point of pDADMAC = 12).[283] Thus, we suggest that strong electrostatic attractions are maintained between the zeolites and nanofiber mats throughout all experiments explored in this study.

Table 10: Mass of Ag-LTA zeolites tested in Figure 58 and the corresponding Ag^+ ion release from each Ag-LTA zeolite/nanofiber mat composite as a function of time.

	Ag-LTA-Large (no nanofiber)	Ag-LTA-Large on nanofiber	Ag-LTA-Small on nanofiber	Ag-LTA-Meso on nanofiber
Ag-LTA (mg)	4	0.3488	0.0697	0.0697
Ion-exchanged Ag^+ (mg) [a]	1.3861	0.1209	0.0242	0.0242
Released Ag^+ (mg) at 30 min [b]	0.3150	0.0275	0.0070	0.0071
Released Ag^+ (mg) at 60 min [b]	0.3038	0.0265	0.0064	0.0072
Released Ag^+ (mg) at 90 min [b]	0.3015	0.0263	0.0065	0.0070

[a] Calculated based on 1.8 mg of fiber mat, TG data and Ag^+ ion-exchange isotherm.
[b] Calculated based on Ag^+ ion release profile in an aqueous $NaNO_3$ solution.

9.4 Conclusion and Future Work

Here, for the first time, Ag^+ ion containing zeolites were successfully fabricated and immobilized on electrospun cellulose nanofiber mats. These composite materials hold potential for use in applications, such as, water treatment and wound healing where porous antibacterial materials are needed. The prepared Ag^+ ion exchanged zeolites (Ag-LTA-Large, Ag-LTA-Small, and Ag-LTA-Meso) immobilized on the nanofiber mats achieved

a high inactivation rate, 92% loss of E. *coli* K12 viability after 60 min incubation. The Ag-LTA-Small and Ag-LTA-Meso zeolites immobilized on the nanofiber mats exhibited the same antibacterial activity. However, due to the lower external surface area of the Ag-LTA-Large zeolites, when immobilized on the nanofiber mats, they exhibited a four times lower antimicrobial performance than the Ag-LTA-Small and Ag-LTA-Meso zeolites attached to the nanofiber mats. Notably, immobilizing zeolites on the nanofiber mats significantly enhanced the initial bacteria inactivation observed after a short incubation time of 30 min, likely because the nanofiber scaffolding provides a high porosity three dimensional microenvironment within which the microorganisms can freely travel. This was supported by the evidence that after a 30 min incubation period, the Ag-LTA-Large zeolites immobilized on the nanofiber mats displayed more than an eleven times greater *E. coli* K12 inactivation than the Ag-LTA-Large zeolites that were not immobilized. For the first time, we have demonstrated that zeolite/nanofiber mat composites offer a rational approach to deliver molecular cargo with a tunable release profile.

The high initial success of inactivation from zeolite coated nanofiber is an excellent platform to building almost 100% zeolite nanofibers, which could be done via core-shell electrospinning, where the outer-solution contains suspended zeolites and the inner-solution contains polymer(s). The advantages of this system would include higher level of zeolites, a complete uniform coating of zeolites and the ability to change the polymer and nanofiber diameter based on application. Additionally, Meso zeolites have the ability to release two different cargo at different release rates. A future objective should exploit this properties to release both an antibacterial agent. Lastly, zeolites can be reloaded with its cargo once depleted and therefore, the reusability of the nanofiber mats should be examined.

CHAPTER 10
SCIENTIFIC CONTRIBUTIONS

The work in this thesis has culminated in various publications and a patent, which are listed in this section. Additionally, dissemination of this work has taken place through various conference presentations and on-campus presentations within different organizations.

- Rieger, K. A., Birch N. P., and Schiffman, J. D, "Designing Electrospun Nanofiber Mats to Promote Wound Healing- A Review." *J. Mater. Chem. B.*, 2013, 1, 4531-4541.
- Schiffman, J. D., Rieger, K. A., "Essential oils or volatile organics thereof electrospun in chitosan nanofiber mats." International Application No.: PCT/US2014/059678, 16.04.2015
- Rieger, K. A.; Schiffman, J. D., Electrospinning an essential oil: Cinnamaldehyde enhances the antimicrobial efficacy of chitosan/poly(ethylene oxide) nanofibers. *Carbohydrate Polymers*, 2014, 113, 561-568.
- Rieger, K. A.; Birch, N. P.; Schiffman, J. D., Electrospinning chitosan/poly(ethylene oxide) solutions with essential oils: Correlating solution rheology to nanofiber formation. *Carbohydrate Polymers*, 2016, 139, 131-138.
- Rieger, K. A.; Eagan, N. M.; Schiffman, J. D., Encapsulation of cinnamaldehyde into nanostructured chitosan films. *Journal of Applied Polymer Science*, 2015, 132 (13).
- Rieger, K. A., Birch, N. P., Eagan, N., Schiffman, J. D., "Green Engineering of Antimicrobial Nanofiber Mats" The Fiber Society 2012 Fall Meeting Rediscovering Fibers in the 21st Century, Boston, MA. Published Full Proceeding.
- Rieger, K. A.; Thyagarajan, R.; Hoen, M. E.; Yeung, H. F.; Ford, D. M.; Schiffman, J. D., Transport of Microorganisms into Cellulose Nanofiber Mats. *RSC Advances*, 2016, 6, 24438-24445.
- Rieger, K. A.; Cho, H. J.; Yeung, H. F.; Fan, W.; Schiffman, J. D., Antimicrobial Activity of Silver Ions Released from Zeolites Immobilized on Cellulose Nanofiber Mats. *ACS Applied Materials and Interfaces*, 2016, 8(5), 3032-3040.
- Rieger, K. A.; Porter, M.; Schiffman, J. D., Polyelectrolyte-Functionalized Nanofiber Mats Control the Collection and Inactivation of *Escherichia coli*. *Materials*, 2016, 9(4), 297.

CHAPTER 11
CONCLUSION AND FUTURE WORK

As antibiotic resistance increases, there is a continual need to develop antibacterial materials that can be utilized within the medical field such as bandages, textiles or coatings. Electrospinning offers a fabrication technique that produces a unique flexible 3D contouring material composed of non-woven nanofibers. The resulting properties are advantageous for wound healing, drug delivery and bacteria adhesion and entrapment. The use of environmentally friendly natural biopolymers and essential oils results in novel antibacterial activity that promotes little to no resistance. Additionally, these natural materials offer additional benefits such as hemostatic activity.

A large part of this work focused on chitosan, which was paired with essential oils to act as a stabilizing agent and offer additional antibacterial activity. Along with PEO, electrospun nanofiber mats were fabricated and the subsequent release of the essential oil was characterized along with the overall antibacterial efficacy of the nanofiber mat. Successful incorporation of the essential oil, CIN, into chitosan/PEO nanofiber mats resulted in high inactivation of both *P. aeruginosa* and *E. coli*. Furthermore, the incorporation of an essential oil based on its structure and properties and the subsequent electrospinning as a function of chitosan's DA and MW was characterized. As a function of aging, the same characterization should be employed to determine storage limitations. Translation of chitosan/essential oil pre-cursor solutions to fabricating thin films was also demonstrated along with exploring the effect of the addition of a surfactant to the incorporation and subsequent release of an essential oil. Specifically, a higher release can be achieved by the addition of a surfactant and the use of a surfactant in electrospunning chitosan/PEO/CIN should be explored in future studies. Overall, the successful utilization

of two structurally different essential oils as antibacterial agents delivered via chitosan electrospun nanofiber mats or thin films has been demonstrated.

An additional objective of demonstrating the of nanofiber mats to uptake potentially harmful bacteria utilized regenerated cellulose nanofiber mats. These nanofiber mats were compared to other commercial fibrous material to assess their potential and outperformed the commercial options. As a function of bacteria concentration, nanofiber mat parameters, bacteria strain, and bacteria viability, the uptake of bacteria by nanofiber mats was quantified. The removal of bacteria from the nanofiber mats post collection for reusability should be assessed and studied as a greener alternative to one-use disposables. Through post functionalization with polyelectrolytes, the surface properties of the cellulose nanofiber mats were optimized to demonstrate control over collection and inactivation. Hydrophilic cationic surfaces resulted in the highest collection and inactivation. Translation of polyelectrolyte functionalized nanofibers for the uptake of viruses in addition to bacteria would be an ideal next step for medical applications.

A final part of this dissertation explored zeolites as a cargo carrier for nanofiber mats, which are advantageous due to their tunable profile release. Three geometrically different LTA zeolites were either grown or attached to cellulose nanofiber mats to access their ability to inactivate bacteria using Ag^{+} ions as the loaded cargo. Successful inactivation was achieved by all zeolite/nanofiber mats composites. Zeolites can be reloaded and the reusability of these composite materials should be studied. Additionally, Meso zeolites offer the unique advantage of delivering two agents, which could provide reusable nanofiber mats capable of delivering either two different antibacterial agents, two essential oils or an antibacterial agent paired with another medical drug.

APPENDIX
FUNCTIONALIZING CELLULOSE NANOFIBER MATS WITH CHITOSAN/CIN

A.1 Summary

Here, the potential of functionalizing via dip-coating the outer surface of electrospun nanofiber mats with an essential oil is investigated. Cellulose nanofiber mats are functionalized using a chitosan-based solution containing CIN through dip-coating. Resultant chitosan/CIN(1:0, 1:0.1, 1:1 and 0:1) functionalized mats morphology and average fiber diameter consistent with cellulose nanofiber mats. The addition of chitosan to the surface results in an increased hydrophobic surface and the addition of CIN further increased the hydrophobicity of the surface. Post-functionalization of chitosan/CIN resulted in higher quantities (~10×) of CIN released in comparison to electrospun chitosan/PEO/CIN mats. The low levels of bacterial uptake paired with the high release of CIN exhibited by all chitosan/CIN functionalized mats demonstrates the potential of this coating to be used when minimal cell adhesion but high inactivation is needed.

A.2 Methods

A.2.1 Chitosan/CIN Synthesis and Quantification

Mass ratios of 1:0, 1:0.1, 1:1 and 0:1 of chitosan/CIN using 2.5 w/v% chitosan dissolved in 0.5 M AA-d4 (500 μL) were prepared as previously described in Chapter 4 Section 4.2.1. ^{1}H NMR was used as previously described in Chapter 4 Section 4.2.1.

A.2.2. Cellulose Nanofiber Mat Fabrication

Details are provided in Chapter 7 Section 7.2.1.

A.2.3. Functionalizing Electrospun Cellulose Mats with chitosan/CIN solution

Each solution (20 mL) was separately poured into a square petri dish with six cellulose nanofiber mats. For the pure CIN coating, only 10 mL of pure CIN was used. Each petri dish was then placed onto a Lab Line 3-D rotator (model #4630, 120 V) for 30 min. After rotation, the mats were removed from solution, washed with DI water, and set out to dry overnight.

A.2.4. Chitosan/CIN Functionalized Cellulose Nanofiber Mat Characterization

SEM Micrographs along with fiber diameter averages and distribution were acquired as previously described in Chapter 4 Section 4.2.3. Contact angle measurements were performed as previously described in Chapter 4 Section 4.2.3.

A.2.5. CIN Release from Chitosan/CIN Functionalized Cellulose Nanofiber Mat

The cumulative release of CIN as liquid from cellulose nanofiber mats functionalized with chitosan/CIN(1:0, 1:0.1, 1:1 and 0:1) as a function of time was performed as previously described in Chapter 4 Section 4.2.4. The solution was placed not replaced to maintain the same gradient flux. As no further cumulative release was seen after 24 hr, it was assumed that the samples had reached equilibrium and therefore, a secondary release study was employed using the same nanofiber mats. Starting at the 24 hr time point, the isotonic solution was replaced each day for five days to attempt to release all “releasable” CIN from the sample.

A.2.6. Quantification of Bacteria Uptake by chitosan/CIN Functionalized Electrospun Mats

The uptake of *E. coli* K12 and *P. aeruginosa* PA01 by chitosan/CIN functionalized cellulose nanofiber mats was performed as previously described in Chapter 7 Section 7.2.3.

A.3 Results and Discussion

A.3.1. Chitosan/CIN Functionalized Cellulose Nanofiber Mat Characteristics

Characteristics of cellulose nanofiber mats are described in Chapter 7 Section 7.3.1.

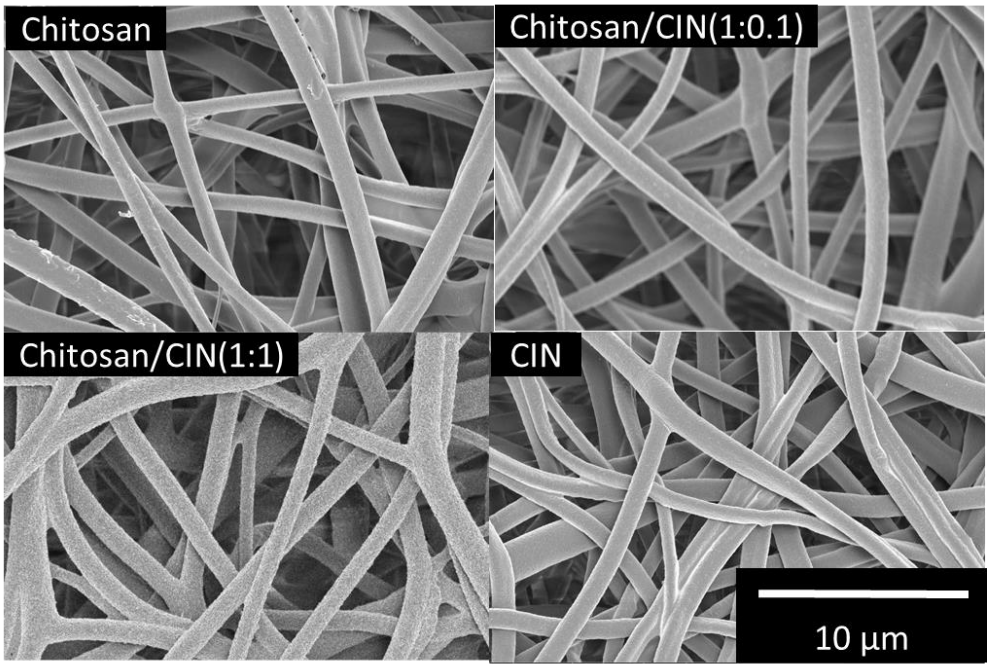

Figure 59: SEM micrographs depicting the morphology of cellulose nanofiber mats functionalized with chitosan, chitosan/CIN(1:0.1 and 1:1 p:o mass ratios) and CIN.

Cellulose nanofiber mats were functionalized with chitosan, chitosan/CIN (1:0.1 and 1:1 p:o mass ratios) and CIN, Figure 59. The average fiber diameter for each sample post functionalization was determined; there was no statistical change in average fiber diameter, Table 11. Based on SEM micrographs (Figure 59), post functionalization with chitosan, chitosan/CIN and CIN, the nanofiber surface appeared smooth and the fiber morphology stayed intact.

Contact angle measurements shown in Table 11 show a sharp contrast between nanofiber mats functionalized and non-functionalized with CIN. Cellulose nanofiber mats have the lowest contact angle. Chitosan-functionalized cellulose nanofiber mats exhibit a statistically increased contact angle. Nanofiber mats functionalized with chitosan/CIN(1:0.1 and 1:1) or CIN have the statistically highest contact angle. The high

standard deviation associated with the majority of CIN functionalization insinuates that this functionalization might not be even or well distributed.

Table 11: Summary of the Materials Properties of chitosan/CIN Functionalized Electrospun Cellulose Nanofiber Mats

Polymer Coating	Average Fiber Diameter (μm)	Contact Angle (°)[1]
N/A	0.85±0.22	35.9±4.8
Chitosan	0.84±0.21	69.2±7.4
Chitosan/CIN (1:0.1 p:o)	0.91±0.18	122.3±10.4
Chitosan/CIN (1:1 p:o)	1.21±0.33	121.4±6.1
CIN	0.88±0.18	127.2±12.6

[1] Glycerol contact angle is reported. The water and diiodomethane contact angles were also tested but the solutions absorbed immediately into all nanofiber mats.

Post functionalization of cellulose nanofiber mats with chitosan/CIN results in hydrophobic fibers whereas electrospinning chitosan/PEO/CIN nanofibers mats results in hydrophilic nanofiber mats. Thus, depending on the application the method of CIN incorporation could be tailored.

A.3.2. Release of CIN from Chitosan/CIN Functionalized Cellulose Nanofiber Mats

The release of CIN in liquid form from chitosan/CIN(1:0, 1:0.1, 1:1 and 0:1) functionalized cellulose nanofiber mats was determined using UV-VIS, Figure 60. For all release experiments, chitosan functionalized cellulose nanofiber mats show no release as expected. A comparison of chitosan/CIN(1:0.1 and 1:1) functionalized mats shows a statistically higher total release, 0.05 ± 0.002 vs. 0.07 ± 0.001 μg, at 180 min from mats functionalized with chitosan/CIN(1:1) vs chitosan/CIN(1:0.1), respectively (Figure 60 Left). Mats coated in CIN demonstrated on average the highest release, releasing 0.10 ± 0.082 μg at 180 min. However, due to the high standard deviation, this is not statistically

significant and further indicates an uneven coating in conjunction with the contact angle results. Thus, CIN functionalization without the use of chitosan might result in unreliable reproducibility.

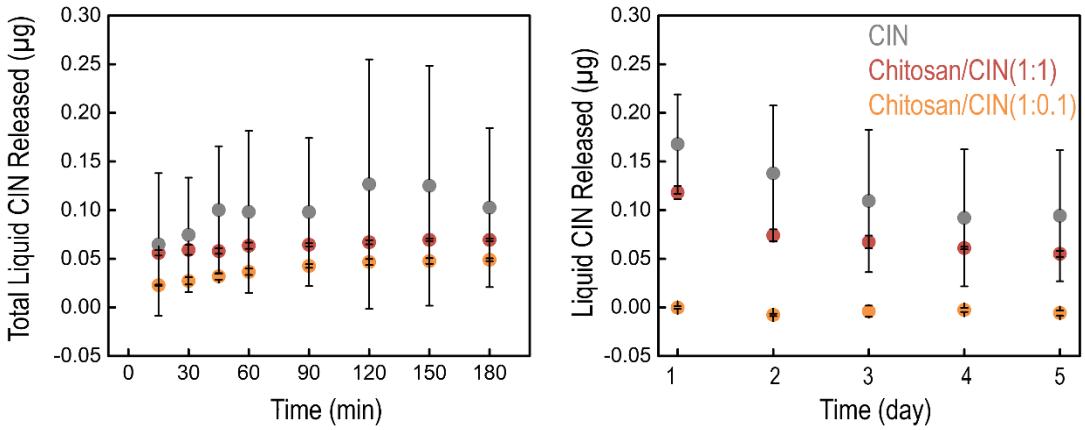

Figure 60: (Left) Cumulative release of CIN over 180 min from nanofiber mats into the same isotonic solution. No further release was seen from 180 min till 24 hr. (Right) The release of CIN over five days using the same nanofiber mats and exchanging the solution for fresh isotonic solution each day.

The overall release at 180 min from nanofiber mats post functionalized with chitosan/CIN is considerably higher (~10×) than the release from electrospun chitosan/PEO/CIN nanofiber mats. Thus, it can be implied that these nanofiber mats would successfully inactivate both *E. coli* K12 and *P. aeruginosa* PA01.

Additionally due to the high release, a second release study was feasible to determine if any more CIN could be extracted from the nanofiber mats by replacing the isotonic solution to create a new gradient flux, Figure 60 (Right). The isotonic solution was then replaced each day for five days to determine if the nanofiber mats would continue to release CIN once it was removed from the surrounding solution. Over the course of five days, continue release of CIN was seen for chitosan/CIN(1:1 and 0:1) functionalized mats with a decreasing trend on the quantity released each day. Similar to the previous initial release experiment, the release of CIN from CIN functionalized mats had high standard

deviations. Chitosan/CIN(1:0.1) functionalized nanofiber mats did not release any more CIN after 180 min.

A.3.3. Uptake of Bacteria using Chitosan/CIN Functionalized Cellulose Nanofiber Mats

Post functionalized chitosan/CIN nanofiber mats had more hydrophobic surfaces, released more CIN and appear to having less reproducibility compared to electrospun chitosan/PEO/CIN nanofiber mats. As the surface hydrophilicity/phobicity plays a critical role in the ability to uptake bacteria, the collection of two strains was examined, Figure 61. Similar quantities of *E. coli* K12 cells were collected by nanofiber mats containing none or low amounts of CIN, specifically chitosan/CIN(1:0 and 1:0.1). These quantities of cells are comparable to the uptake by chitosan or PAA functionalized cellulose nanofiber mats, Figure 49. Nanofiber mats functionalized in only CIN with no chitosan showed the highest collection of bacteria but with very high standard deviations. Based on previous results (Figure 49), we expect that the most *E. coli* K12 cell will be collected by nanofiber mats with the most hydrophilic surface. One potential explanation is that as the CIN released, the nanofiber mat changed from hydrophobic to hydrophilic and bacteria attached.

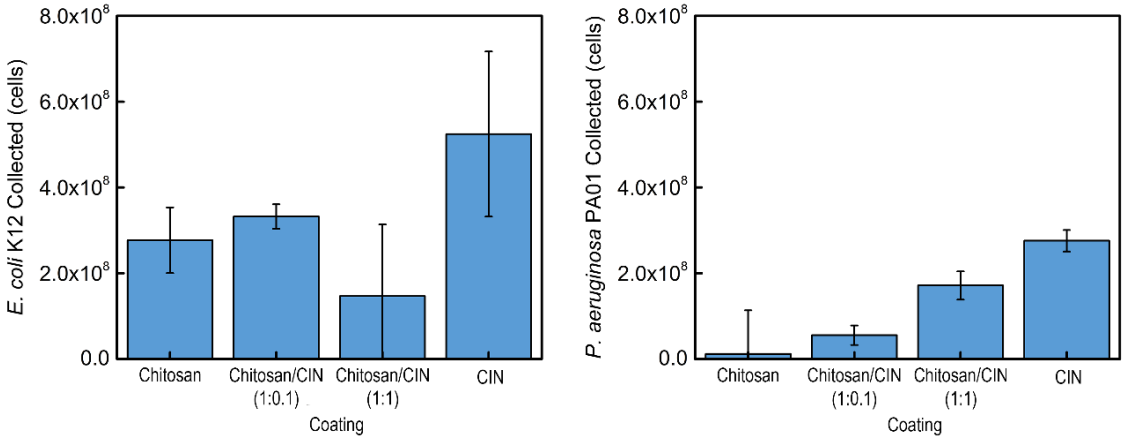

Figure 61: The average number of *E. coli* K12 cells (Left) and *P. aeruginosa* PA01 (Right) collected after 120 min using cellulose nanofiber mats functionalized with chitosan/CIN(1:0, 1:0.1, 1:1 and 0:1).

The collection of *P. aeruginosa* PA01 cells correlates directly with the level of CIN within the functionalization coating. A higher quantity of CIN lead to a higher quantity of cells collected. However, the highest number of cells collected is similar to the lowest quantity collected by polyelectrolyte functionalized nanofiber mats (Figure 49). Unfortunately due to the size of the nanofibers produced from electrospinning chitosan/PEO/CIN, the uptake of bacteria could not be determined and therefore a direct comparison cannot be made. However, the relationship between surface hydrophilicity/phobicity and bacteria uptake would suggest that the electrospun chitosan/PEO/CIN would provide an ideal surface for cell adhesion. Overall, post-functionalization of chitosan/CIN can be potentially used as one method that could result in nanofiber mats that can inactivate bacteria with minimal cell adhesion but must be further optimized to ensure reproducibility.

REFERENCES

(1) Donlan, R. M. *Emerg. Infect. Dis.* **2002**, *8* (9), 881–890.

(2) de Kievit, T. R. *Microbiol.* **2009**, *11* (2), 279–288.

(3) Hall-Stoodley, L.; Costerton, J. W.; Stoodley, P. *Nat. Rev. Microbiol.* **2004**, *2* (2), 95–108.

(4) Rasmussen, T. B.; Givskov, M. *Med. Microbiol.* **2006**, *296* (2-3), 149–161.

(5) *Cent. Diesease Control Prev.* **2013**.

(6) Jr, F. R. In *Pseudomonas aeruginosa, the Opportunist, Pathogensis and Disease*; Fick RB Jr, Ed.; 1993.

(7) Page, M. G. P.; Heim, J. *Curr. Opin. Pharmacol.* **2009**, *9* (5), 558–565.

(8) Carmeli, Y.; Troillet, N.; Eliopoulos, G. M.; Samore, M. H. *Antimicrob. Agents Chemother.* **1999**, *43* (6), 1379–1382.

(9) Hota, S.; Hirji, Z.; Stockton, K.; Lemieux, C.; Dedier, H.; Wolfaardt, G.; Gardam, M. A. *Infect. Control Hosp. Epidemiol.* **2009**, *30* (1), 25–33.

(10) Skindersoe, M. E.; Alhede, M.; Phipps, R.; Yang, L.; Jensen, P. O.; Rasmussen, T. B.; Bjarnsholt, T.; Tolker-Nielsen, T.; Høiby, N.; Givskov, M. *Antimicrob. Agents Chemother.* **2008**, *52* (10), 3648–3663.

(11) Lee, J.; Zhang, L. *Protein Cell* **2015**, *6* (1), 26–41.

(12) Clatworthy, A. E.; Pierson, E.; Hung, D. T. *Nat. Chem. Biol.* **2007**, *3* (9), 541–548.

(13) Bakkali, F.; Averbeck, S.; Averbeck, D.; Idaomar, M. *Food Chem. Toxicol.* **2008**, *46* (2), 446–475.

(14) Pattnaik, S.; Suramanyam, V. R.; Bapaji, M.; Kole, C. R. *Microbiol.* **1997**, *89*, 39–46.

(15) Burt, S. *Int. J. Food Microbiol.* **2004**, *94* (3), 223–253.

(16) Hammer, K. A.; Carson, C. F.; Riley, T. V. *J. Appl. Microbiol.* **1999**, *86* (6), 985–990.

(17) Kavanaugh, N. L.; Ribbeck, K. *Appl. Environ. Microbiol.* **2012**, *78* (11), 4057–4061.

(18) Bouhdid, S.; Abrini, J.; Amensour, M.; Zhiri, A.; Espuny, M. J.; Manresa, A. *J. Appl. Microbiol.* **2010**, *109* (4), 1139–1149.

(19) Chan, K.-G.; Liu, Y.-C.; Chang, C.-Y. *Front. Microbiol.* **2015**, *6*, 1173.

(20) Schiffman, J. D.; Schauer, C. L. *Polym. Rev.* **2008**, *48* (2), 317–352.

(21) Vishakha Kulkarni, K. B. *Int. J. Res. Pharm. Biomed. Sci.* **2012**, *3* (4), 1597–1613.

(22) Shirwaikar, A.; Shirwaikar, A.; Prabu, S. L.; Kumar, G. A. *Indian J. Pharm. Sci. 70* (4), 415–422.

(23) Schiffman, J. D.; Blackford, A. C.; Wegst, U. G. K.; Schauer, C. L. *Carbohydr. Polym.* **2011**, *84* (4), 1252–1257.

(24) Schiffman, J. D.; Stulga, L. A.; Schauer, C. L. *Poly. Eng. Sci.* **2009**, *49* (10), 1918–1928.

(25) Ohkawa, K.; Cha, D.; Kim, H.; Nishida, A.; Yamamoto, H. *Macromol. Rapid Commun.* **2004**, *25* (18), 1600–1605.

(26) Klossner, R. R.; Queen, H. A.; Coughlin, A. J.; Krause, W. E. *Solutions* **2008**, 2947–2953.

(27) Penchev, H.; Paneva, D.; Manolova, N.; Rashkov, I. *Macromol. Biosci.* **2009**, *9* (9), 884–894.

(28) Liu, H.; Hsieh, Y.-L. *J. Polym. Sci., Part B Polym. Phys.* **2002**, *40* (18), 2119–2129.

(29) Chen, L.; Bromberg, L.; Hatton, T. A.; Rutledge, G. C. *Polymer (Guildf).* **2008**, *49* (5), 1266–1275.

(30) Frey, M. W. *Polym. Rev.* **2008**, *48* (2), 378–391.

(31) Wang, L.; Wang, M.; Topham, P. D.; Huang, Y. *RSC Adv.* **2012**, *2* (6), 2433.

(32) Brenner, E. K.; Schiffman, J. D.; Thompson, E. A.; Toth, L. J.; Schauer, C. L. *Carbohydr. Polym.* **2012**, *87* (1), 926–929.

(33) Uppal, R.; Ramaswamy, G. N.; Arnold, C.; Goodband, R.; Wang, Y. *J. Biomed. Mater. Res., Part B* **2011**, *97* (1), 20–29.

(34) Lin, J.; Li, C.; Zhao, Y.; Hu, J.; Zhang, L.-M. *ACS Appl. Mater. Interfaces* **2012**, *4* (2), 1050–1057.

(35) Matthews, J. A.; Wnek, G. E.; Simpson, D. G.; Bowlin, G. L. *Biomacromolecules* **2002**, *3* (2), 232–238.

(36) Liu, S.-J.; Kau, Y.-C.; Chou, C.-Y.; Chen, J.-H.; Wu, R.-C.; Yeh, W.-L. *J. Membr. Sci.* **2010**, *355* (1-2), 53–59.

(37) Wharram, S. E.; Zhang, X.; Kaplan, D. L.; McCarthy, S. P. *Macromol. Biosci.* **2010**, *10* (3), 246–257.

(38) Ayutsede, J.; Gandhi, M.; Sukigara, S.; Micklus, M.; Chen, H.-E.; Ko, F. *Polymer (Guildf).* **2005**, *46* (5), 1625–1634.

(39) Jin, H.-J.; Fridrikh, S. V; Rutledge, G. C.; Kaplan, D. L. *Biomacromolecules 3* (6), 1233–1239.

(40) Li, C.; Vepari, C.; Jin, H.-J.; Kim, H. J.; Kaplan, D. L. *Biomaterials* **2006**, *27* (16), 3115–3124.

(41) Rieger, K. A.; Birch, N. P.; Schiffman, J. D. *J. Mater. Chem. B* **2013**, *1* (36), 4531.

(42) Vulcani, V. A. S.; Franzo, V. S.; Rabelo, R. E.; Rabbers, A. S.; Assis, B. M.; D'Ávila, M. A.; Antoni, S. M. B. *Arq. Bras. Med. Veterinária e Zootec.* **2015**, *67* (4), 1039–1044.

(43) Bhattarai, N.; Edmondson, D.; Veiseh, O.; Matsen, F. A.; Zhang, M. *Biomaterials* **2005**, *26* (31), 6176–6184.

(44) Gombotz, W. R.; Pettit, D. K. *Bioconjugate Chem.* **1995**, *6* (4), 332–351.

(45) Casper, C. L.; Yamaguchi, N.; Kiick, K. L.; Rabolt, J. F. *Biomacromolecules 6* (4), 1998–2007.

(46) Ojha, S. S.; Stevens, D. R.; Hoffman, T. J.; Stano, K.; Klossner, R.; Scott, M. C.; Krause, W.; Clarke, L. I.; Gorga, R. E. *Biomacromolecules* **2008**, *9* (9), 2523–2529.

(47) Deitzel, J. M.; Kleinmeyer, J. D.; Hirvonen, J. K.; Tan, N. C. B. *Polymer (Guildf).* **2001**, *42*, 8163–8170.

(48) Ignatova, M.; Manolova, N.; Markova, N.; Rashkov, I. *Macromol. Biosci.* **2009**, *9* (1), 102–111.

(49) Luu, Y. K.; Kim, K.; Hsiao, B. S.; Chu, B.; Hadjiargyrou, M. *J. Control. Release* **2003**, *89* (2), 341–353.

(50) Said, S. S.; El-Halfawy, O. M.; El-Gowelli, H. M.; Aloufy, A. K.; Boraei, N. A.; El-Khordagui, L. K. *Eur. J. Pharm. Biopharm.* **2012**, *80* (1), 85–94.

(51) Yang, F.; Murugan, R.; Wang, S.; Ramakrishna, S. *Biomaterials* **2005**, *26* (15), 2603–2610.

(52) Thakur, R. A. A.; Florek, C. A. A.; Kohn, J.; Michniak, B. B. B. *Int. J. Pharm* **2008**, *364* (1), 87–93.

(53) Gümüşderelioğlu, M.; Dalkıranoğlu, S.; Aydın, R. S. T.; Cakmak, S. *J. Biomed. Mater. Res., Part A* **2011**, *98* (3), 461–472.

(54) Jannesari, M.; Varshosaz, J.; Morshed, M.; Zamani, M. *Int. J. Nanomedicine* **2011**, *6*, 993–1003.

(55) Zhang, Y.; Ouyang, H.; Lim, C. T.; Ramakrishna, S.; Huang, Z.-M. *J. Biomed. Mater. Res., Part B* **2005**, *72* (1), 156–165.

(56) Gunn, J.; Zhang, M. *Trends Biotechnol.* **2010**, *28* (4), 189–197.

(57) Gilbert, W. *P. Short. London* **1628**.

(58) Larmor, J. *Proc. R. Soc. Lond. A. Math. Phys. Sci.* **1898**, *63*, 365.

(59) Cooley, J. F. Apparatus for Electrically dispersing Fluids US Paten 692,631, 1902.

(60) Morton, W. J. Method of dispersing fluids U.S. Patent 705,691, 1902.

(61) Formhals, A. A method and apparatus for the production of fibers., 1938.

(62) Formhals, A. Method and apparatus for spinning., 1939.

(63) Formhals, A. A Method and apparatus for the production of artificial fibers, 1939.

(64) Doshi, J.; Reneker, D. H. *J. Electrost.* **2012**, *35* (2-3), 1–10.

(65) Persano, L.; Camposeo, A.; Tekmen, C.; Pisignano, D. *Macromol. Mater. Eng.* **2013**, *298* (5), 504–520.

(66) Teo, W. E.; Ramakrishna, S. *Nanotechnology* **2006**, *17* (14), R89–R106.

(67) Taylor, G. *Proc. R. Soc. Lond. A. Math. Phys. Sci.* **1966**, *291*, 145.

(68) Taylor, G. *Proc. R. Soc. London. Ser. A, Math. Phys. Eng. Sci.* **1969**, *313*, 453.

(69) Shin, Y. .; Hohman, M. .; Brenner, M. P.; Rutledge, G. . *Polymer (Guildf).* **2001**, *42* (25), 9955–9967.

(70) Mckee, M. G.; Wilkes, G. L.; Colby, R. H.; Long, T. E. *Macromolecules* **2004**, *37* (5), 1760–1767.

(71) McKee, M. G.; Hunley, M. T.; Layman, J. M.; Long, T. E. *Macromolecules* **2006**, *39* (2), 575–583.

(72) Zong, X. H.; Kim, K.; Fang, D. F.; Ran, S. F.; Hsiao, B. S.; Chu, B. *Polymer (Guildf).* **2002**, *43*, 4403.

(73) Geng, X. Y.; Kwon, O. H.; Jang, J. H. *Biomaterials* **2005**, *26*, 5427.

(74) Mit-Uppatham, C.; Nithitanakul, M.; Supaphol, P. *Macromolecules* **2004**, *205*, 2327.

(75) Behonick, D. J.; Werb, Z. *Mech. Dev.* **2003**, *120* (11), 1327–1336.

(76) Schiffman, J. D.; Austero, M.; Oroho, A. E.; Wegst, U. G. .; Schauer, C. L. *J. Polym. Sci. Part A Polym. Chem.*

(77) Li, D.; Wang, Y.; Xia, Y. *Nano Lett.* **2003**, *3* (8), 1167–1171.

(78) Li, D.; Wang, Y.; Xia, Y. *Adv. Mater.* **2004**, *16* (4), 361–366.

(79) Schiffman, J. D.; Elimelech, M. *ACS Appl. Mater. Interfaces* **2011**, *3* (2), 462–468.

(80) Kenawy, E.-R.; Abdel-Hay, F. I.; El-Newehy, M. H.; Wnek, G. E. *Mater. Chem. Phys.* **2009**, *113* (1), 296–302.

(81) Suwantong, O.; Opanasopit, P.; Ruktanonchai, U.; Supaphol, P. *Polymer (Guildf).* **2007**, *48* (26), 7546–7557.

(82) Rujitanaroj, P.; Pimpha, N.; Supaphol, P. *Polymer (Guildf).* **2008**, *49* (21), 4723–4732.

(83) Nguyen, T.-H.; Kim, Y.-H.; Song, H.-Y.; Lee, B.-T. *J. Biomed. Mater. Res., Part B* **2011**, *96* (2), 225–233.

(84) Zhang, Y.; Lim, C. T.; Ramakrishna, S.; Huang, Z.-M. *J. Mater. Sci. Mater. Med.* **2005**, *16* (10), 933–946.

(85) Charernsriwilaiwat, N.; Opanasopit, P.; Rojanarata, T.; Ngawhirunpat, T. *Int. J. Pharm.* **2012**, *427* (2), 379–384.

(86) Huang, X.; Brazel, C. S. *J. Control. Release* **2001**, *73* (2-3), 121–136.

(87) Cantón, I.; Mckean, R.; Charnley, M.; Blackwood, K. A.; Fiorica, C.; Ryan, A. J.; MacNeil, S. *Biotechnol. Bioeng.* **2010**, *105* (2), 396–408.

(88) Zhang, X.; Suresh Kumar, P.; Aravindan, V.; Liu, H. H.; Sundaramurthy, J.; Mhaisalkar, S. G.; Duong, H. M.; Ramakrishna, S.; Madhavi, S. *J. Phys. Chem. C* **2012**, *116* (28), 14780–14788.

(89) He, X.; Tan, L.; Wu, X.; Yan, C.; Chen, D.; Meng, X.; Tang, F. *J. Mater. Chem.* **2012**, *22* (35), 18471.

(90) Saquing, C. D.; Tang, C.; Monian, B.; Bonino, C. A.; Manasco, J. L.; Alsberg, E.; Khan, S. A. *Ind. Eng. Chem. Res.* **2013**, *52* (26), 8692–8704.

(91) Choi, J. S.; Choi, S. H.; Yoo, H. S. *J. Mater. Chem.* **2011**, *21* (14), 5258.

(92) Jiang, H.; HU, Y.; LI, Y.; ZHAO, P.; Zhu, K.; CHEN, W. *J. Control. Release* **2005**, *108* (2-3), 237–243.

(93) Liu, J.-J.; Wang, C.-Y.; Wang, J.-G.; Ruan, H.-J.; Fan, C.-Y. *J. Biomed. Mater. Res., Part A* **2011**, *96* (1), 13–20.

(94) Pakravan, M.; Heuzey, M.-C.; Ajji, A. *Biomacromolecules* **2012**, *13* (2), 412–421.

(95) Nguyen, T. T. T.; Chung, O. H.; Park, J. S. *Carbohydr. Polym.* **2011**, *86* (4), 1799–1806.

(96) Reznik, S. N.; Yarin, A. L.; Zussman, E.; Bercovici, L. *Phys. Fluids* **2006**, *18* (6), 062101.

(97) Yarin, a. L. *Polym. Adv. Technol.* **2011**, *22* (3), 310–317.

(98) Su, Y.; Li, X.; Liu, Y.; Su, Q.; Qiang, M. L. W.; Mo, X. *J. Biomater. Sci., Polym. Ed.* **2010**, No. 1, 165–177.

(99) Qi, H.; Hu, P.; Xu, J.; Wang, A.; Qi; Wang. *Biomacromolecules* **2006**, *7* (8), 2327–2330.

(100) Liao, Y.; Zhang, L.; Gao, Y.; Zhu, Z.-T.; Fong, H. *Polymer (Guildf).* **2008**, *49* (24), 5294–5299.

(101) Xu, X.; Yang, L.; Xu, X.; Wang, X.; Chen, X.; Liang, Q.; Zeng, J.; Jing, X. *J. Control. Release* **2005**, *108* (1), 33–42.

(102) Yang, Y.; Li, X.; Cui, W.; Zhou, S.; Tan, R.; Wang, C. *J. Biomed. Mater. Res., Part A* **2008**, *86* (2), 374–385.

(103) Xu, X.; Zhuang, X.; Chen, X.; Wang, X.; Yang, L.; Jing, X. *Macromol. Rapid Commun.* **2006**, *27* (19), 1637–1642.

(104) Briggs, T.; Arinzeh, T. L. *J. Biomed. Mater. Res. A* **2014**, *102* (3), 674–684.

(105) Yang, Y.; Li, X.; Cheng, L.; He, S.; Zou, J.; Chen, F.; Zhang, Z. *Acta Biomater.* **2011**, *7* (6), 2533–2543.

(106) Xu, X.; Chen, X.; Ma, P.; Wang, X.; Jing, X. *Eur. J. Pharm. Biopharm.* **2008**, *70* (1), 165–170.

(107) Sanders, E. H.; Kloefkorn, R.; Bowlin, G. L.; Simpson, D. G.; Wnek, G. E. *Macromolecules* **2003**, *36* (11), 3803–3805.

(108) Angeles, M.; Cheng, H.; Velankar, S. S. *Polym. Adv. Technol.* **2008**, *19* (7), 728–733.

(109) Li, Y.; Ko, F. K.; Hamad, W. Y. *Biomacromolecules* **2013**, *14* (11), 3801–3807.

(110) Xu, X.; Zhong, W.; Zhou, S.; Trajtman, A.; Alfa, M. *J. Appl. Poly. Sci.* **2010**, n/a – n/a.

(111) Schiffman, J. D.; Wang, Y.; Giannelis, E. P.; Elimelech, M. *Langmuir* **2011**, *27* (21), 13159–13164.

(112) Kang, Y. O.; Yoon, I.-S.; Lee, S. Y.; Kim, D.-D.; Lee, S. J.; Park, W. H.; Hudson, S. M. *J. Biomed. Mater. Res., Part B* **2010**, *92* (2), 568–576.

(113) Spasova, M.; Paneva, D.; Manolova, N.; Radenkov, P.; Rashkov, I. *Macromol. Biosci.* **2008**, *8* (2), 153–162.

(114) Chen, L.; Bromberg, L.; Lee, J. A.; Zhang, H.; Schreuder-Gibson, H.; Gibson, P.; Walker, J.; Hammond, P. T.; Hatton, T. A.; Rutledge, G. C. *Chem. Mat.* **2010**, *22* (4), 1429–1436.

(115) Kim, H. S.; Yoo, H. S. *J. Control. Release* **2010**, *145* (3), 264–271.

(116) Woo, Y. I.; Park, B. J.; Kim, H.-L.; Lee, M. H.; Kim, J.; Yang, Y.-I.; Kim, J. K.; Tsubaki, K.; Han, D.-W.; Park, J.-C. *Biomed. Mater.* **2010**, *5* (4), 044109.

(117) Choi, J. S.; Leong, K. W.; Yoo, H. S. *Biomaterials* **2008**, *29* (5), 587–596.

(118) Nicknejad, E. T.; Ghoreishi, S. M.; Habibi, N. *AAPS PharmSciTech* **2015**, *16* (6), 1480–1486.

(119) Maeda, N.; Miao, J.; Simmons, T. J.; Dordick, J. S.; Linhardt, R. J. *Carbohydr. Polym.* **2014**, *102*, 950–955.

(120) Deng, L.; Young, R. J.; Kinloch, I. A.; Zhu, Y.; Eichhorn, S. J. *Carbon N. Y.* **2013**, *58*, 66–75.

(121) Konwarh, R.; Karak, N.; Misra, M. *Biotechnol. Adv.* **2013**, *31* (4), 421–437.

(122) Fischer, R. L.; McCoy, M. G.; Grant, S. A. *J. Mater. Sci. Mater. Med.* **2012**, *23* (7), 1645–1654.

(123) Bürck, J.; Heissler, S.; Geckle, U.; Ardakani, M. F.; Schneider, R.; Ulrich, A. S.; Kazanci, M. *Langmuir* **2013**, *29* (5), 1562–1572.

(124) Zhang, Y. Z.; Venugopal, J.; Huang, Z.-M.; Lim, C. T.; Ramakrishna, S. *Polymer (Guildf).* **2006**, *47* (8), 2911–2917.

(125) Choktaweesap, N.; Arayanarakul, K.; Aht-ong, D.; Meechaisue, C.; Supaphol, P. *Polym. J.* **2007**, *39* (6), 622–631.

(126) Zhang, X.; Reagan, M. R.; Kaplan, D. L. *Adv. Drug Deliv. Rev.* **2009**, *61* (12), 988–1006.

(127) Li, M.; Mondrinos, M. J.; Gandhi, M. R.; Ko, F. K.; Weiss, A. S.; Lelkes, P. I. *Biomaterials* **2005**, *26* (30), 5999–6008.

(128) Araujo, J.; Padrão, J.; Silva, J. P.; Dourado, F.; Correia, D. M.; Botelho, G.; Gomez Ribelles, J. L.; Lanceros-Méndez, S.; Sencadas, V. *Appl. Phys. A* **2013**, *115* (4), 1291–1298.

(129) McKenna, K. A.; Hinds, M. T.; Sarao, R. C.; Wu, P.-C.; Maslen, C. L.; Glanville, R. W.; Babcock, D.; Gregory, K. W. *Acta Biomater.* **2012**, *8* (1), 225–233.

(130) Frey, M. W.; Li, L.; Xiao, M.; Gould, T. *Cellulose* **2006**, *13* (2), 147–155.

(131) Viswanathan, G.; Murugesan, S.; Pushparaj, V.; Nalamasu, O.; Ajayan, P. M.; Linhardt, R. J. *Biomacromolecules* **2006**, *7* (2), 415–418.

(132) Ahn, Y.; Hu, D.-H.; Hong, J. H.; Lee, S. H.; Kim, H. J.; Kim, H. *Carbohydr. Polym.* **2012**, *89* (2), 340–345.

(133) Kulpinski, P. *J. Appl. Polym. Sci.* **2005**, *98* (4), 1855–1859.

(134) Kriegel, C.; Arecchi, A.; Arrechi, A.; Kit, K.; McClements, D. J.; Weiss, J. *Crit. Rev. Food Sci. Nutr.* **2008**, *48* (8), 775–797.

(135) Rodríguez, K.; Gatenholm, P.; Renneckar, S. *Cellulose* **2012**, *19* (5), 1583–1598.

(136) Rezaei, A.; Nasirpour, A.; Fathi, M. *Compr. Rev. Food Sci. Food Saf.* **2015**, *14* (3), 269–284.

(137) Ma, H.; Burger, C.; Hsiao, B. S.; Chu, B. *Biomacromolecules* **2012**, *13* (1), 180–186.

(138) Song, J.; Birbach, N. L.; Hinestroza, J. P. *Cellulose* **2012**, *19* (2), 411–424.

(139) Schiffman, J. D.; Schauer, C. L. *Biomacromolecules* **2007**, *8* (9), 2665–2667.

(140) Sangsanoh, P.; Supaphol, P. *Biomacromolecules* **2006**, *7* (10), 2710–2714.

(141) Wu, L.; Li, H.; Li, S.; Li, X. X.; Yuan, X.; Zhang, Y. *J. Biomed. Mater. Res. Part B Appl. Biomater.* **2009**, *9999A* (2), NA – NA.

(142) Pakravan, M.; Heuzey, M. C.; Ajji, A. *Polymer (Guildf).* **2011**, *52* (21), 4813–4824.

(143) Chen, L.; Zhu, C.; Fan, D.; Liu, B.; Ma, X.; Duan, Z.; Zhou, Y. *J. Biomed. Mater. Res. A* **2011**, *99* (3), 395–409.

(144) Min, B.-M.; Lee, S. W.; Lim, J. N.; You, Y.; Lee, T. S.; Kang, P. H.; Park, W. H. *Polymer (Guildf).* **2004**, *45* (21), 7137–7142.

(145) Lakshman, L.; Shalumon, K. T.; Nair, S.; Jayakumar, R.; Nair, S. V. *J. Macromol. Sci. Part A* **2010**, *47* (10), 1012–1018.

(146) Son, W. K.; Youk, J. H.; Park, W. H. *Carbohydr. Polym.* **2006**, *65* (4), 430–434.

(147) Zhang, Q.; Wu, D.; Qi, S.; Wu, Z.; Yang, X.; Jin, R. *Mat. Lett.* **2007**, *61* (19-20), 4027–4030.

(148) Azad, A.-M.; Hershey, R.; Ali, S.; Goel, V. *J. Mat. Res.* **2010**, *25* (09), 1761–1770.

(149) Yan, L.; Si, S.; Chen, Y.; Yuan, T.; Fan, H.; Yao, Y.; Zhang, Q. *Fibers Polym.* **2011**, *12* (2), 207–213.

(150) Amna, T.; Hassan, M. S.; Barakat, N. A. M.; Pandeya, D. R.; Hong, S. T.; Khil, M.-S.; Kim, H. Y. *Appl. Microbiol. Biotechnol.* **2012**, *93* (2), 743–751.

(151) Hu, W.; Peng, C.; Luo, W.; Lv, M.; Li, X.; Li, D.; Huang, Q.; Fan, C. *ACS Nano* **2010**, *4* (7), 4317–4323.

(152) Kang, S.; Mauter, M. S.; Elimelech, M. *Environ. Sci. Tech.* **2009**, *43* (7), 2648–2653.

(153) Lyon, D. Y.; Alvarez, P. J. J. *Environ. Sci. Tech.* **2008**, *42* (21), 8127–8132.

(154) Kang, S.; Pinault, M.; Pfefferle, L. D.; Elimelech, M. *Langmuir* **2007**, *23* (17), 8670–8673.

(155) Liu, S.; Wei, L.; Hao, L.; Fang, N.; Chang, M. W.; Xu, R.; Yang, Y.; Chen, Y. *ACS Nano* **2009**, *3* (12), 3891–3902.

(156) Han, J.; Chen, T.-X.; Branford-White, C. J.; Zhu, L.-M. *Int. J. Pharm.* **2009**, *382* (1-2), 215–221.

(157) Kontogiannopoulos, K. N.; Assimopoulou, A. N.; Tsivintzelis, I.; Panayiotou, C.; Papageorgiou, V. P. *Int. J. Pharm.* **2011**, *409* (1-2), 216–228.

(158) Miao, J.; Pangule, R. C.; Paskaleva, E. E.; Hwang, E. E.; Kane, R. S.; Linhardt, R. J.; Dordick, J. S. *Biomaterials* **2011**, *32* (36), 9557–9567.

(159) Edris, A. E. *Phyther. Res.* **2007**, *21* (4), 308–323.

(160) Dorman, H. J.; Deans, S. G. *J. Appl. Microbiol.* **2000**, *88* (2), 308–316.

(161) Ojagh, S. M.; Rezaei, M.; Razavi, S. H.; Hosseini, S. M. H. *Food Chem.* **2010**, *122* (1), 161–166.

(162) Zodrow, K. R.; Schiffman, J. D.; Elimelech, M. *Langmuir* **2012**, *39*, 13993–13999.

(163) Badawy, M. E. I.; Rabea, E. I. *Int. J. Biol. Macromol.* **2013**, *57*, 185–192.

(164) Klossner, R. R.; Queen, H. A.; Coughlin, A. J.; Krause, W. E. *Biomacromolecules* **2008**, *9* (10), 2947–2953.

(165) Iamsamai, C.; Hannongbua, S.; Ruktanonchai, U.; Soottitantawat, A.; Dubas, S. T. *Carbon N. Y.* **2010**, *48* (1), 25–30.

(166) Yan, L. Y.; Poon, Y. F.; Chan-Park, M. B.; Chen, Y.; Zhang, Q. *J. Phys. Chem. C* **2008**, *112* (20), 7579–7587.

(167) Rodri-guez, M.; Albertengo, L. A.; Agullo, E. *Carbohydr. Polym.* **2002**, *48* (3), 271–276.

(168) Schulz, P. C.; Rodríguez, M. S.; Del Blanco, L. F.; Pistonesi, M.; Agulló, E. *Colloid Polym. Sci.* **1998**, *276* (12), 1159–1165.

(169) Guinesi, L. . *Carbohydr. Polym.* **2006**, *65* (4), 557–561.

(170) Cordes, E. H.; Jencks, W. P. *J. Am. Chem. Soc.* **1962**, *84* (5), 832–837.

(171) Marin, L.; Moraru, S.; Popescu, M.-C.; Nicolescu, A.; Zgardan, C.; Simionescu, B. C.; Barboiu, M. *Chemistry* **2014**, *20* (16), 4814–4821.

(172) Marin, L.; Simionescu, B.; Barboiu, M. *Chem. Commun.* **2012**, *48* (70), 8778.

(173) Abrigo, M.; Kingshott, P.; McArthur, S. L. *ACS Appl. Mater. Interfaces* **2015**, *7* (14), 7644–7652.

(174) Tufenkji, N. *Adv. Water Resour.* **2007**, *30* (6-7), 1455–1469.

(175) Nielsen, S. M.; Nesterov, I.; Shapiro, A. A. *Transp. Porous Media* **2014**, *102* (2), 227–259.

(176) Liu, J.; Ford, R. M. *Environ. Sci. Technol.* **2009**, *43* (23), 8874–8880.

(177) Saino, E.; Focarete, M. L.; Gualandi, C.; Emanuele, E.; Cornaglia, A. I.; Imbriani, M.; Visai, L. *Biomacromolecules* **2011**, *12* (5), 1900–1911.

(178) Xie, J.; Liu, W.; MacEwan, M. R.; Bridgman, P. C.; Xia, Y. *ACS Nano* **2014**, *8* (2), 1878–1885.

(179) Ku, S. H.; Lee, S. H.; Park, C. B. *Biomaterials* **2012**, *33* (26), 6098–6104.

(180) Soliman, S.; Sant, S.; Nichol, J. W.; Khabiry, M.; Traversa, E.; Khademhosseini, A. *J. Biomed. Mater. Res. A* **2011**, *96* (3), 566–574.

(181) Kim, J.; Kim, D.-H.; Lim, K. T.; Seonwoo, H.; Park, S. H.; Kim, Y.-R.; Kim, Y.; Choung, Y.-H.; Choung, P.-H.; Chung, J. H. *Tissue Eng. Part C. Methods* **2012**, *18* (12), 913–923.

(182) Kim, K.; Luu, Y. K.; Chang, C.; Fang, D.; Hsiao, B. S.; Chu, B.; Hadjiargyrou, M. *J. Control. Release* **2004**, *98* (1), 47–56.

(183) Zheng, F.; Wang, S.; Wen, S.; Shen, M.; Zhu, M.; Shi, X. *Biomaterials* **2013**, *34* (4), 1402–1412.

(184) Kong, H.; Jang, J. *Langmuir* **2008**, *24* (5), 2051–2056.

(185) Abrigo, M.; Kingshott, P.; McArthur, S. L. *Biointerphases* **2015**, *10* (4), 04A301.

(186) Rad, L. R.; Momeni, A.; Ghazani, B. F.; Irani, M.; Mahmoudi, M.; Noghreh, B. *Chem. Eng. J.* **2014**, *256*, 119–127.

(187) Singaravel, G. P.; Hashaikeh, R. *J. Mater. Sci.* **2015**, *51* (2), 1133–1141.

(188) Lalueza, P.; Monzón, M.; Arruebo, M.; Santamaría, J. *Mater. Res. Bull.* **2011**, *46* (11), 2070–2076.

(189) Lalueza, P.; Monzón, M.; Arruebo, M.; Santamaria, J. *Chem. Commun. (Camb).* **2011**, *47* (2), 680–682.

(190) Kwakye-Awuah, B.; Williams, C.; Kenward, M. A.; Radecka, I. *J. Appl. Microbiol.* **2008**, *104* (5), 1516–1524.

(191) Ferreira, L.; Fonseca, A. M.; Botelho, G.; Aguiar, C. A.-; Neves, I. C. *Micropor. Mesopor. Mat.* **2012**, *160*, 126–132.

(192) Krishnani, K. K.; Zhang, Y.; Xiong, L.; Yan, Y.; Boopathy, R.; Mulchandani, A. *Bioresour. Technol.* **2012**, *117*, 86–91.

(193) Belkhair, S.; Kinninmonth, M.; Fisher, L.; Gasharova, B.; Liauw, C. M.; Verran, J.; Mihailova, B.; Tosheva, L. *RSC Adv.* **2015**, *5* (51), 40932–40939.

(194) Jiraroj, D.; Tungasmita, S.; Tungasmita, D. N. *Powder Technol.* **2014**, *264*, 418–422.

(195) Jatunov, S.; Franconetti, A.; Gomez-Guillen, M.; Cabrera-Escribano, F. In *Sciforum Electronic Conference Series*; 2012; Vol. 16.

(196) Eral, H. B.; 't Mannetje, D. J. C. M.; Oh, J. M. *Colloid Polym. Sci.* **2012**, *291* (2), 247–260.

(197) Yang, J.; Kuang, X.; Li, B.; Zhou, B.; Li, J.; Cui, B.; MA, M. *J. Food Saf.* **2012**, *32* (2), 189–197.

(198) Talrose, V.; Yermakov, A. N.; Usov, A. A.; Goncharova, A. A.; Leskin, A. .; Messineva, N. A.; Trusova, N. V.; Efimkina, M. V. *NIST Chem. WebBook, NIST Stand. Ref. Database Number 69, Eds. P.J. Linstrom W.G. Mallard, Natl. Inst. Stand. Technol.* **2007**.

(199) Friedman, M.; Kozukue, N.; Harden, L. A. *J. Agric. Food Chem* **2000**, *48* (11), 5702–5709.

(200) Wiegand, I.; Hilpert, K.; Hancock, R. E. W. *Nat. Protoc.* **2008**, *3* (2), 163–175.

(201) *Am. Soc. Test. Mater. ASTM E2149-01* **2004**.

(202) Fu, J.; Ji, J.; Yuan, W.; Shen, J. *Biomaterials* **2005**, *26* (33), 6684–6692.

(203) Fernandez-Megia, E.; Novoa-Carballal, R.; Quiñoá, E.; Riguera, R. *Carohydr. Polym.* **2005**, *61*, 155–161.

(204) Hirai, A.; Odani, H.; Nakajima, A. *Polym. Bull.* **1991**, *26*, 87–94.

(205) Varum, K. M.; Antohonsen, M. W.; Grasdalen, H.; Smidsrød, O. *Carbohydr. Res.* **1991**, *211*, 17–23.

(206) Pine, S. H.; Hendrickson, J.; Cram, D. J.; Hammono, G. S. *Organic Chemistry*, 4th ed.; McGrawHill: New York, 1980.

(207) Guinesi, L. S.; Cavalheiro, É. T. G. *Thermochim. Acta* **2006**, *444* (2), 128–133.

(208) Ganjian, I.; Baumgarten, R. L.; Valenzuela, R. J. *J. Chem. Educ.* **1992**, *69* (6), 511.

(209) An, J.; Zhang, H.; Zhang, J.; Zhao, Y.; Yuan, X. *Colloid Polym. Sci.* **2009**, *287* (12), 1425–1434.

(210) Schiffman, J. D.; Schauer, C. L. *Biomacromolecules* **2007**, *8* (2), 594–601.

(211) Peppas, N. A.; Bures, P.; Leobandung, W.; Ichikawa, H. *Eur. J. Pharm. Biopharm.* **2000**, *50* (1), 27–46.

(212) Siepmann, J.; Peppas, N. A. *Int. J. Pharm* **2011**, *418* (1), 6–12.

(213) Verreck, G.; Chun, I.; Rosenblatt, J.; Dijck, A. V; J, M.; Noppe, M.; Brewster, M. E. *J. Control. Release* **2003**, *92*, 349–360.

(214) Helander, I. .; Nurmiaho-Lassila, E.-L.; Ahvenainen, R.; Rhoades, J.; Roller, S. *Int. J. Food Microbiol.* **2001**, *71* (2-3), 235–244.

(215) Krajewska, B.; Wydro, P.; Kyzioł, A. *Colloids Surfaces A Physicochem. Eng. Asp.* **2013**, *434*, 349–358.

(216) Krajewska, B.; Wydro, P.; Jańczyk, A. *Biomacromolecules* **2011**, *12* (11), 4144–4152.

(217) Krajewska, B.; Kyzioł, A.; Wydro, P. *Colloids Surfaces A Physicochem. Eng. Asp.* **2013**, *434*, 359–364.

(218) Liu, H.; Du, Y.; Wang, X.; Sun, L. *Int. J. Food Microbiol.* **2004**, *95* (2), 147–155.

(219) Oussalah, M.; Caillet, S.; Lacroix, M. *J. Food Prot.* **2006**, *69* (5), 1046–1055.

(220) López, P.; Sanchez, C.; Batlle, R.; Nerín, C. *J. Agric. Food Chem* **2007**, *55* (11), 4348–4356.

(221) Yuan, Y.; Chesnutt, B. M.; Haggard, W. O.; Bumgardner, J. D. *Materials.* **2011**, *4* (12), 1399–1416.

(222) Barck, K.; Butler, M. F. *J. Appl. Polym. Sci.* **2005**, *98* (4), 1581–1593.

(223) Rieger, K. A.; Schiffman, J. D. *Carbohydr. Polym.* **2014**, *113*, 561–568.

(224) Dapčević Hadnađev, T.; Dokić, P.; Krstonošić, V.; Hadnađev, M. *Eur. J. Lipid Sci. Technol.* **2013**, *115* (3), 313–321.

(225) Palangetic, L.; Reddy, N. K.; Srinivasan, S.; Cohen, R. E.; McKinley, G. H.; Clasen, C. *Polymer (Guildf).* **2014**, *55* (19), 4920–4931.

(226) Rošic, R.; Pelipenko, J.; Kocbek, P.; Baumgartner, S.; Bešter-Rogač, M.; Kristl, J. *Eur. Polym. J.* **2012**, *48* (8), 1374–1384.

(227) Bordi, F.; Colby, R. H.; Cametti, C.; De Lorenzo, L.; Gili, T. *J. Phys. Chem. B* **2002**, *106* (27), 6887–6893.

(228) Kong, L.; Ziegler, G. R. *Biomacromolecules* **2012**, *13* (8), 2247–2253.

(229) Morrison, F. . *Understanding Rheology*; Gubbins, K. F., Barteau, M. A., Lauffenburger, D. A., Morari, M., Ray, W. H., Russel, W. B., Tirrell, M. V., Eds.; Eds.: Oxford University Press: New York, 2001.

(230) Thompson, C. J.; Chase, G. G.; Yarin, A. L.; Reneker, D. H. *Polymer (Guildf).* **2007**, *48* (23), 6913–6922.

(231) Yao, L.; Woll, A. R.; Watkins, J. J. *Macromolecules* **2013**, *46* (15), 6132–6144.

(232) Vazquez, M. A.; Munoz, F.; Donoso, J.; Gracia Blanco, F. *Biochem* **1992**, *11*, 241–254.

(233) Zeng, B.; Gao, Y.; Bartoli, F. J. *Sci. Rep.* **2013**, *3*, 2840.

(234) Murray, C. A.; Dutcher, J. R. *Biomacromolecules* **2006**, *7* (12), 3460–3465.

(235) Heriot, S. Y.; Jones, R. A. L. *Nat. Mater.* **2005**, *4* (10), 782–786.

(236) Yuan, Y.; Lee, T. . *Surf. Sci. Tech. Springer Ser. Surf. Sci.* **2013**, *51*, 3–34.

(237) Villalobos, R.; Chanona, J.; Hernández, P.; Gutiérrez, G.; Chiralt, A. *Food Hydrocoll.* **2005**, *19* (1), 53–61.

(238) Ma, Z.; Kotaki, M.; Ramakrishna, S. *J. Membr. Sci.* **2005**, *265* (1), 115–123.

(239) Dornath, P.; Fan, W. *Micropor. Mesopor. Mat.* **2014**, *191*, 10–17.

(240) Ruthven, D. M. *Principles of Adsorption and Adsorption Processes*; John Wiley & Sons, Inc., 1984.

(241) Crank, J. *The Mathematics of Diffusion*, 2nd ed.; Oxford University Press: New York, 1975.

(242) Lu, P.; Hsieh, Y.-L. *ACS Appl. Mater. Interfaces* **2010**, *2* (8), 2413–2420.

(243) Celebioglu, A.; Uyar, T. *Mater. Lett.* **2011**, *65* (14), 2291–2294.

(244) Schreuder-Gibson, H. L.; Truong, Q.; Walker, J. E.; Owens, J. R.; Wander, J. D.; Jones, W. E. *MRS Bullentin* **2003**, *28* (8), 574–578.

(245) Zahedi, P.; Rezaeian, I.; Ranaei-Siadat, S.-O.; Jafari, S.-H.; Supaphol, P. *Polym. Adv. Technol.* **2009**, *21*, 77–95.

(246) Carpenter, A. W.; de Lannoy, C.-F.; Wiesner, M. R. *Environ. Sci. Technol.* **2015**, *49* (9), 5277–5287.

(247) Dods, S. R.; Hardick, O.; Stevens, B.; Bracewell, D. G. *J. Chromatogr. A* **2015**, *1376*, 74–83.

(248) Zhang, L.; Menkhaus, T.; Fong, H. *J. Membr. Sci.* **2008**, *319* (1-2), 176–184.

(249) Aussawasathien, D.; Teerawattananon, C.; Vongachariya, A. *J. Membr. Sci.* **2008**, *315* (1-2), 11–19.

(250) Ramakrishna, S.; Jose, R.; Archana, P. S.; Nair, A. S.; Balamurugan, R.; Venugopal, J.; Teo, W. E. *J. Mater. Sci.* **2010**, *45* (23), 6283–6312.

(251) Ma, H.; Burger, C.; Hsiao, B. S.; Chu, B. *J. Mater. Chem.* **2011**, *21* (21), 7507.

(252) Ma, H.; Hsiao, B. S.; Chu, B. *J. Membr. Sci.* **2014**, *452*, 446–452.

(253) Abrigo, M.; Kingshott, P.; McArthur, S. L. *ACS Appl. Mater. Interfaces* **2015**, *7* (14), 7644–7652.

(254) Rivera-Utrilla, J.; Bautista-Toledo, I.; Ferro-Garcia, M.; Moreno-Castilla, C. *J. Chem. Technol. Biotechnol.* **2001**, *76* (12), 1209–1215.

(255) Katsikogianni, M.; Missirlis, Y. F. *Eur. Cell. Mater.* **2004**, *8*, 37–57.

(256) Dunne, W. M. *Clin. Microbiol. Rev.* **2002**, *15* (2), 155–166.

(257) Foster, T. J.; Höök, M. *Trends Microbiol.* **1998**, *6* (12), 484–488.

(258) Clarke, S. R.; Foster, S. J. *Adv. Microb. Physiol.* **2006**, *51*, 187–224.

(259) Makin, S. A.; Beveridge, T. J. *Microbiology* **1996**, *142* (2), 299–307.

(260) Cerf, A.; Cau, J.-C.; Vieu, C.; Dague, E. *Langmuir* **2009**, *25* (10), 5731–5736.

(261) Deng, H.; Zhou, X.; Wang, X.; Zhang, C.; Ding, B.; Zhang, Q.; Du, Y. *Carbohydr. Polym.* **2010**, *80* (2), 474–479.

(262) Da Róz, A. L.; Leite, F. L.; Pereiro, L. V.; Nascente, P. A. P.; Zucolotto, V.; Oliveira, O. N.; Carvalho, A. J. F. *Carbohydr. Polym.* **2010**, *80* (1), 65–70.

(263) Rieger, K. A.; Cho, H. J.; Yeung, H. F.; Fan, W.; Schiffman, J. D. *ACS Appl. Mater. Interfaces* **2016**, *8* (5), 3032–3040.

(264) Adewuyi, S.; Ondigo, D. A.; Zugle, R.; Tshentu, Z.; Nyokong, T.; Torto, N. *Anal. Methods* **2012**, *4* (6), 1729.

(265) Rodríguez, K.; Sundberg, J.; Gatenholm, P.; Renneckar, S. *Carbohydr. Polym.* **2014**, *100*, 143–149.

(266) Huang, F. L.; Wang, Q. Q.; Wei, Q. F.; Gao, W. D.; Shou, H. Y.; Jiang, S. D. *eXPRESS Polym. Lett.* **2010**, *4* (9), 551–558.

(267) Lee, S.-D.; Hsiue, G.-H.; Chang, P. C.-T.; Kao, C.-Y. *Biomaterials* **1996**, *17* (16), 1599–1608.

(268) Bumgardner, J. D.; Wiser, R.; Elder, S. H.; Jouett, R.; Yang, Y.; Ong, J. L. *J. Biomater. Sci. Polym. Ed.* **2003**, *14* (12), 1401–1409.

(269) Terada, A.; Yuasa, A.; Kushimoto, T.; Tsuneda, S.; Katakai, A.; Tamada, M. *Microbiology* **2006**, *152* (Pt 12), 3575–3583.

(270) An, Y. H.; Friedman, R. J. *J. Biomed. Mater. Res.* **1998**, *43* (3), 338–348.

(271) No, H. K.; Park, N. Y.; Lee, S. H.; Meyers, S. P. *Int. J Food Microbiol.* **2002**, *74* (1-2), 65–72.

(272) Goy, R. C.; Britto, D. de; Assis, O. B. G. *Polímeros* **2009**, *19* (3), 241–247.

(273) Timofeeva, L. M.; Kleshcheva, N. A.; Moroz, A. F.; Didenko, L. V. *Biomacromolecules* **2009**, *10* (11), 2976–2986.

(274) Mi, X.; Vijayaragavan, K. S.; Heldt, C. L. *Carbohydr. Res.* **2014**, *387*, 24–29.

(275) Sato, A.; Wang, R.; Ma, H.; Hsiao, B. S.; Chu, B. *J. Electron Microsc. (Tokyo).* **2011**, *60* (3), 201–209.

(276) Huang, A.; Caro, J. *Chem. Mater.* **2010**, *22* (15), 4353–4355.

(277) Xu, X.; Yang, W.; Liu, J.; Lin, L.; Stroh, N.; Brunner, H. *J. Membr. Sci.* **2004**, *229* (1-2), 81–85.

(278) Chen, H.; Wydra, J.; Zhang, X.; Lee, P.-S.; Wang, Z.; Fan, W.; Tsapatsis, M. *J. Am. Chem. Soc.* **2011**, *133* (32), 12390–12393.

(279) Fan, W.; Snyder, M. A.; Kumar, S.; Lee, P.-S.; Yoo, W. C.; McCormick, A. V; Lee Penn, R.; Stein, A.; Tsapatsis, M. *Nat. Mater.* **2008**, *7* (12), 984–991.

(280) Cho, H. J.; Dornath, P.; Fan, W. *ACS Catal.* **2014**, *4* (6), 2029–2037.

(281) Bedi, R. S.; Cai, R.; O'Neill, C.; Beving, D. E.; Foster, S.; Guthrie, S.; Chen, W.; Yan, Y. *Micropor. Mesopor. Mat.* **2012**, *151*, 352–357.

(282) International Zeolite Association, I.-S. .

(283) Strydom, S. J.; Otto, D. P.; Liebenberg, W.; Lvov, Y. M.; de Villiers, M. M. *Int. J. Pharm.* **2011**, *404* (1-2), 57–65.

(284) Meyer, M.; Leiggener, C.; Calzaferri, G. *Chemphyschem* **2005**, *6* (6), 1071–1080.